AD-A063 870 OHIO STATE UNIV COLUMBUS ELECTROSCIENCE LAB F/G 9/5
ASYMPTOTIC HIGH FREQUENCY TECHNIQUES FOR UHF AND ABOVE ANTENNAS--ETC(U)
OCT 78 R C RUDDUCK, R J MARHEFKA N00123-76-C-1371
UNCLASSIFIED ESL-4508-12 NL

1 OF 2
AD A063870

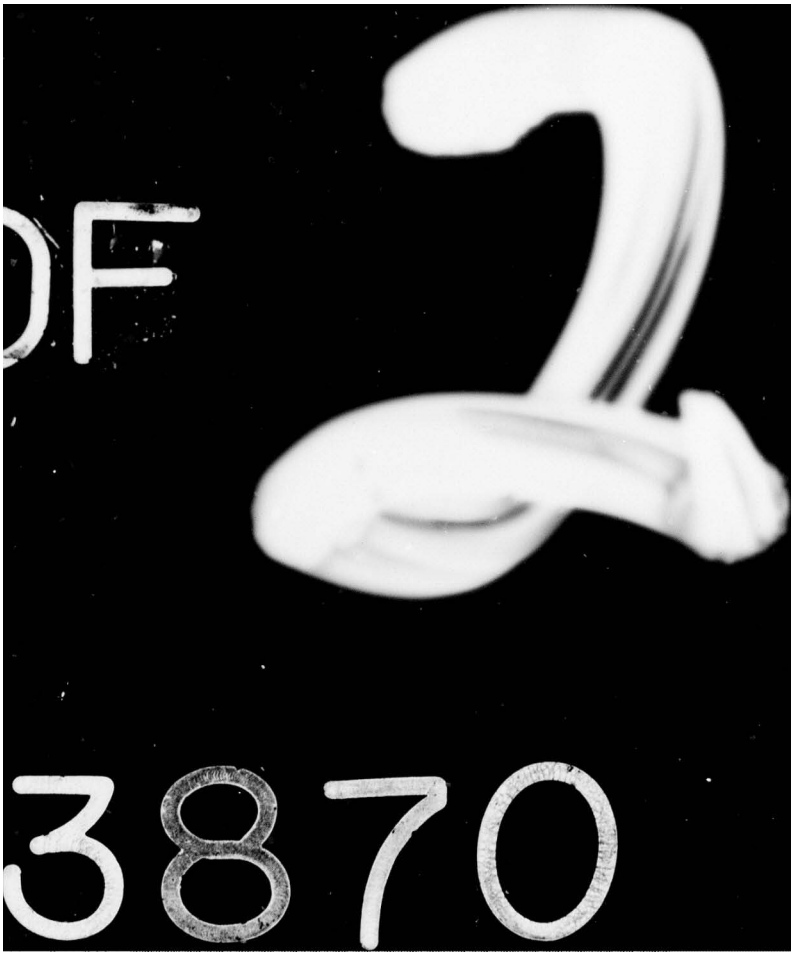
OF
3870

LEVEL II

(12)

(6) ASYMPTOTIC HIGH FREQUENCY TECHNIQUES FOR UHF AND ABOVE ANTENNAS.

(10) R. C. Rudduck,
R. J. Marhefka,
W. D. Burnside,
R. G. Kouyoumjian
C. H. Walter

The Ohio State University

ElectroScience Laboratory

Department of Electrical Engineering
Columbus, Ohio 43212

(9) Annual Report, 4508-12 (784508)
1 Aug [redacted]77 [redacted] 31 Jul [redacted]978,
Oct [redacted]978

(11)

(12) 99 p.

(14) ESL-4508-12,
ESL-784508

(15) N00123-76-C-1371

Naval Regional Procurement Office
Long Beach, California 90822

NOTICES

When Government drawings, specifications, or other data are used for any purpose other than in connection with a definitely related Government procurement operation, the United States Government thereby incurs no responsibility nor any obligation whatsoever, and the fact that the Government may have formulated, furnished, or in any way supplied the said drawings, specifications, or other data, is not to be regarded by implication or otherwise as in any manner licensing the holder or any other person or corporation, or conveying any rights or permission to manufacture, use, or sell any patented invention that may in any way be related thereto.

UNCLASSIFIED

SECURITY CLASSIFICATION OF THIS PAGE *(When Data Entered)*

REPORT DOCUMENTATION PAGE		READ INSTRUCTIONS BEFORE COMPLETING FORM
1. REPORT NUMBER	2. GOVT ACCESSION NO.	3. RECIPIENT'S CATALOG NUMBER
4. TITLE *(and Subtitle)* ASYMPTOTIC HIGH FREQUENCY TECHNIQUES FOR UHF AND ABOVE ANTENNAS		5. TYPE OF REPORT & PERIOD COVERED Annual Report 1 August 1977 to 31 July 1978 6. PERFORMING ORG. REPORT NUMBER ESL 4508-12 (784508)
7. AUTHOR(s) R. C. Rudduck, R. G. Kouyoumjian, R. J. Marhefka, C. H. Walter, W. D. Burnside		8. CONTRACT OR GRANT NUMBER(s) Contract N00123-76-C-1371
9. PERFORMING ORGANIZATION NAME AND ADDRESS The Ohio State University ElectroScience Laboratory, Department of Electrical Engineering Columbus, Ohio 43212		10. PROGRAM ELEMENT, PROJECT, TASK AREA & WORK UNIT NUMBERS
11. CONTROLLING OFFICE NAME AND ADDRESS Naval Regional Procurement Office Long Beach, California 90822		12. REPORT DATE October 1978 13. NUMBER OF PAGES 96
14. MONITORING AGENCY NAME & ADDRESS*(if different from Controlling Office)*		15. SECURITY CLASS. *(of this report)* Unclassified 15a. DECLASSIFICATION/DOWNGRADING SCHEDULE
16. DISTRIBUTION STATEMENT *(of this Report)* This document has been approved for public release and sale; its distribution is unlimited.		
17. DISTRIBUTION STATEMENT *(of the abstract entered in Block 20, if different from Report)*		
18. SUPPLEMENTARY NOTES		
19. KEY WORDS *(Continue on reverse side if necessary and identify by block number)* Computer code Algorithm Geometrical Theory of Diffraction Far Field Pattern Reflector Antenna Aperture Integration Cylinders		

20. ABSTRACT *(Continue on reverse side if necessary and identify by block number)*

The overall scope of the program on Contract No. N00123-76-C-1371 between The Ohio State University ElectroScience Laboratory and the Naval Electronics Laboratory Center is to develop the necessary theory, algorithms and computer codes for simulating antennas at UHF and above in a complex ship environment. The work consists of a) basic scattering code development, b) reflector antenna code development and c) basic studies to support items a) and b). This report describes the progress in each of these three areas for the period 1 August 1977 to 31 July 1978.

DD FORM 1 JAN 73 1473 EDITION OF 1 NOV 65 IS OBSOLETE

UNCLASSIFIED

SECURITY CLASSIFICATION OF THIS PAGE *(When Data Entered)*

CONTENTS

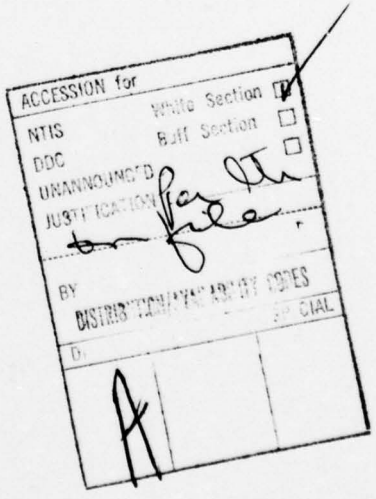

I. INTRODUCTION

This report describes the work done on Contract No. N00123-76-C-1371 for the year 1 August 1977 to 31 July 1978.

The overall program is divided into three areas. These are 1) basic scattering code development, 2) reflector antenna code development and 3) basic theoretical studies to support the first two areas. The following sections describe the research accomplished in each of the three areas mentioned above.

II. PROGRAM SCOPE

The scope of the work under Contract No. N00123-76-C-1371 is to develop the necessary theory, algorithms and computer codes for simulating antennas at UHF and above in a complex ship environment. A revised milestone chart for the three year program is shown in Table I. The revised milestone chart shows the inclusion of the more useful source representation (item C of the Basic Scattering Code). The more useful source representation is being given priority in the current three-year program over the near field analysis of coupled structures which was shown in previous milestone charts.

III. BASIC SCATTERING CODE DEVELOPMENT

The analytic modeling of a ship to predict the radiation patterns of antennas mounted on shipboard is being accomplished by the use of the Geometrical Theory of Diffraction (GTD) [1,2,3]. This is a high frequency technique that allows a complicated structure to be approximated by basic shapes representing canonical problems in the GTD. These shapes include flat and curved wedges and convex curved surfaces. The GTD is a ray optical technique and it therefore allows one to gain some physical insight into the various scattering and diffraction mechanisms involved. Consequently, one is able to quickly seek out the dominant or significant scattering and diffraction mechanism for a given geometrical configuration. This, in turn, leads to an accurate engineering solution to practical antenna problems. For example, the performance of an antenna at UHF and above in the presence of a complex ship environment can be modeled using flat plates, box-like structures and a finite elliptic cylinder to represent the various component parts of a ship as illustrated in Figure 1. A user oriented computer code is being developed to aid the antenna and system designer to accomplish this task.

This section briefly describes the basic operation of the third generation of this scattering code for the analysis of antennas in a shipboard environment. This version of the code allows analysis of scattering structures that can be modeled by concave flat plate structures, an infinite ground plane, and a finite elliptic cylinder all of which are built up from the basic canonical structures. These shapes allow one to model a wide variety of structures in the UHF range and above where the scattering

TABLE I

REVISED MILESTONE CHART (04/12/78)

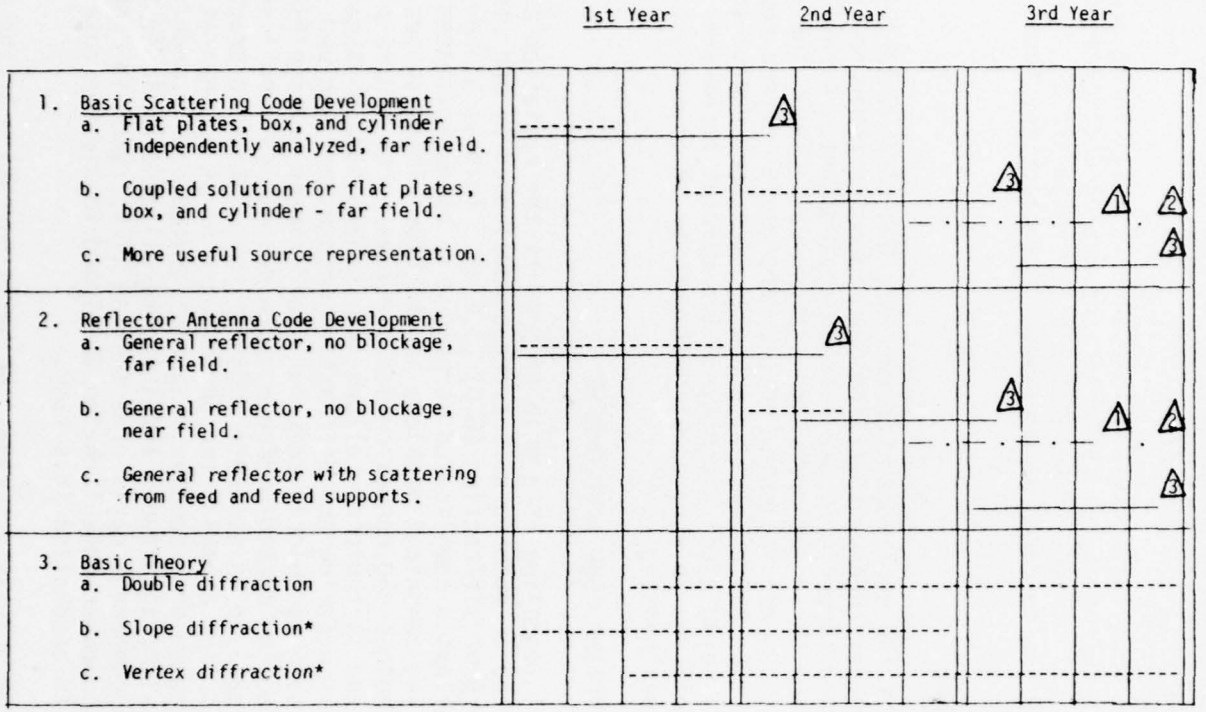

----- Theoretical development

——— Formulate algorithms and write and implement codes (including integration with NEC and User's Manual)

—·— Write Code Manual

*To be jointly supported by ONR Block Funding (Associate JSEP)

1 Rough Draft

2 Final Version

3 Computer Code Delivered to NOSC

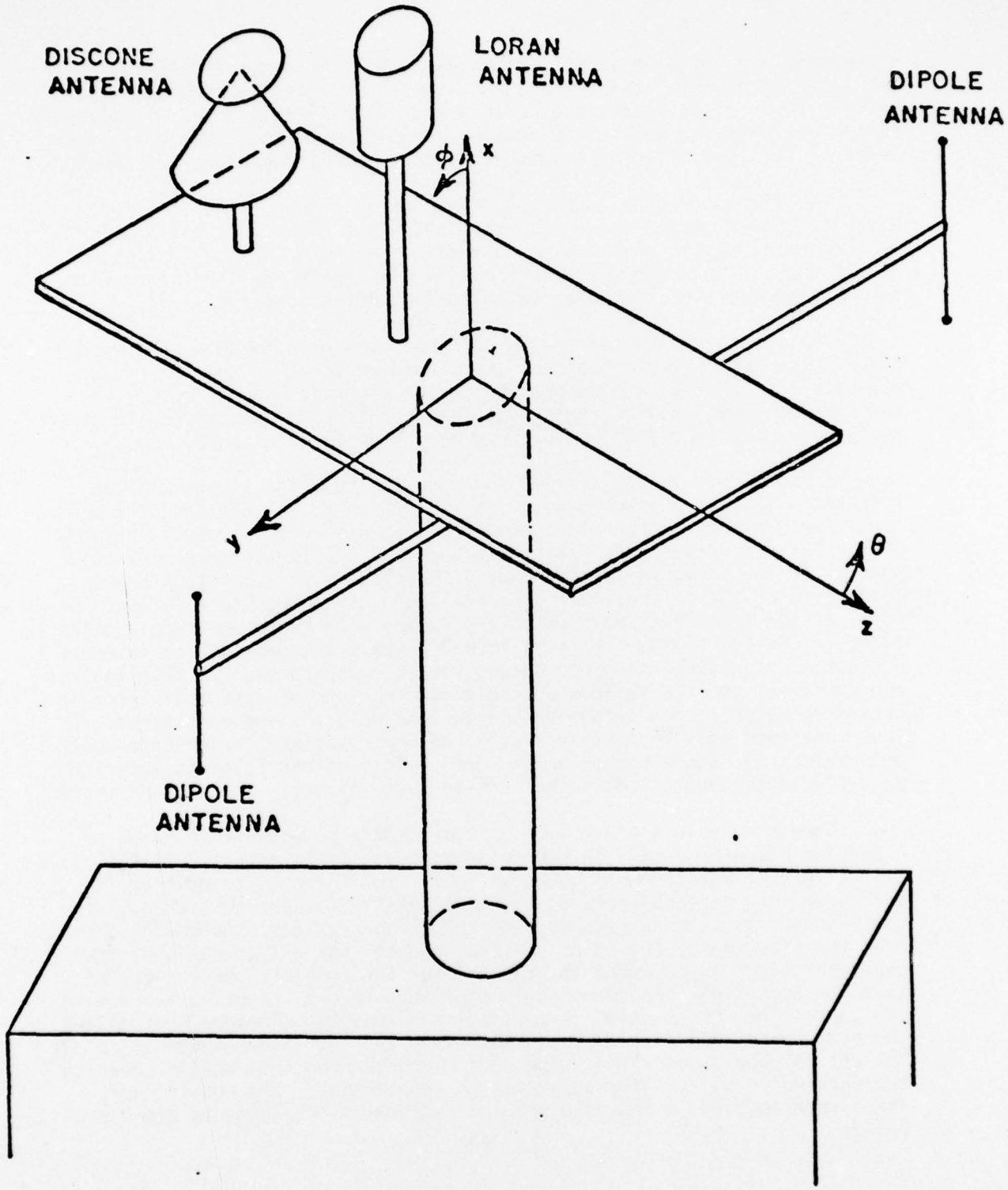

Figure 1. Sample UHF antenna problem.

structures are large in terms of a wavelength. The general rule is that the lower frequency limit of this solution is dictated by the spacings between the various scattering centers and their overall size. In practice this means that the smallest dimensions should be on the order of a wavelength. This can often be relaxed to approximately a quarter-wavelength.

The GTD approach allows other types of solutions to be interfaced with it. For example, the modal solution can be used for a small cylinder or the moment method can be used to model wire segments, small structures or antennas. The present scattering code is capable of interfacing with the wire segments of the Numerical Electromagnetic Code (NEC) [4].

The positive time convention $e^{j\omega t}$ has been used in this scattering code. Also, the radiation patterns are assumed to be in the far field. The term e^{-jkR}/R has been suppressed unless otherwise specified by the user of the code. All of the structures in this code are assumed to be perfectly-conducting and the surrounding medium is free space.

As mentioned above, the GTD approach is ideal for a general high frequency study of shipboard antennas in that only the most basic structural features of an otherwise very complicated structure need to be modeled. This is because ray optical techniques are used to determine components of the field incident on and diffracted by various structures. Components of the diffracted fields are found using the GTD solutions in terms of the individual rays which are summed with the geometrical optics terms in the far field. The rays from a given scatterer tend to interact with other structures causing various higher-order terms. In this way one can trace out the various possible combinations of rays that interact between scatterers and determine and include only the dominant terms. Thus, one need only be concerned with the important scattering components and neglect all other higher-order terms. This method leads to accurate and efficient computer codes that can be systematically written and tested.

Complex problems are built up from simpler components in terms of a modular computer code. This modular approach is illustrated in the block diagram of the main program shown in Table II. The scattering code is broken up into many subroutines that represent different scattered field components, ray tracing methods, and shadowing routines. As can be seen from the flow chart, the code is structured so that all of one type of scattered field is computed at one time for the complete pattern cut so that the amount of core swapping is minimized thereby reducing overlaying and increasing efficiency. This also is an important feature that allows the code to be used on small computers that are not large enough to accept the entire code at one time. The code can be broken into smaller overlay segments which will individually fit in the machine. The results are, then, superimposed in the main program as the various segments are executed.

TABLE II
Block Diagram of the Main Program for the Computer Code

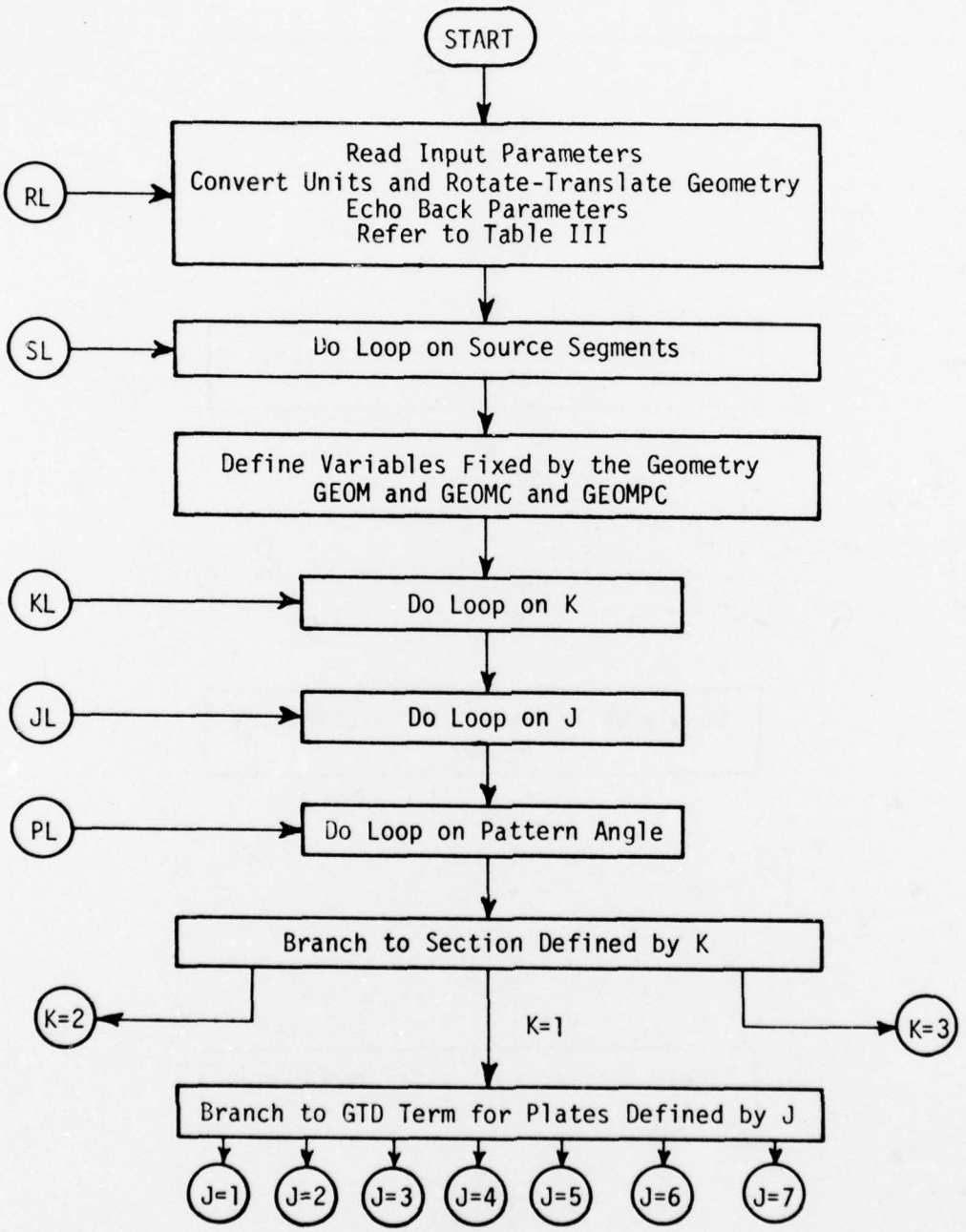

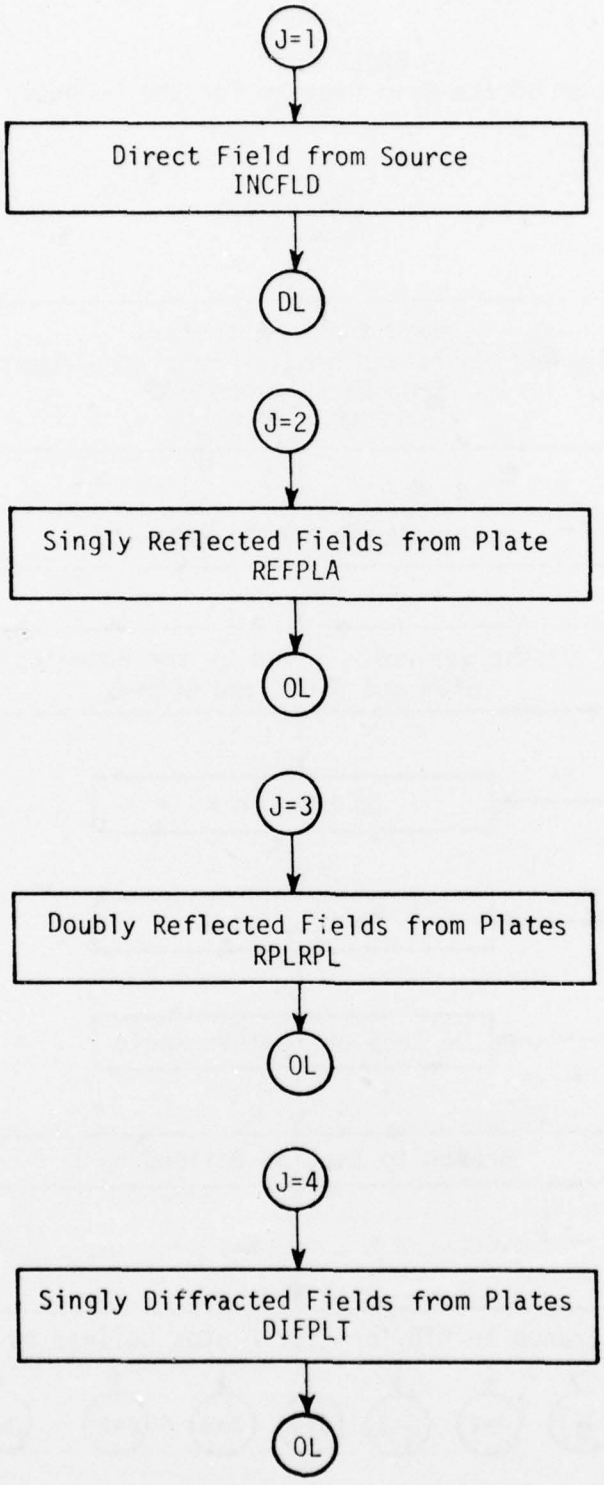
J=1
Direct Field from Source
INCFLD
DL
J=2
Singly Reflected Fields from Plate
REFPLA
OL
J=3
Doubly Reflected Fields from Plates
RPLRPL
OL
J=4
Singly Diffracted Fields from Plates
DIFPLT
OL

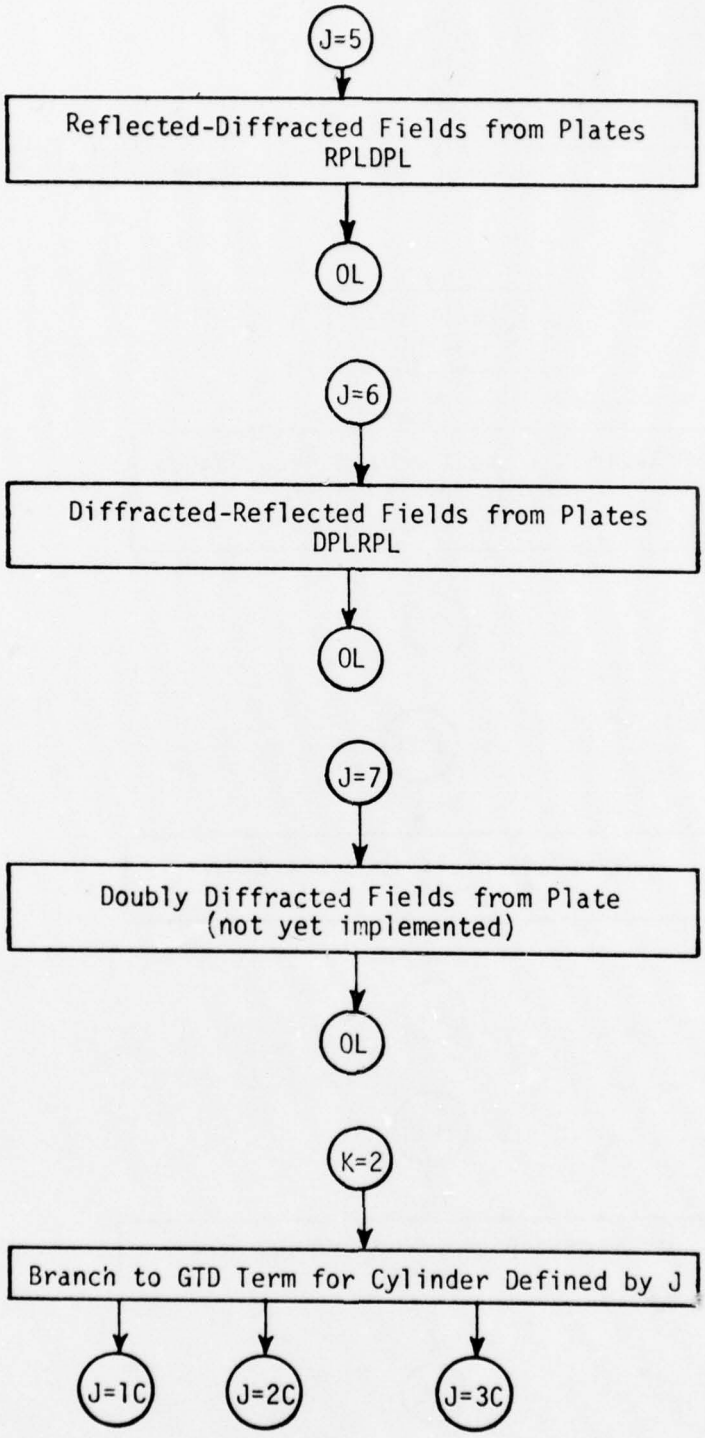
J=5
Reflected-Diffracted Fields from Plates
RPLDPL
OL
J=6
Diffracted-Reflected Fields from Plates
DPLRPL
OL
J=7
Doubly Diffracted Fields from Plate
(not yet implemented)
OL
K=2
Branch to GTD Term for Cylinder Defined by J
J=1C
J=2C
J=3C

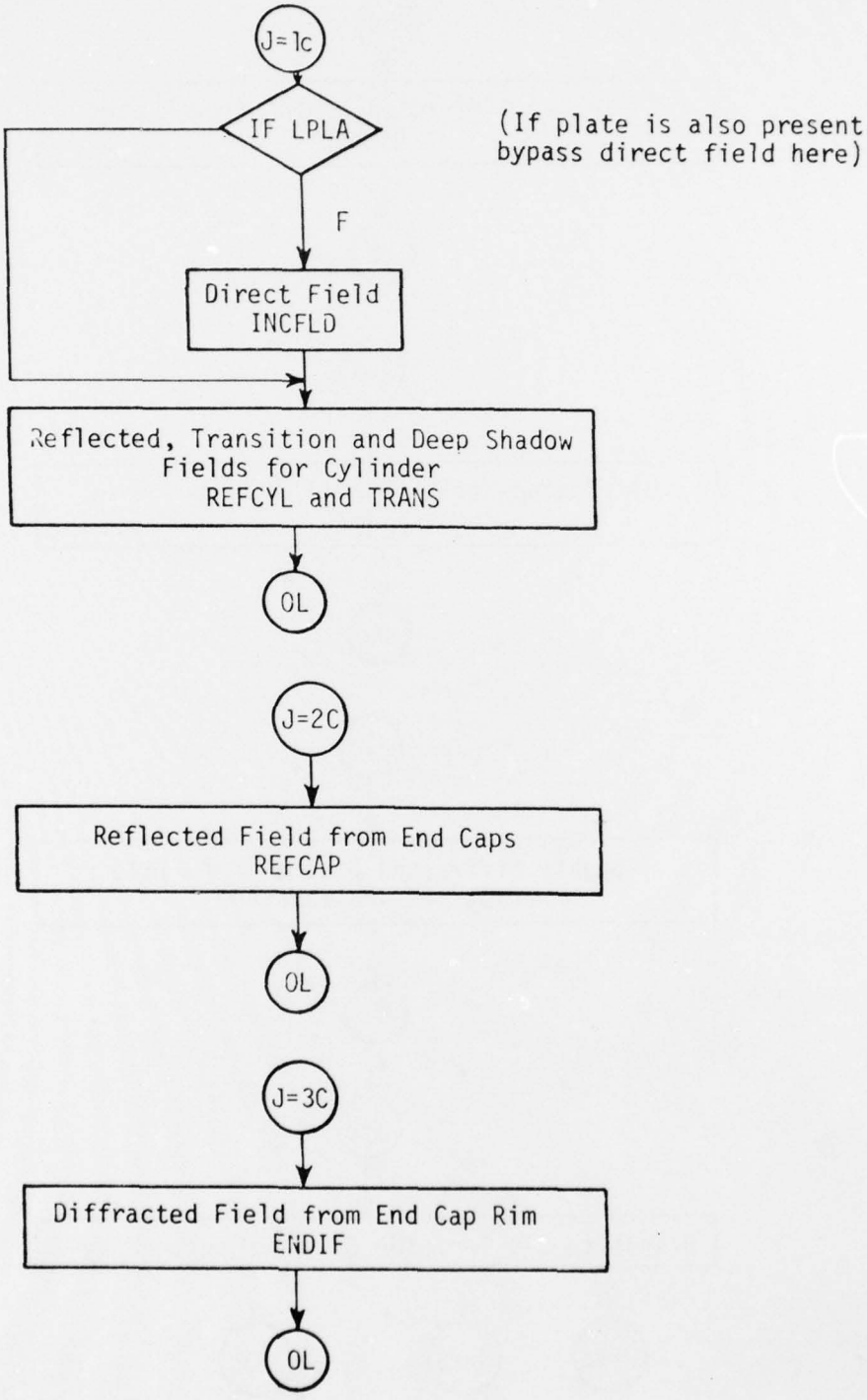
J=1C
IF LPLA
(If plate is also present bypass direct field here)
F
Direct Field
INCFLD
Reflected, Transition and Deep Shadow Fields for Cylinder
REFCYL and TRANS
OL
J=2C
Reflected Field from End Caps
REFCAP
OL
J=3C
Diffracted Field from End Cap Rim
ENDIF
OL

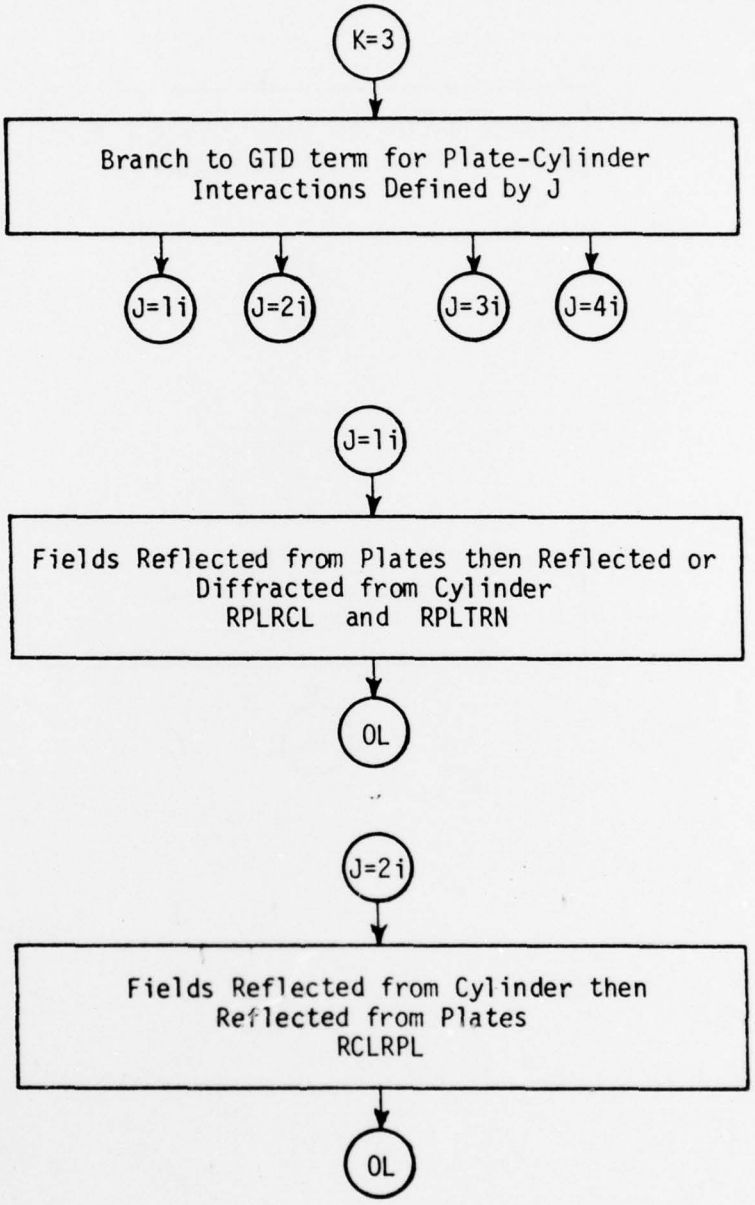
K=3
Branch to GTD term for Plate-Cylinder Interactions Defined by J
J=1i
J=2i
J=3i
J=4i
J=1i
Fields Reflected from Plates then Reflected or Diffracted from Cylinder
RPLRCL and RPLTRN
OL
J=2i
Fields Reflected from Cylinder then Reflected from Plates
RCLRPL
OL

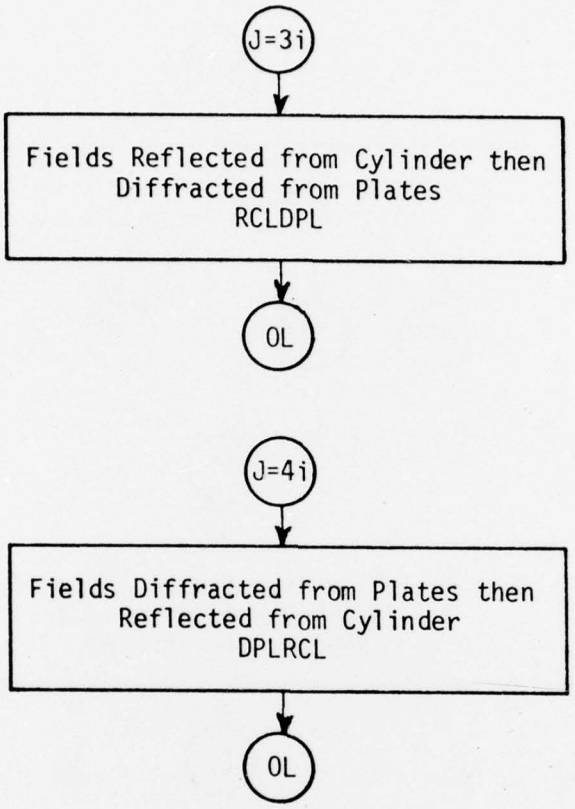
J=3i
Fields Reflected from Cylinder then Diffracted from Plates
RCLDPL
OL
J=4i
Fields Diffracted from Plates then Reflected from Cylinder
DPLRCL
OL

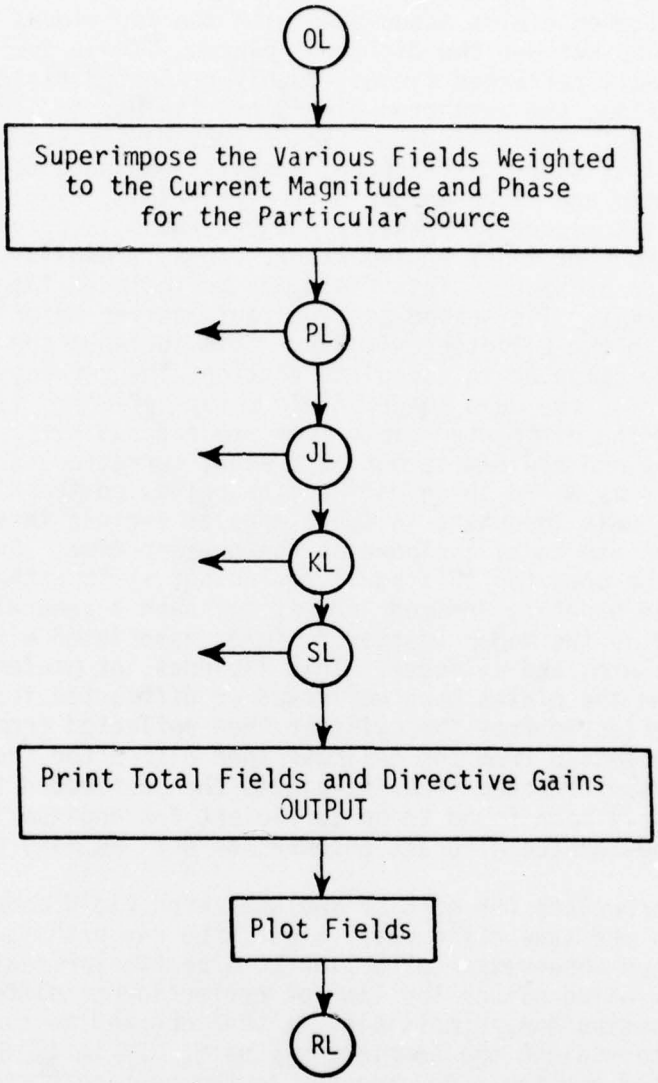
OL
Superimpose the Various Fields Weighted to the Current Magnitude and Phase for the Particular Source
PL
JL
KL
SL
Print Total Fields and Directive Gains OUTPUT
Plot Fields
RL

The code is divided into three large sections. The first two sections were included in the second generation code. The third section is being included in the third generation of the code. The first section contains the major scattered fields associated with the individual flat plates and the interactions between the different plates. These include the direct field, the singly reflected fields, doubly reflected fields, the singly diffracted fields, the reflected-diffracted fields, and the diffracted-reflected fields. The diffracted fields include the normal diffracted fields as well as slope diffraction, a newly developed heuristic corner diffracted field and slope-corner diffracted field. The double diffracted fields are not included at present, but a warning is provided wherever this field component might be important. This is usually only a small angular section of space. This field may be included later whenever time and effort permit. The second section contains the major scattered fields associated with the elliptic cylinder. This includes the direct field, if not already computed in the plate section, the reflected field, the transition field, the deep shadow fields, the reflected field from the end caps, and the diffracted field from the end cap rims. The diffracted field from the end cap rim is not at present corrected in the pseudo caustic regions. This is where three diffraction points on the rim coalesce into one. This is only important in small angular regions in space and is not deemed appropriate to be included at the present time. An equivalent current method could be used for this small region but it is rather time consuming to use for the benefits derived from it for such a general code. The third section contains the major scattered fields associated with the interactions between the plates and cylinder. This includes, at present, the fields reflected from the plates then reflected or diffracted from the cylinder, the fields reflected from the cylinder then reflected from the plates, the fields reflected from the cylinder then diffracted from the plates, and the fields diffracted from the plates then reflected from the cylinder. These terms have been found to be sufficient for engineering purposes when analyzing wing-mounted aircraft antennas as well as many other structures[5].

The subroutines for each of the scattered field components are all structured in the same basic way. First, the ray path is traced backward from the chosen observation direction to a particular scatterer and subsequently to the source using either the laws of reflection or diffraction. Each ray path, assuming one is possible, is then checked to see if it is shadowed by any structure along the complete ray path. If it is shadowed the field is not computed and the code proceeds to the next scatterer or observation direction. If the path is not interrupted the scattered field is computed using the appropriate GTD solutions. The fields are then superimposed in the main program. This shadowing process is often speeded up by making various decisions based on bounds associated with the geometry of the structure. This type of knowledge is used wherever possible.

The shadowing of rays is a very important part of the GTD scattering code. It is obvious that this approach should lead to various discontinuities in the resulting pattern. However, the GTD diffraction coefficients are designed to smooth out the discontinuities in the fields such that a continuous field is obtained. When a scattered field is not included in the result, therefore, the lack of its presence is apparent. This can be used to advantge in analyzing complicated problems. Obviously in a complex problem not

all the possible scattered fields can be included. In the GTD code the importance of the neglected terms are determined by the size of the so-called gliches or jumps in the pattern trace. If the gliches are small no additional terms are needed for a good engineering solution. If the gliches are large it may be necessary to include more terms in the solution. In any case the user has a gauge with which he can examine the accuracy of the results and is not falsely led into believing a result is correct when in fact there could be an error. In order to show the versatility of the code and to test its accuracy a large number of example problems were run and compared with measurements whenever possible. These results are included in user's manuals [6,7] that illustrate the above ideas.

The method used to input data into the computer code is presently based on a command word system. This is especially convenient when more than one problem is to be analyzed during a computer run. The code stores the previous input data such that one need only input that data which needs to be changed from the previous execution. Also, there is a default list of data so for any given problem the amount of data that needs to be input has been shortened. The command words that are presently implemented in the computer code are listed in Table III. The input parameters for the third generation code will be a modified version of those used in the second generation code [7]. A more detailed description of the modified parameters will be given in the next quarterly report and the user's manual for the third generation code.

The input/output format of the basic scattering code may differ slightly between the NOSC and OSU versions. NOSC personnel will make the modifications in the input/output for their needs and will furnish an appendix to the user's manual detailing their modifications. The two versions of the codes will be the same other than the differences in format.

In order to confirm the validity of the GTD and the numerical accuracy of the basic scattering code over a wide range of geometries, the code's results are being tested against measurements made at OSU. Whenever possible, the code's results are also being checked against measurements made at other facilities or against results found in the literature. For example, the basic scattering code has been checked against measurements made by Bach [8] on a variety of satellite shapes. The code's calculated results for a dipole in the presence of an eight sided box as illustrated in Figure 2, is compared against measurements in Figure 3. The calculated results for various locations about a finite circular cylinder as shown in Figures 4a,b, and c, are compared against measurements in Figures 5a,b, and c respectively. In all cases the agreement is very good, confirming the validity of the basic scattering code's results. The small discrepencies that exist between the patterns can be contributed to measurement inaccuracies and to the lack of double diffraction effects in both the geometries and, in the case of the cylinder, to the pseudo caustic caused by the coalescence of rays on the endcap rims.

TABLE III

COMMAND WORDS FOR INPUT DATA

CM:	Comment card
CE:	Last or only comment card
TO:	Test data options
UN:	Units of input
FR:	Frequency
PD:	Pattern Data
RG:	Far Field Range
RT:	Translate and/or rotation of geometry
PG:	Plate geometry input
GP:	Infinite ground plane
CG:	Cylinder geometry input
SG:	Source geometry input
AM:	Source input from NEC/AMP
LP:	Line printer output
PP:	Pen plotter output
XQ:	Execute program
NX:	Next problem
EN:	End program

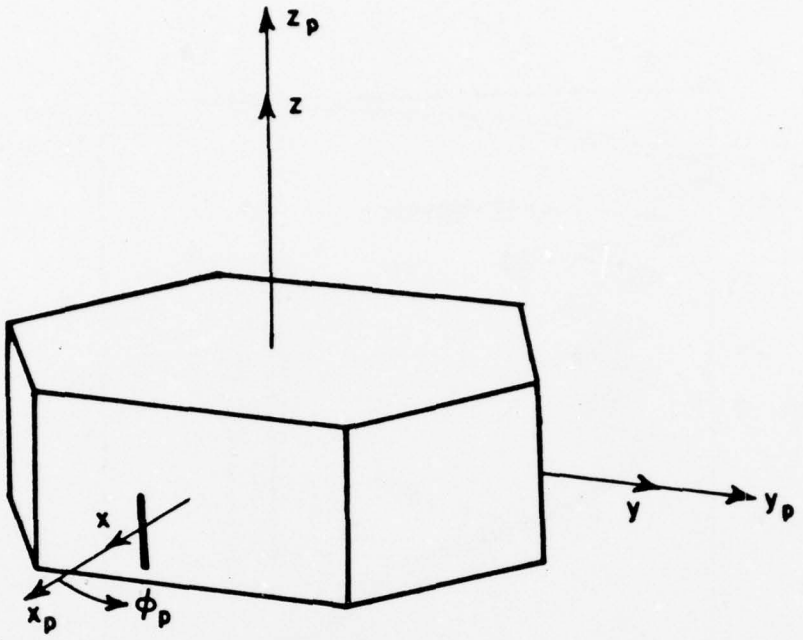

Figure 2. Electric dipole in the presence of an eight sided box.

The two geometries considered above are composed of either plates alone or a finite cylinder by itself. These separate shapes can be analyzed using the second generation of the scattering code. The third generation of the code, however, has the plate-cylinder interaction fields included so that geometries containing both plates and a finite elliptic cylinder can be analyzed. This is a much more difficult problem, due to the more complicated nature of equations defining the ray paths and the fields. In order to test the accuracy of the five interaction fields that are being included, a series of measurements were made at OSU on a simplified geometry that resembles a situation that may arise on shipboard. The geometry is shown in Figure 6. This is a very difficult problem because of the multiple bounces of the fields that can occur between the plate and the cylinder. This, however, illustrates the engineering solution that can be obtained using the scattering code. For comparison purposes, the separate pieces are first studied individually. The calculated and measured pattern of the half-wavelength dipole is compared in Figure 7a. The results for the square plate are compared against measurements in Figure 7b. The results for the finite circular cylinder are shown in Figure 7c. In all of these three cases the comparisons are quite good. The radiation pattern of the dipole in the presence of both the plate and the cylinder is compared to the calculated result from the second generation scattering code, in Figure 7d. The second generation code does not include the plate-cylinder interaction fields. Although the basic structure of the pattern is there, the proper levels and fine details are missing. The measured result is compared to the third generation code result

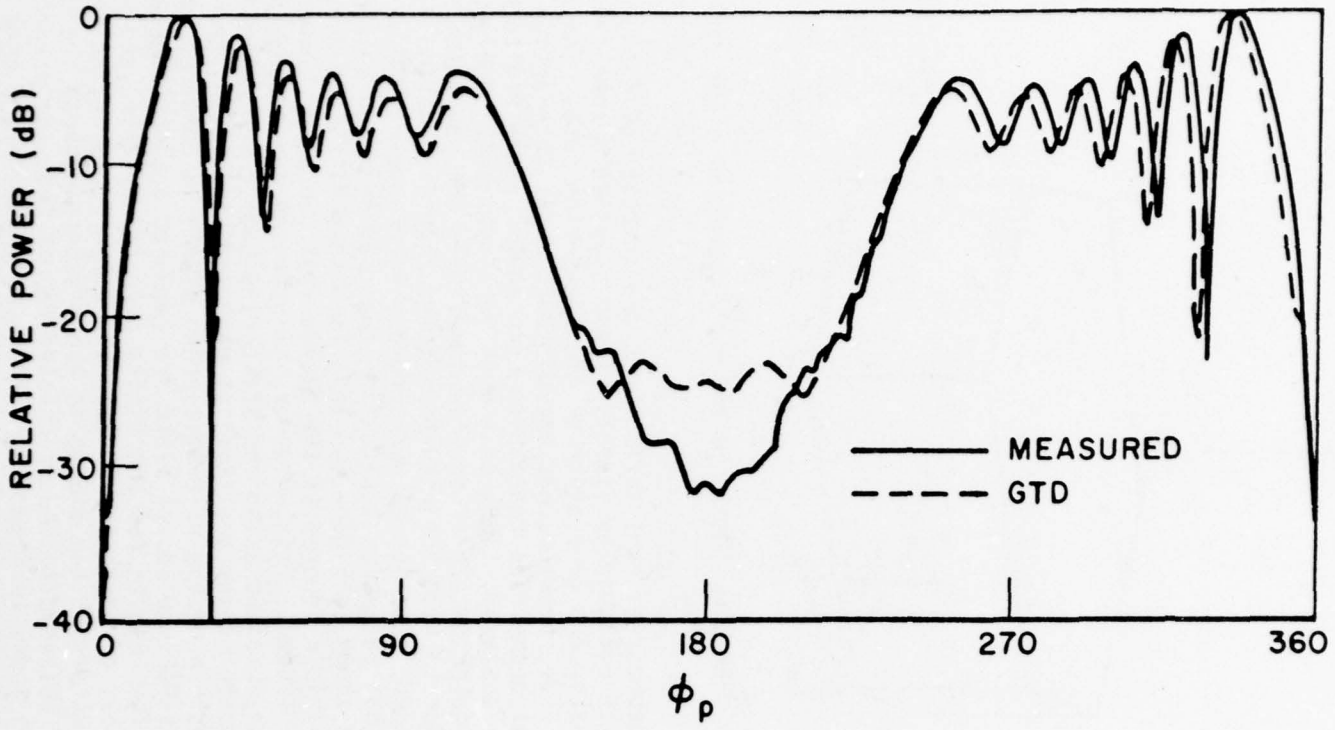

Figure 3. Comparison of measured (Bach) and calculated radiation pattern for E_{θ_p} for an electric dipole in the presence of an eight sided box.

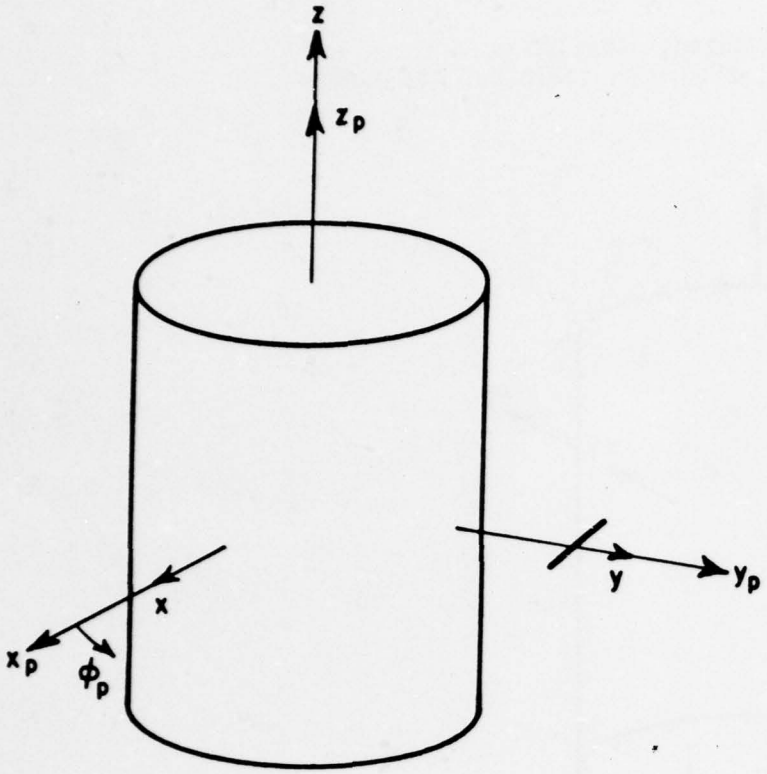

Figure 4a. An electric dipole in the presence of a finite circular cylinder (pattern taken in x-y plane).

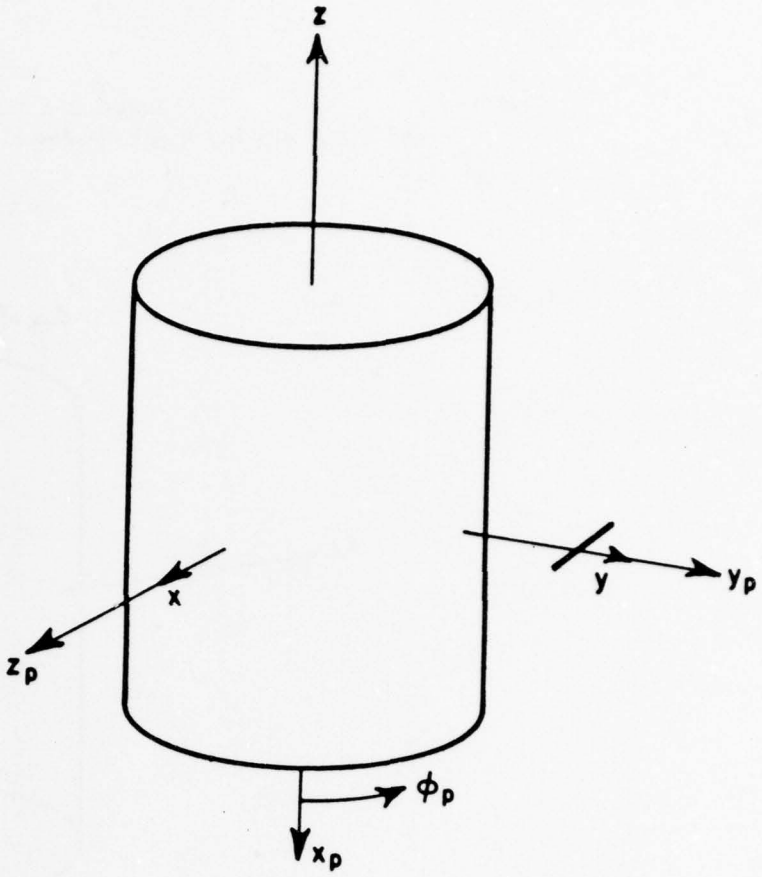

Figure 4b. An electric dipole in the presence of a finite circular cylinder (pattern taken in y-z plane).

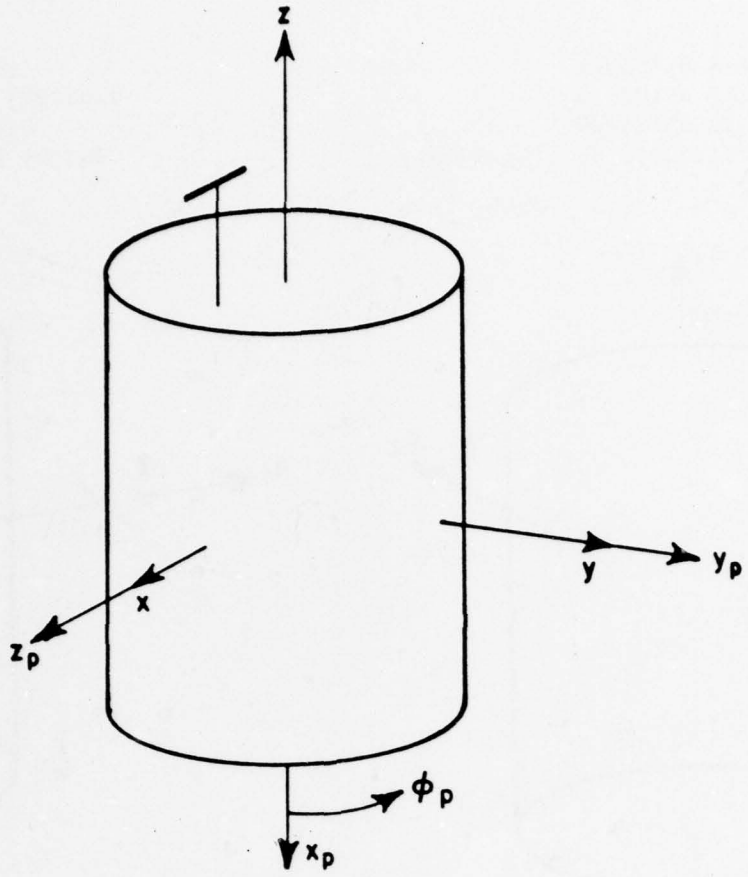

Figure 4c. An electric dipole in the presence of a finite circular cylinder (pattern in the y-z plane).

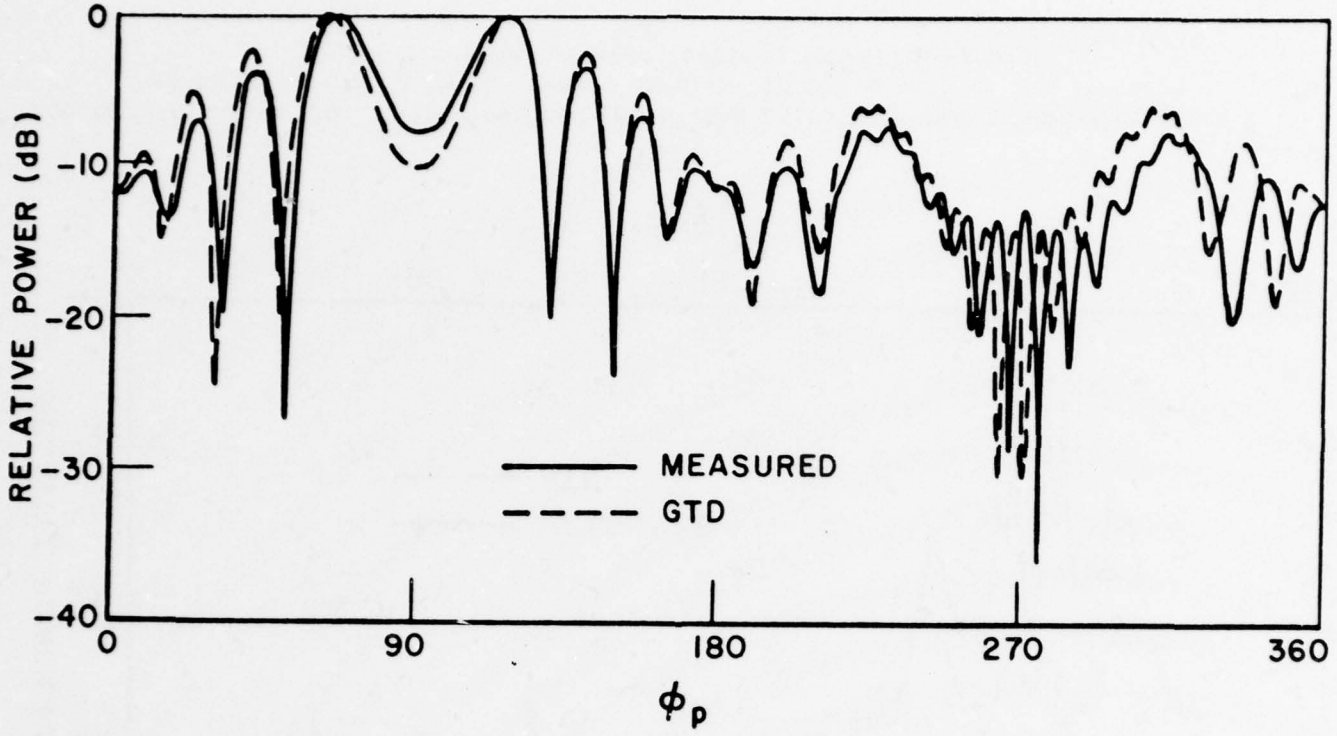

Figure 5a. Comparison of the measured (Bach) and calculated radiation pattern for E_{ϕ_p} of an electric dipole on the y-axis parallel to the x-axis in the presence of a finite circular cylinder (pattern taken in x-y plane).

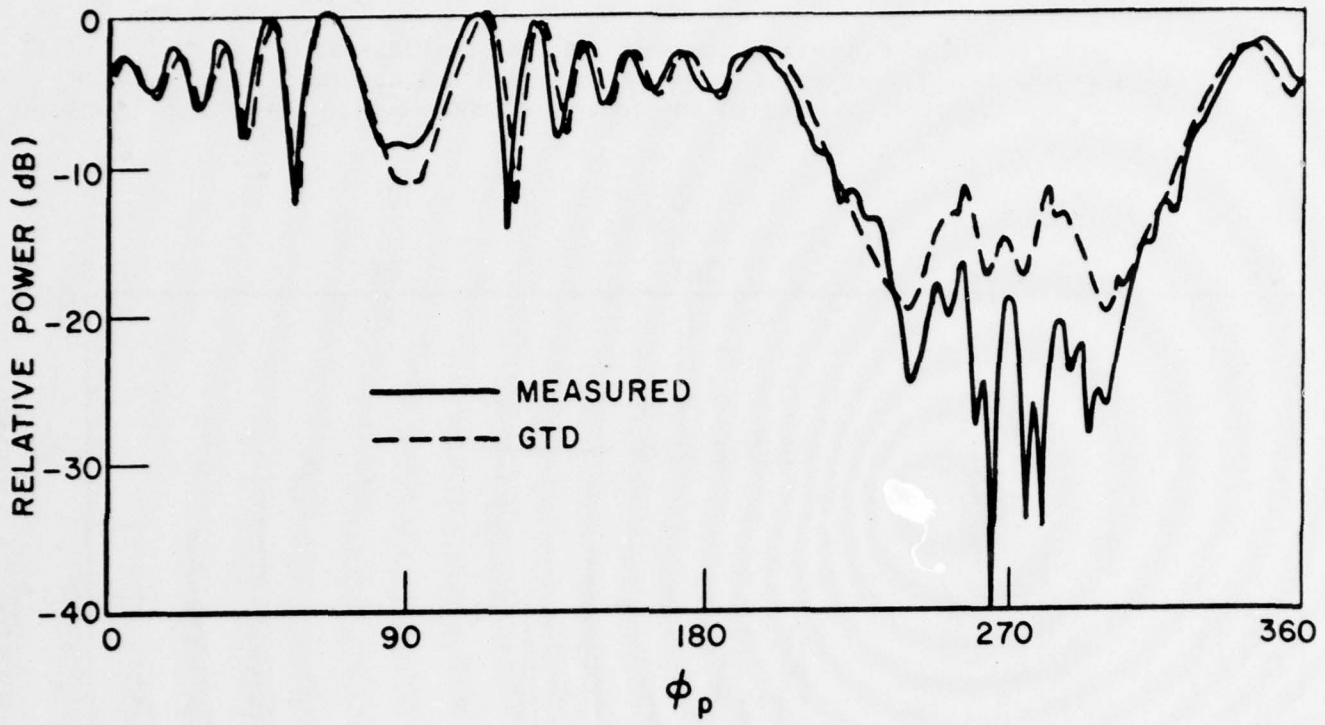

Figure 5b. Comparison of the measured (Bach) and calculated radiation pattern for E_{θ_p} of an electric dipole on the y-axis parallel to the x-axis in the presence of a finite circular cylinder (pattern taken in y-z plane).

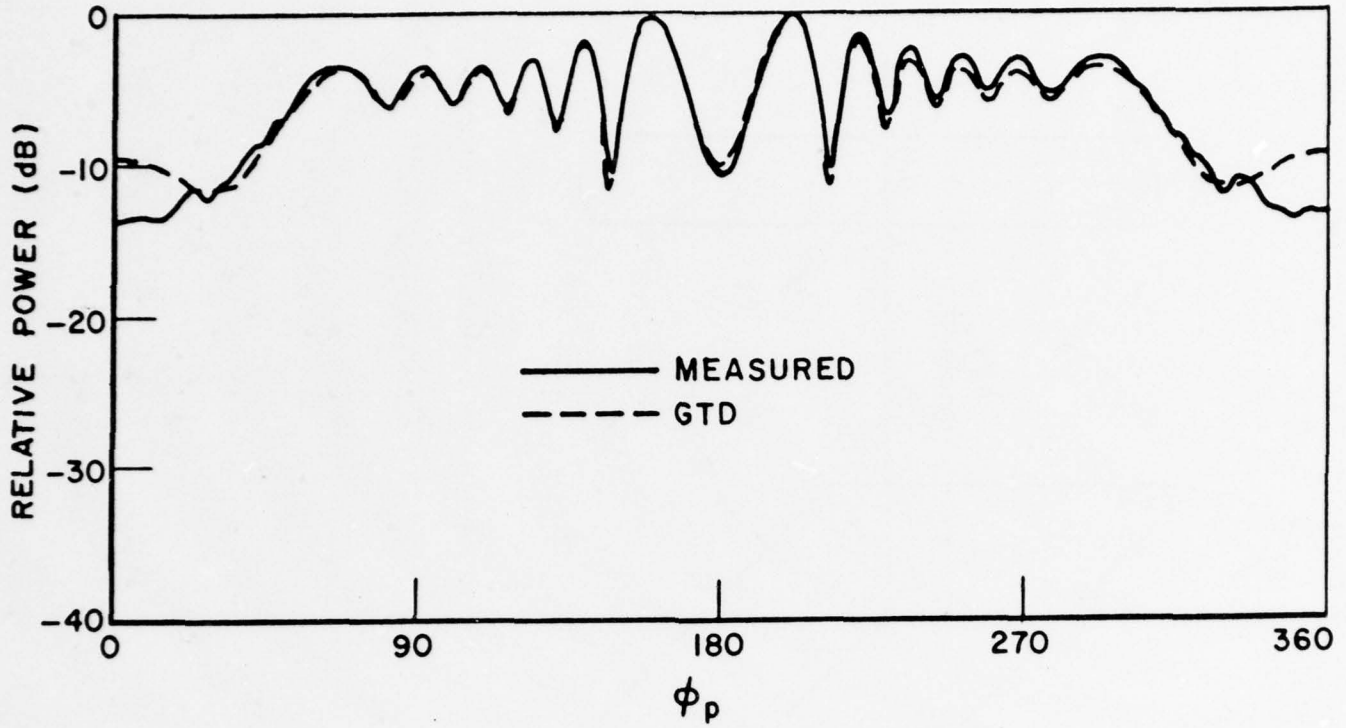

Figure 5c. Comparison of the measured (Bach) and calculated radiation pattern for E_{θ_p} of an electric dipole in the x-z plane parallel to the x-axis in the presence of a finite circular cylinder (pattern taken in the y-z plane).

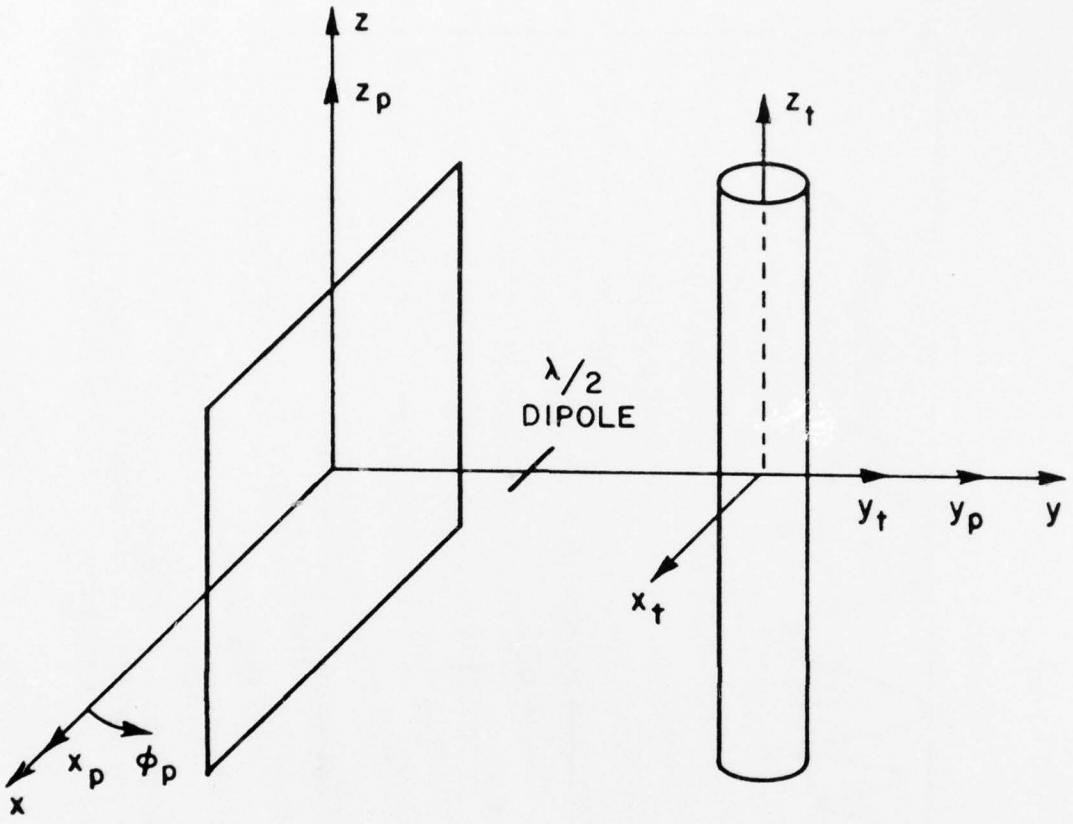

Figure 6. A λ/2 dipole in the presence of a square plate.

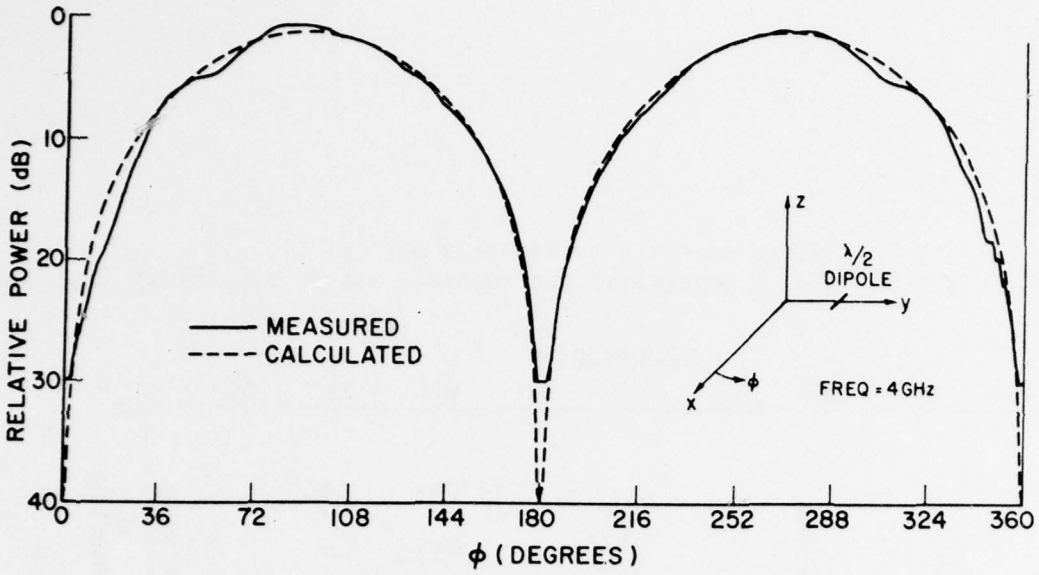

Figure 7a. Comparison of the measured and calculated E_ϕ radiation pattern of a $\lambda/2$ dipole.

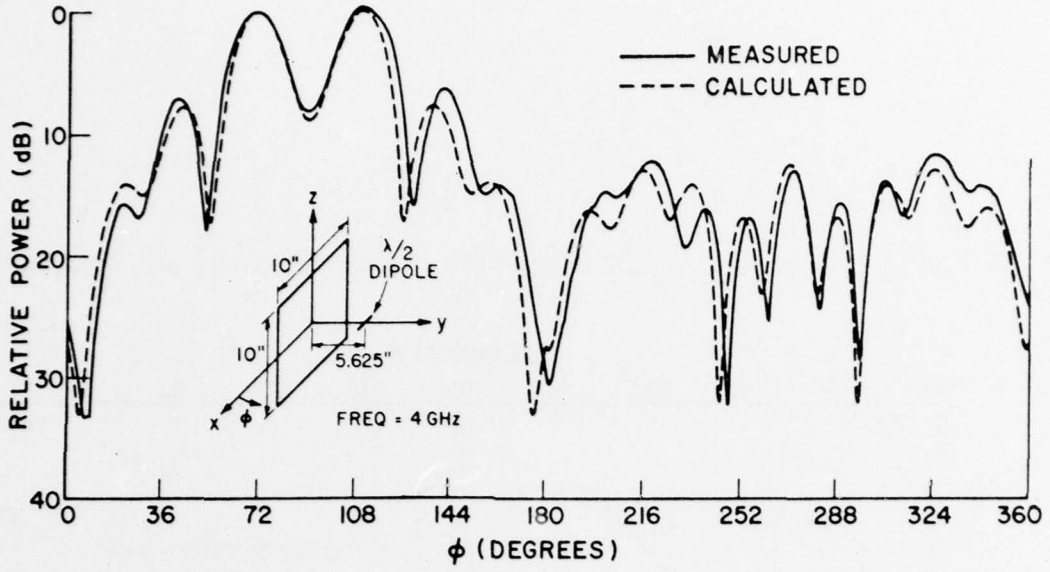

Figure 7b. Comparison of the measured and calculated E_ϕ radiation pattern of a dipole in the presence of a square plate.

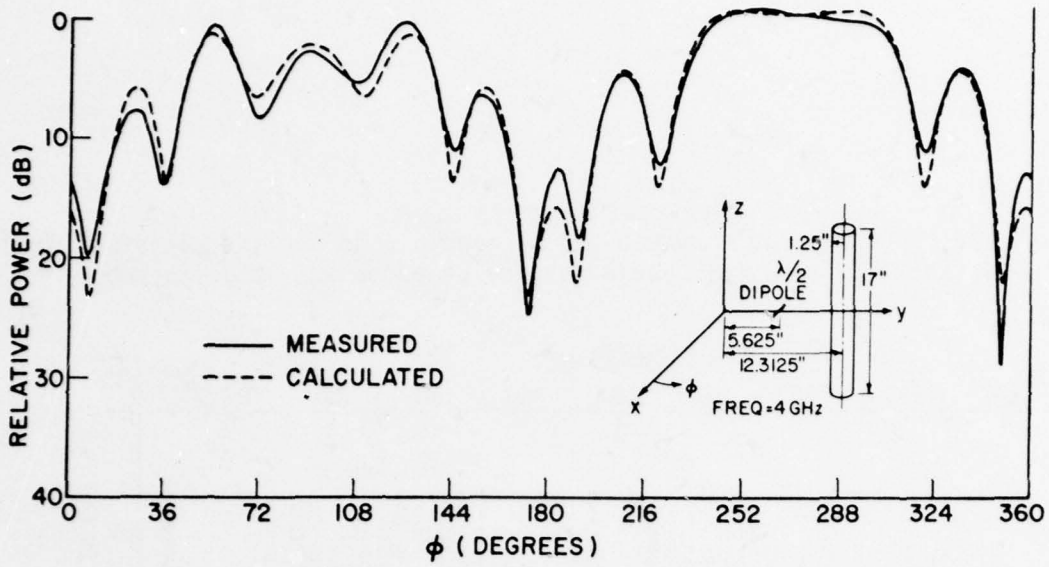

Figure 7c. Comparison of the measured and calculated E_ϕ radiation pattern of a dipole in the presence of a finite circular cylinder.

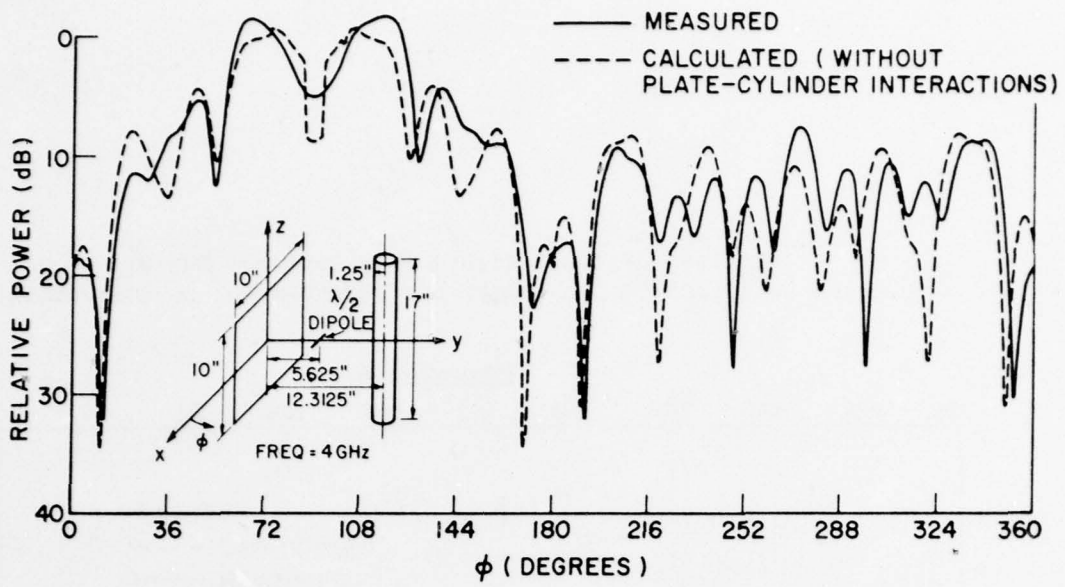

Figure 7d. Comparison of the measured and calculated (without plate-cylinder interactions) E_ϕ radiation pattern of a dipole in the presence of a square plate and a finite circular cylinder.

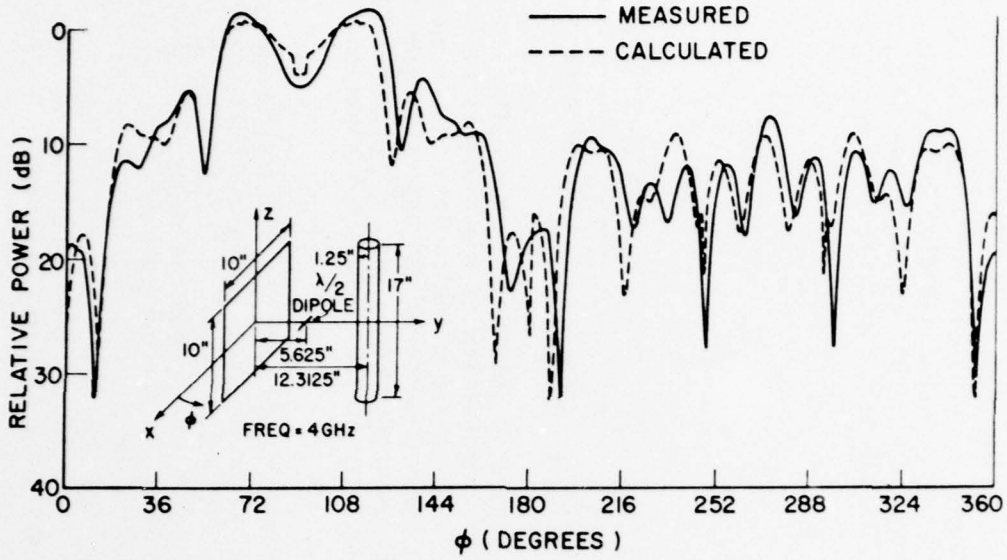

Figure 7e. Comparison of the measured and calculated (with plate-cylinder interactions) E_ϕ radiation pattern of a dipole in the presence of a square plate and a finite circular cylinder.

in Figure 7e. This result contains five plate-cylinder interaction fields as is listed above. It can be noted that the levels are better and that the fine details have the right trends. The plate-cylinder interations are still being improved and more tests are being made on different varieties of shapes to see if the code is functioning properly. However, the results in Figure 7e indicate that the third generation code is giving good results for engineering purposes.

In all of the examples above the scattering code uses an analytic representation for the antenna. The antenna presently considered in the computer code is an electric or magnetic radiator with a cosine distribution, arbitrary length and width, arbitrary magnitude and phase, and arbitrary orientation. This antenna is specified as follows for an electric source

$$I(z') = I_m \cos\left(\frac{\pi z'}{\ell}\right)$$

$$E_{\theta'} = \frac{j\eta_0}{2\pi} I_m \frac{\sin\theta' \left(\frac{\pi}{k\ell}\right) \cos\left(\frac{k\ell}{2} \cos\theta'\right)}{\left(\frac{\pi}{k\ell}\right)^2 - \cos^2\theta'} \frac{w \sin\left(k\frac{\omega}{2}\sin\theta'\cos\phi'\right)}{k\frac{\omega}{2}\sin\theta'\cos\phi'} \frac{e^{-jkr'}}{r'}$$

The result for a magnetic source is obtained using duality. Any arbitrary antenna can be simulated by superposition of the elements by making the length ℓ small ($\ell \approx 0.1\lambda$), spacing the elements less than a quarter wavelength, and then weighting their magnitudes and phases to simulate the current distribution of the desired antenna [9]. Since the radiation pattern is relatively insensitive to the current distribution this method works very well.

The NEC code is also interfaced with the GTD scattering code. This allows complicated antennas to be analyzed using the best features of the moment methods to find the antenna's impedance characteristics and current distribution. Then the GTD scattering code can be used to calculate the radiation pattern of the antenna in the presence of large scattering structures. At present, the scattering code is written to use only the wire segment capabilities of the NEC code and not the patch segments. The NEC currents are assumed to be the value of the current at the center of a segment that is approximately 0.15λ or less in length. The field [10] of an individual segment is set to

$$E_{\theta'} = \frac{j\eta_0 k\ell}{4\pi} I_m \sin\theta' \frac{e^{-jkr'}}{r'}$$

which gives consistent results with the NEC code. The scattering code is normalized in the far field to exp(-jkR)/R unless otherwise specified. The fields are output in volts/meter, however, it should be noted that unless a range R is defined the units are actually volts. The directive gain is also calculated by using the power radiated as supplied by the NEC code.

The interfacing of the NEC and GTD codes has been tested by using two examples obtained from Mr. Jim Logan at NOSC. Both examples are composed of antennas that were modeled by wire segments over a perfectly-conducting infinite ground plane. Using the assumption that the current distributions obtained in this way will not be perturbed appreciably by slightly changing the environment, the currents from the NEC code can be used to simulate the radiation pattern for the antennas mounted over a finite plate which is over an infinite ground plane as shown in Figure 8.

To test the compatibility of the current distribution used in the GTD code with the current weights obtained from the NEC code, the GTD code was used to calculate the field for the example problem of four quarter-wavelength dipoles. The locations of the four dipoles are illustrated in Figure 8 as the four solid lines parallel to the x-axis. The infinite ground plane is coincident with the square plate for this first test. The dipoles were divided into a total of 20 segments. The fields obtained from this calculation resulted in a directive gain within 0.2 dB of the NEC result as shown in Figures 9a and b for the plane $\phi=0^{o}$ and $\phi=90^{o}$, respectively.

The GTD code was next used to show how the directive gain changes when the four dipoles are placed over a square plate over a ground plane as shown in Figure 8. The comparisons between the infinite ground plane and square plate cases are shown in Figures 10a and 10b for the two pattern planes.

The second example is composed of four sets of crossed dipoles as shown in Figure 8 where solid and dashed lines are used to represent the crossed dipoles. The results obtained from NOSC for this example were obtained from an AMP code print out rather than an NEC code print out; however, the results are still useful for comparison purposes. The GTD and AMP results for 48 segment dipoles over an infinite ground plane are compared in Figures 11a and 11b, where Figure 11a shows the vertical component and Figure 11b the horizontal component. The solid curves represent the GTD code result and the X's show the AMP result. Again the two results compare within 0.2 dB. Square plate results are also shown in Figures 11a and 11b. Directive gains for the infinite ground plane and square plate cases are compared in Figures 12a and 12b for the $\phi=0^{o}$ and $\phi=45^{o}$ planes, respectively. The two examples confirm that the GTD and NEC code are compatible.

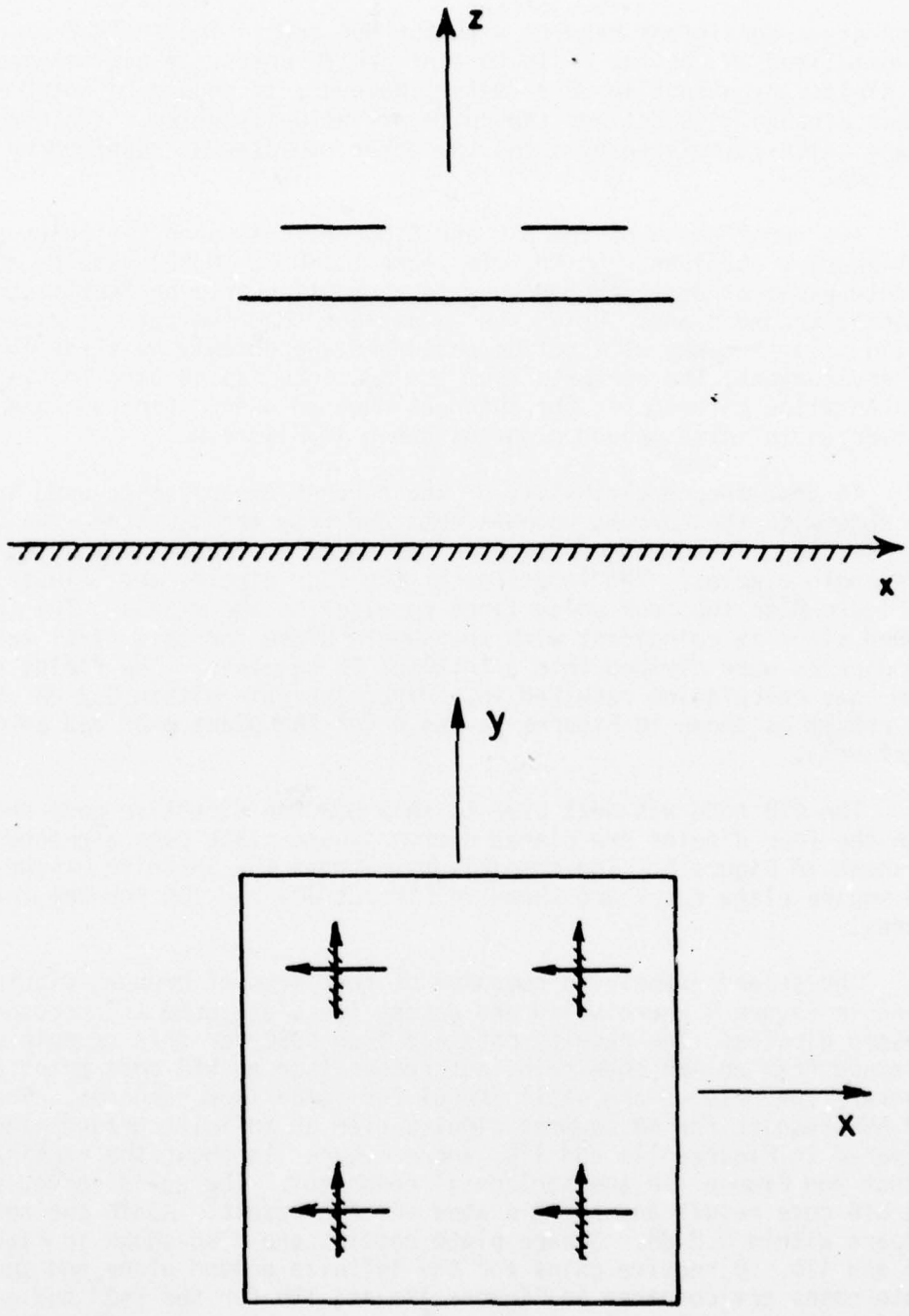

Figure 8. Geometry for the problems of dipoles over a square plate and infinite ground plane showing the side and top views.

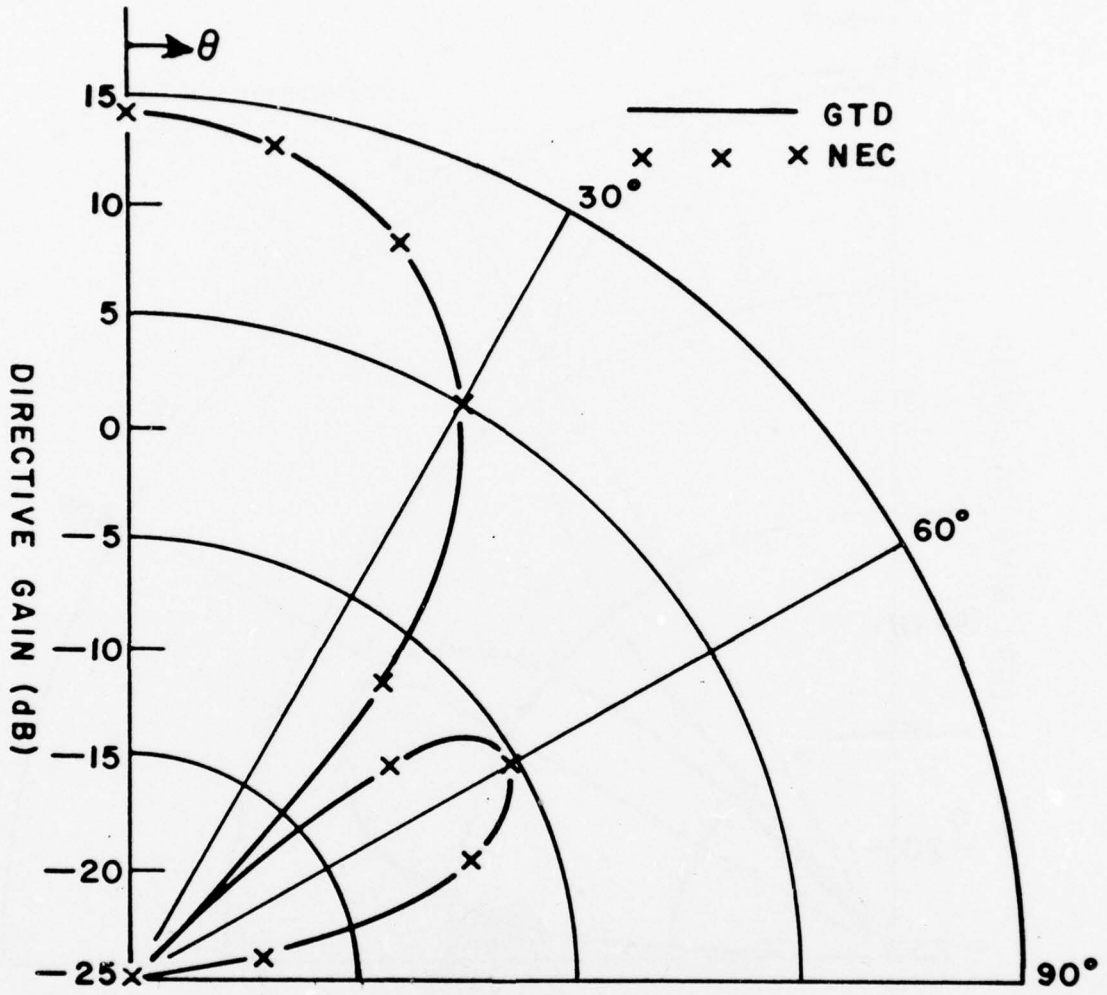

Figure 9a. Comparison of the directive gain of four dipoles over an infinite ground plane obtained from the NEC code and from the GTD code using the NEC currents ($\phi=0^{o}$ vertical polarization).

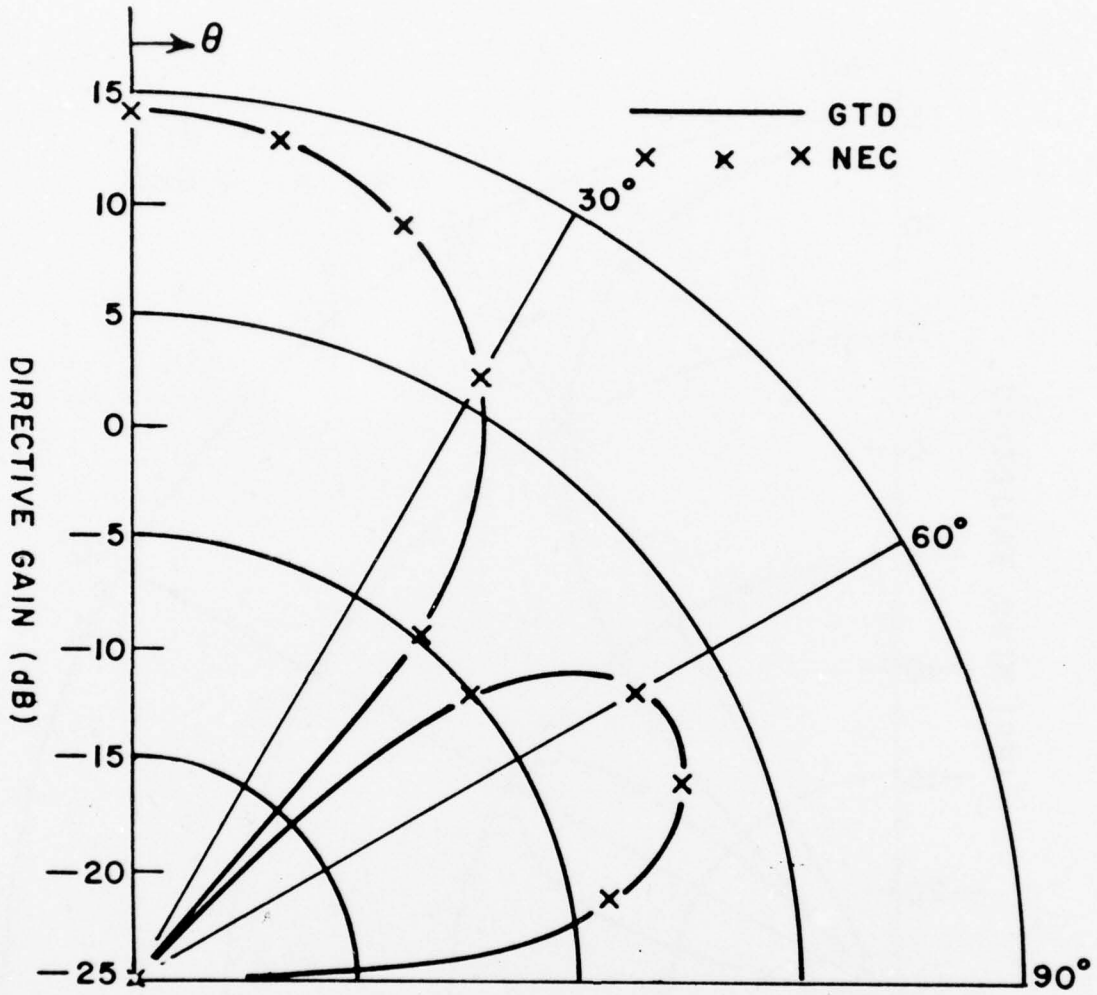

Figure 9b. Comparison of the directive gain of four dipoles over an infinite ground plane obtained from the NEC code and from the GTD code using the NEC currents ($\phi = 90^{\circ}$ horizontal polarization).

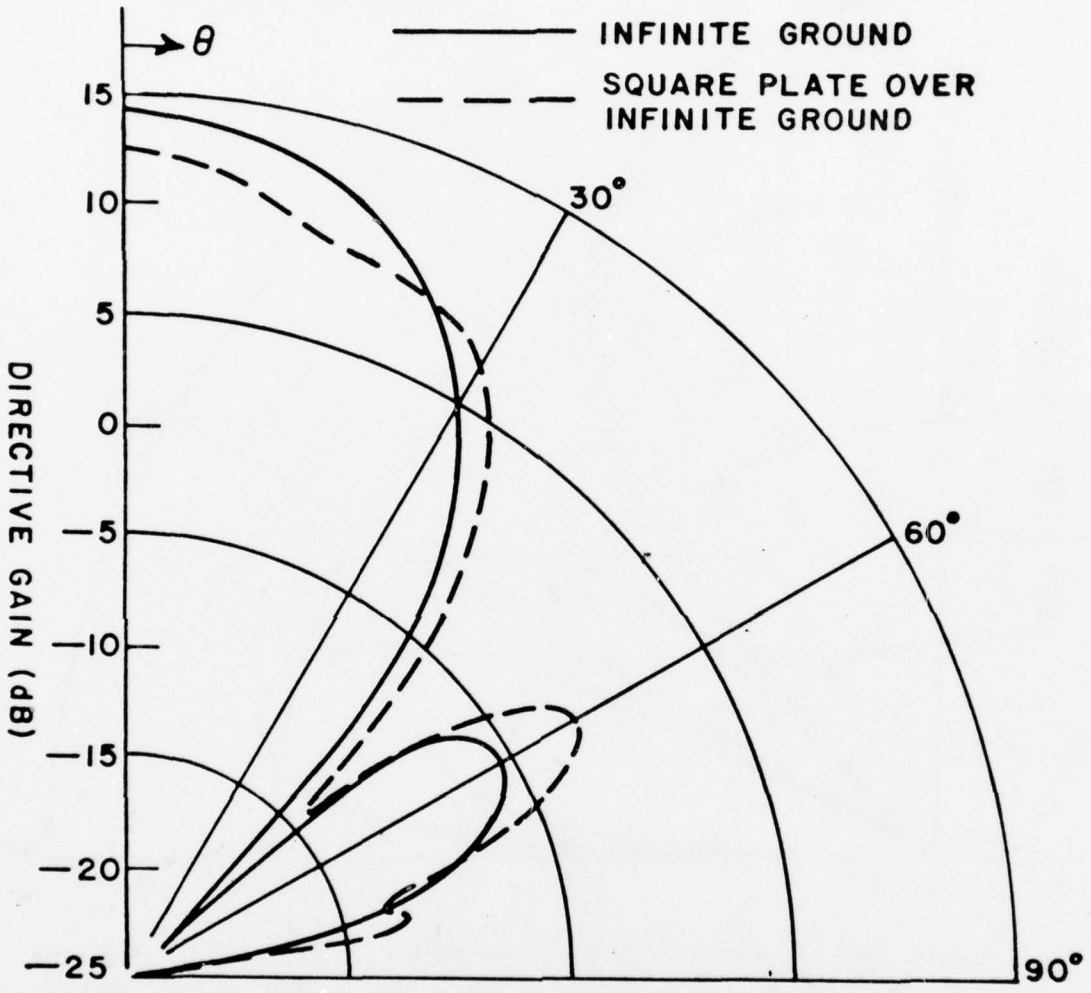

Figure 10a. Comparison of the directive gain of four dipoles over an infinite ground with four dipoles over a square plate over a square plate over an infinite ground plane ($\phi = 0^{0}$, vertical polarization).

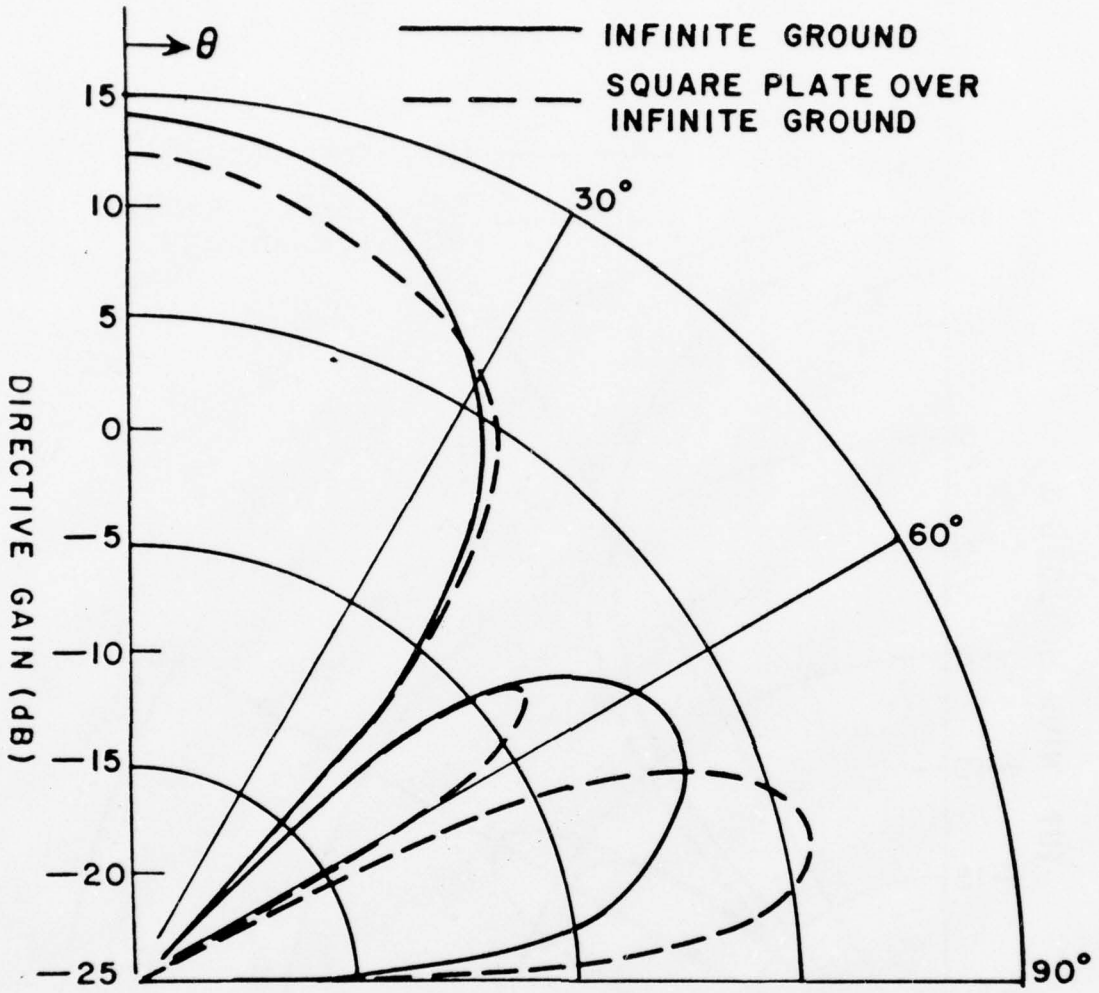

Figure 10b. Comparison of the directive gain of four dipoles over an infinite ground with four dipoles over a square plate over an infinite ground plane ($\phi=90^0$, horizontal polarization).

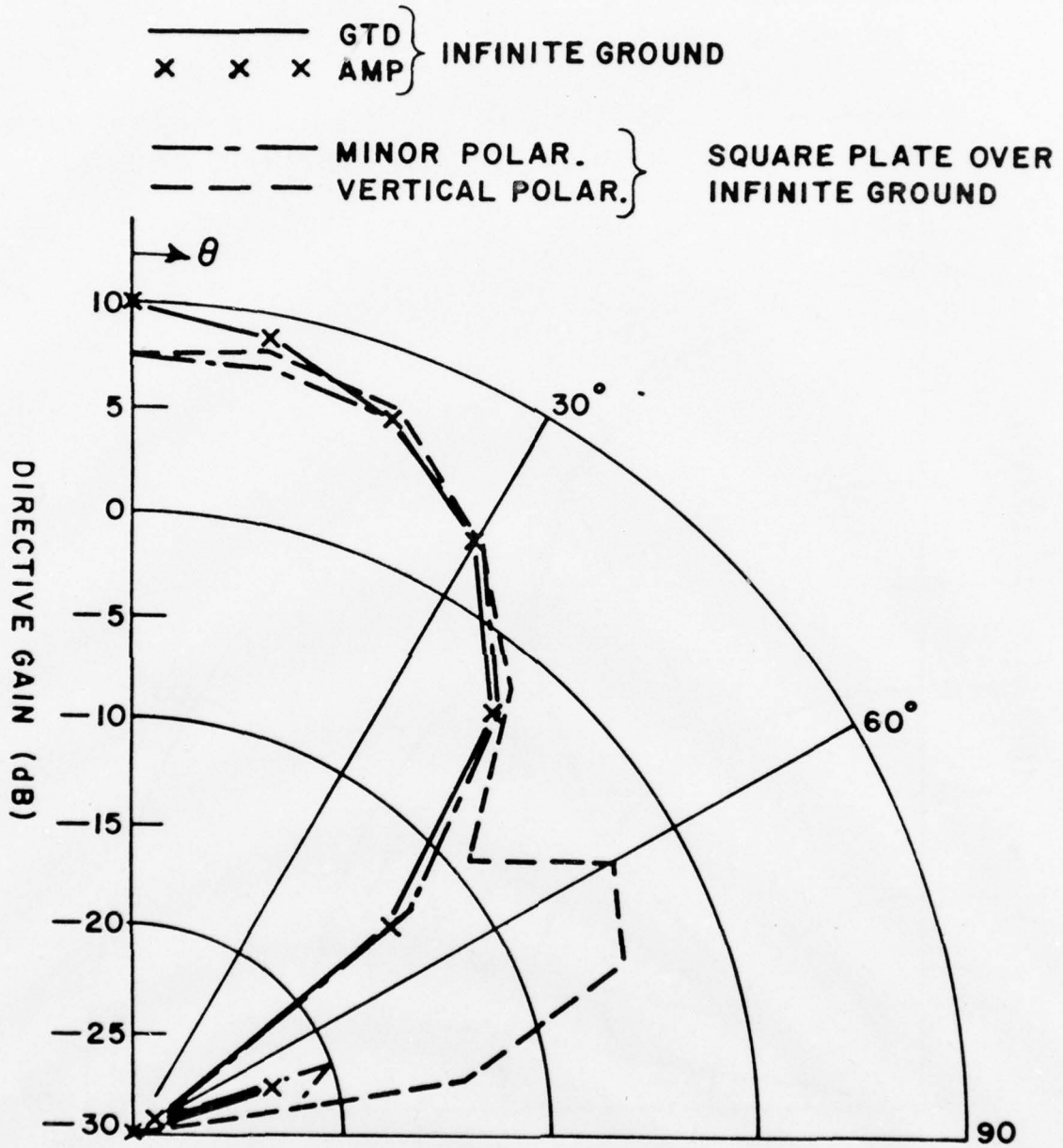

Figure 11a. Comparison of the directive gain of four sets of crossed dipoles over an infinite ground and over a square plate over an infinite ground ($\phi=0^{o}$, vertical polarization).

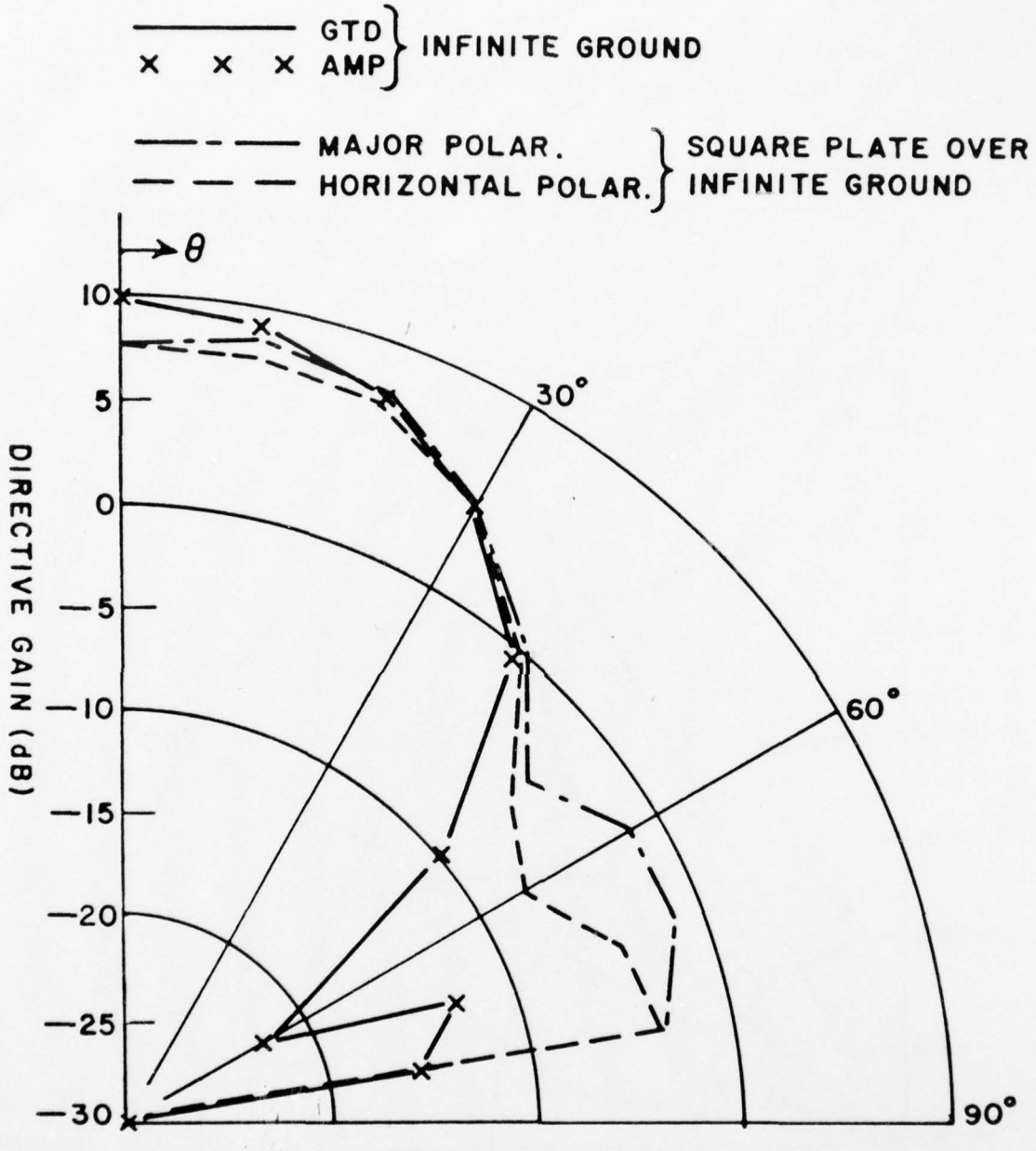

Figure 11b. Comparison of the directive gain of four sets of crossed dipoles over an infinite ground and over a square plate over an infinite ground ($\phi=0^{o}$, horizontal polarization).

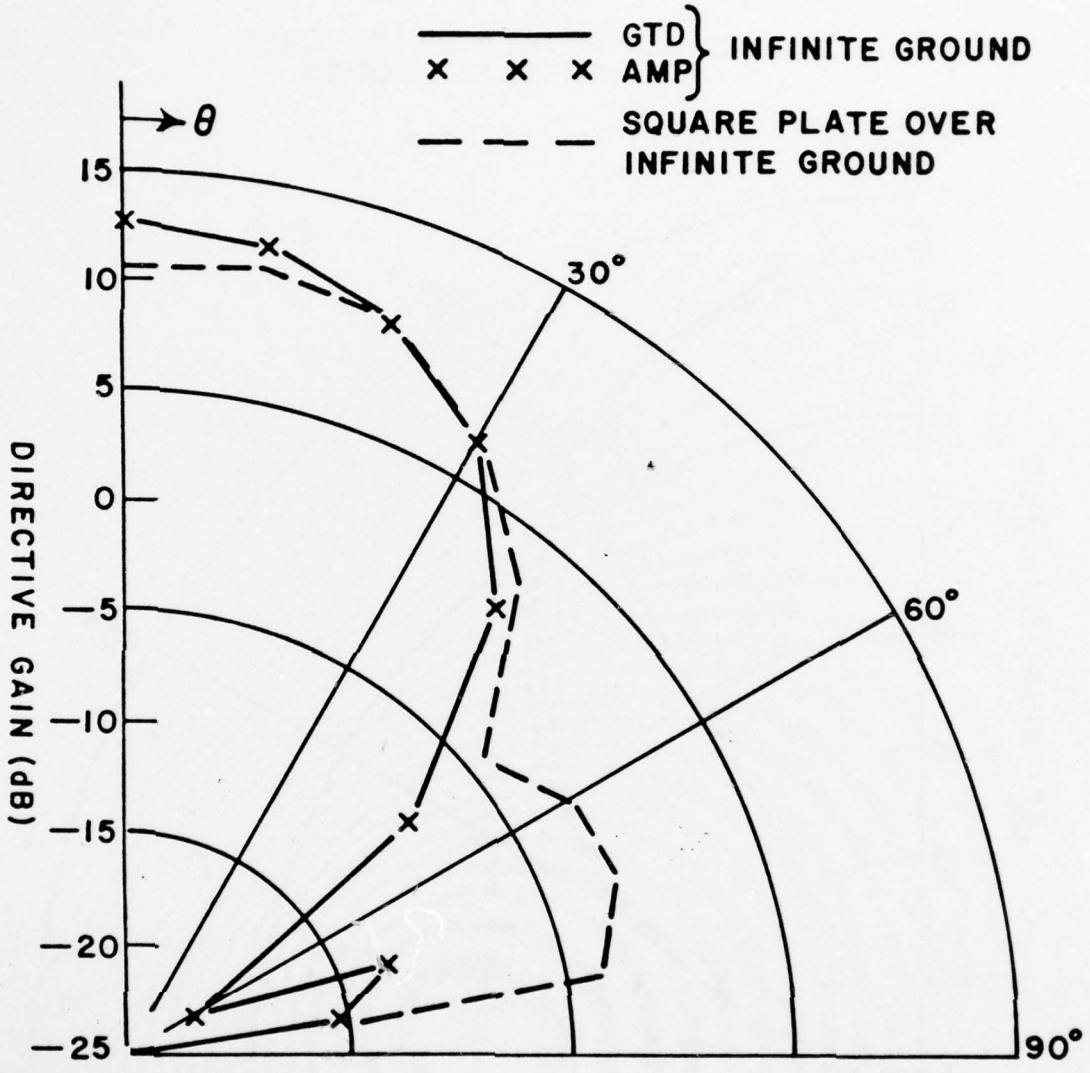

Figure 12a. Comparison of the total directive gain of four sets of crossed dipoles over an infinite ground and over a square plate over an infinite ground ($\phi=0^{0}$).

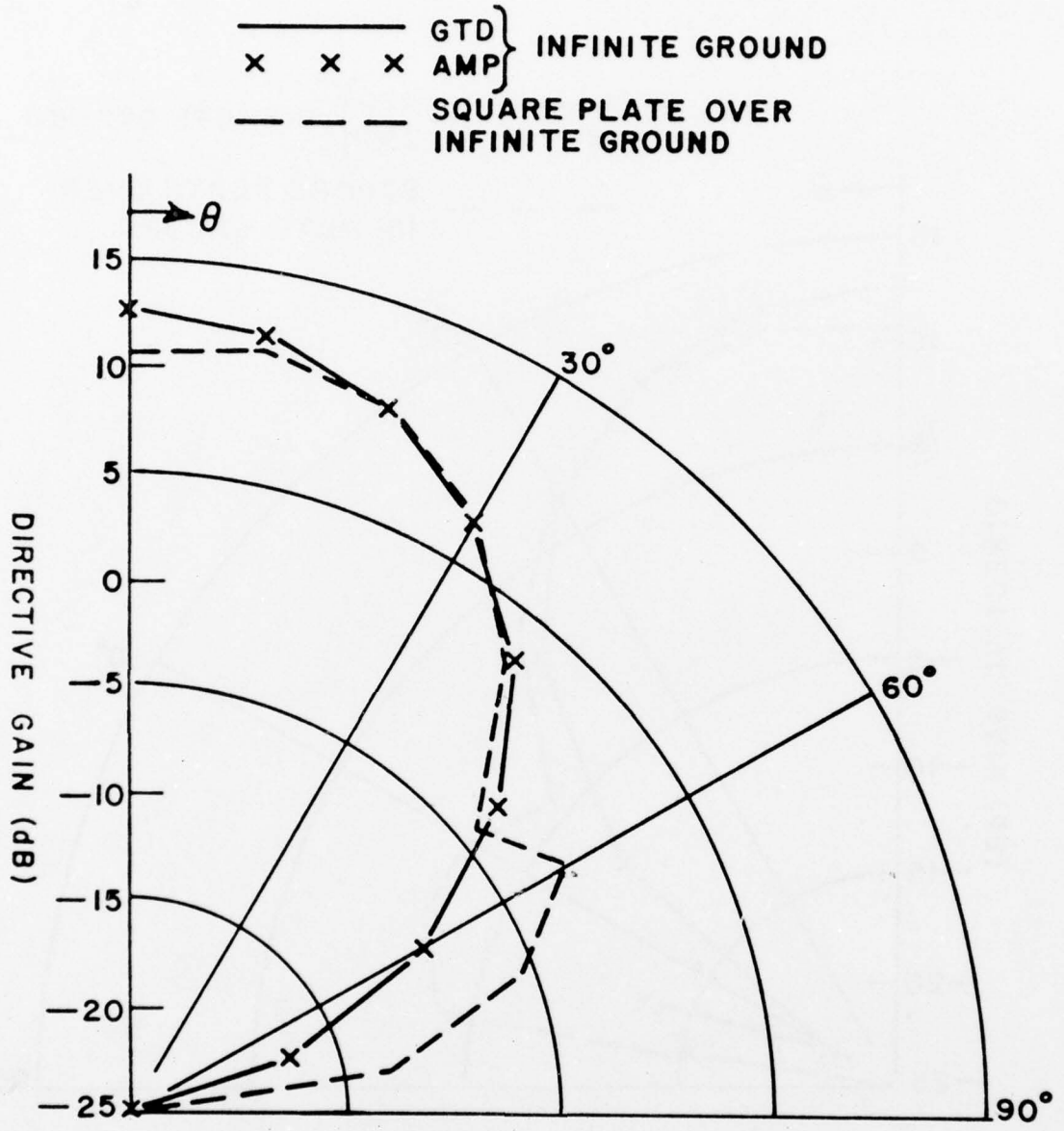

Figure 12b. Comparison of the total directive gain of four sets of crossed dipoles over an infinite ground and over a square plate over an infinite ground (ϕ=45°).

The main disadvantage of using the NEC currents in the scattering code is the time required to compute the results. At present, the time for one pattern computation increases by a linear factor of the number of NEC segments specified. In the next year, ways of increasing the efficiency of this process will be studied. A more useful source representation capability will be implemented. The inclusion of a width to the source representation is a step in this direction. It is hoped that this will be compatible with the patch segments of the NEC code. Also, a study will be made of summing up the incident fields from each of the source dipole elements so that the diffraction calculations need not be made for each individual dipole. The effect of a group of dipole sources will, thus, be more efficiently computed.

In the next contract year the third generation of the scattering code will be completed along with a user's manual. The code will be delivered to NOSC by October 31, 1978. A code manual, which has already been started, will be written giving details of all the individual subroutines in the scattering code. Also, as mentioned above, a more useful source representation will be studied and included in the code when it is completed.

The scattering code has been much in demand over the past year and has been sent to many agencies. Because of its versatility it can be used to simulate numerous antenna pattern distortion effects. The following is a partial list of how the first generation code has been used and by whom:

- Westinghouse (baltimore, Maryland) is using the code to analyze the scattering effects of a radar (search and track) mounted on a tank.

- Electronic Communications Inc. (St. Petersburg, Florida) is using the code to determine the optimum location for various antennas mounted on and around a communication van.

- Naval Research Laboratory (Washington, D.C.) is using the code to locate antennas on an F-14 aircraft.

The second generation code has been or is in the process of being sent to the following:

- Martin Marietta Corp. (Denver, Colorado)
- Atlantic Research Corp. (Rome, New York)

IV. REFLECTOR ANTENNA CODE DEVELOPMENT

The task of the reflector antenna code development is to develop user-oriented computer program packages by which the fields of typical Navy reflector antennas can be calculated. These codes are being developed as part of a larger effort to develop computer models for simulating antennas at UHF and above frequencies in a complex ship environment.

The first task under the reflector antenna code development was to develop the computer program package for calculating far field patterns. Feed blockage and scattering effects were not included in this phase. These will be included later (see Table I). The second task of this effort is the development of a second generation computer code by which the near fields of a typical Navy reflector can also be calculated. The second generation reflector code, capable of both near field and far field computations, will be completed in the near future and is scheduled for delivery at the end of the next quarter as seen in Table I.

These computer program packages are designed to have the flexibility to compute the fields of most reflector antennas. One important feature of the codes is their capability for a general reflector rim shape. Another important feature is their capability to input a practically arbitrary volumetric feed pattern.

Since the majority of Navy reflector antennas have parabolic surfaces, only the class of parabolic surfaces are implemented in the computer codes. The geometry of the reflector rim is treated as piece-wise linear. The codes are flexible enough to include general reflector rim shapes such as elliptical and rectangular with chopped corners.

The theoretical approach for computing the far field pattern of the general reflector is based on a combination of the Geometrical Theory of Diffraction (GTD) and Aperture Integration (AI) techniques. AI is used to compute the main beam and near sidelobes; GTD is used to compute the wide-angle sidelobes and the backlobes. To implement the computer algorithms based on these theories, efficient ways were developed to handle calculations involving the feed pattern, the aperture field and the far field pattern computation.

The development of the first generation reflector code for far field patterns was completed and delivered to NOSC in February. A user's manual [11] has been published for the first generation code. Further testing was done on the far field code and its accuracy has been verified by comparisons with independent pattern data. The results of these comparisons are given later in this report.

A. Feed Patterns

Sampled data from each measured feed pattern cut is input and stored in the code. Linear interpolation is then used to obtain a piece-wise linear representation of the input pattern cut. The feed patterns in planes other than those corresponding to the input pattern cuts also are calculated by linear interpolation. This method provides a computationally efficient way of calculating the aperture fields and feed spillover radiation without requiring large amounts of computer storage for the measured feed pattern. Only relatively few data points need to be stored for essentially complete feed pattern information. Furthermore, the piece-wise

linear method has the advantages of flexibility and simplicity for general feed patterns. No cut-and-try procedures are needed; the sample feed values can be obtained directly from measured feed pattern data.

An option has been added to the second generation reflector code, currently under development, for convenience in specifying the feed patterns for offset-fed reflector antennas. Part of the logic for the offset feed pattern was built into the first generation code; but some minor additions were necessary to run the offset feed option. This option enables the user to specify the patterns of the feed in the coordinate system of the tilted feed horn axis. The code then automatically transforms the feed patterns to the coordinate system of the reflector. This feature simplifies the input of data for a symmetrical feed horn in an offset-fed reflector.

Several subroutines have been developed to treat a feed with a general pattern and general polarization. These subroutines decompose the feed radiation into components to provide the necessary information for the following: 1) aperture fields, 2) GTD edge illuminations, and 3) direct feed radiation. Detailed equations for the feed patterns are given in the Seventh Quarterly Report [12].

The far field reflector code uses either a piece-wise linear feed pattern, or the analytic functions described below. For sum patterns the analytic function is given by

$$F_{\Sigma}(\psi) = \frac{e^{-A\left(\frac{\psi}{\psi_0}\right)^2} \cos^N\left(\frac{\pi\psi}{2\psi_0}\right) + C}{1 + C} \qquad (1)$$

where the constants A, ψ_0 and C can be controlled for each input pattern cut ϕ_n. The pattern value in Equation (1) is normalized such that $F_{\Sigma}(0) \equiv 1$ for all ϕ-plane cuts. The constants A, C and N control the shape of the pattern. The constant ψ_0 permits a given pattern shape to be stretched or compressed. For difference feed patterns the analytic function is given by

$$f_{\Delta}(\psi) = C\, e^{-A\left(\frac{\psi}{\psi_0}\right)^2} \sin^N\left(\frac{\pi\psi}{2\psi_0}\right) \qquad (2)$$

B. Reflector Geometry and Aperture Integration

The reflector rim geometry is specified by the X- and Y-coordinates of each junction point on the rim. Thus the projection of the reflector rim onto the aperture plane is specified as piece-wise linear. The rim points P_k are numbered in a counter-clockwise sequence. A typical reflector rim shape with eight rim points is shown in Figure 13a. A rectangular

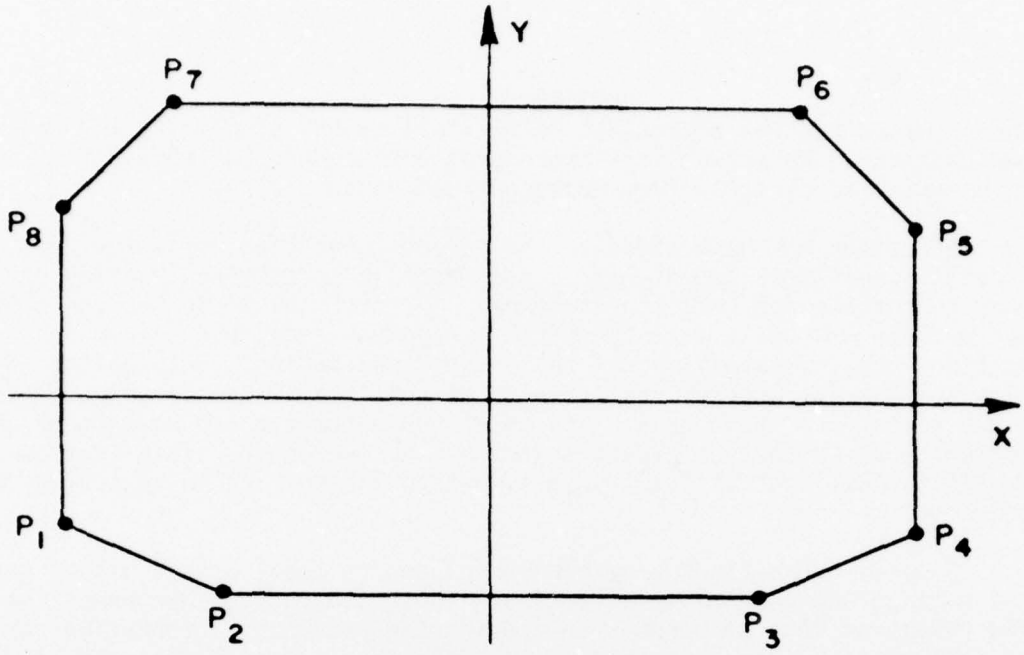

(a)

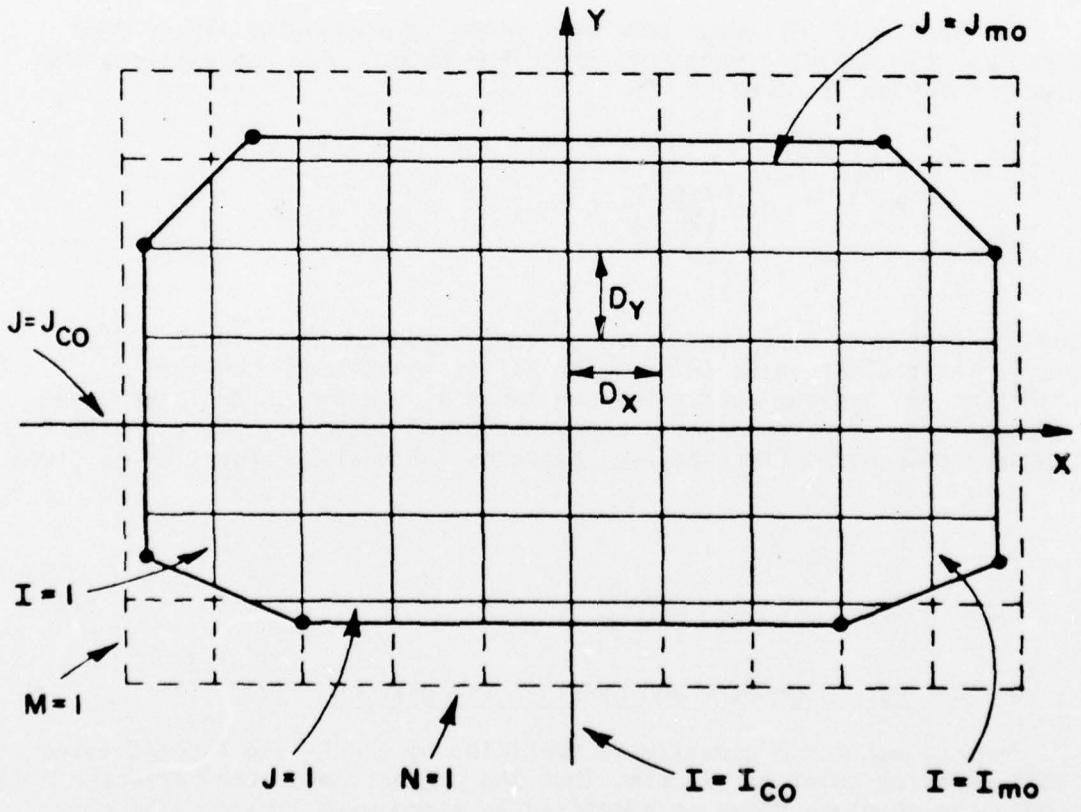

(b)

Figure 13. Reflector rim geometry and principal rectangular grid.

grid size (D_x and D_y) is then chosen so that the aperture can be divided into a principal rectangular grid as shown in Figure 13b.

The aperture fields are calculated and stored on the principal grid for use in the aperture integration. The principal grid values are used for all output pattern cuts. The aperture fields are calculated at points off the principal grid by using linear interpolation from the principal grid. This is more efficient than calculating the aperture fields from the feed pattern for each rotated grid that is used for off-principal plane cuts.

The rotating grid method described in Reference [13] is used for the aperture integration. This method provides good efficiency because it combines several features. One feature is the use of overlapping sub-apertures which allows a piece-wise linear representation for the aperture distribution. Thus variations in the aperture fields can be represented with relatively few subapertures. Furthermore, the subapertures can be electrically large; thus minimizing the computer storage and also the amount of numerical integration required. Another feature of the rotating grid method is that the y-integrations are carried out for each column of the aperture and each one-dimensional integration result is stored. The stored values for the y-integration are then used for each pattern angle in the plane perpendicular to the y-axis; thus the efficiency approaches that of a one-dimensional integration. Even though the integration grid must be rotated to obtain the pattern in other planes, the required grid rotation is computationally much faster than the numerous two-dimensional integrations that would otherwise be required.

C. GTD

The rotating grid method is used to calculate the far field pattern in the main beam and near sidelobe region. The GTD is used to calculate the wide-angle sidelobe and backlobe regions for the reflector antenna computer code. Advantage was taken of the existing GTD computer subroutines used in the basic scattering code. The GTD analysis of the reflector is similar to that of diffraction by a flat plate [5], except that the curvature of the reflector surface must be taken into account. It was found that the reflector rim must be subdivided into nearly straight segments. A suitable criterion is that each segment of the reflector rim be small enough that the focus lies in the far field of the rim segment.

The GTD method used in the reflector code increments around the rim and determines whether a diffraction occurs for each linear rim segment. This is done by comparing the diffraction angle with the bounds on the permissible range of angles. If no diffraction occurs for that segment the code checks the next rim segment. If a diffraction does occur, the diffraction point and the vector for the incident ray from the feed are calculated. This procedure is the same as that used for the flat plate scattering code except that the geometry information associated with the parabolic reflector surface is changed.

Each diffracted field contribution is first calculated in components perpendicular and parallel to the specific rim segment. The perpendicular and parallel field components, $E_\perp$ and $E_\parallel$, are then transformed to E_θ and E_ϕ components in the reflector coordinate system, so that the diffracted field contributions can be summed for all rim segments. This process of calculating and summing the diffracted fields for all the rim segments is repeated for all GTD pattern angles.

Most of the far field pattern calculations are performed in terms of the E_θ and E_ϕ components; but are then converted to principal and cross polarized components for the output pattern. A Huygen's source representation is used as a reference for the principal and cross polarizations[14].

D. Summary of Computer Code

The reflector code for far field pattern computations requires approximately 125 Kbytes of storage. Typical CPU times are less than 1 second per pattern angle on the ElectroScience Laboratory Datacraft computer. For example, the patterns in Figure 17 require about 300 seconds each of CPU time to give a printout for 361 pattern values ($\Delta\theta=0.5^0$). The corresponding CPU time for Figure 23 is about 210 seconds. The code is expected to run 3 to 5 times faster on machines comparable to a CDC-6600.

The capabilities of the code may be summarized as follows:

1. A general reflector rim shape may be used (piece-wise linear).

2. The required input data for the feed pattern is minimized by piece-wise linear pattern fitting.

3. Storage and computation time of aperture data for AI is minimized by using a principal rectangular grid and interpolation of the aperture field.

4. The efficiency of the far field pattern computation is maximized by the use of GTD for wide pattern angles and the use of the rotating grid method for near-axis angles (main beam region).

5. The feed may be linearly polarized with any orientation or circularly polarized.

The GTD and AI approaches used for the code have a basic limitation on the minimum size reflector that can be modeled. This limitation is probably on the order of 1λ to 3λ for the reflector diameter. However, virtually all practical reflector antennas exceed 3λ diameter. There is no basic limitation on the maximum size of the reflector for the basic analysis. In the code, the reflector surface is assumed to be a perfect paraboloid. Thus, an actual reflector antenna must have sufficiently good tolerances, especially at high frequencies, so that it can be accurately modeled by the code.

The practical limitations on this version of the code can be summarized as follows:

1. The feed must be located at the focus and have a constant phase pattern.

2. The reflector surface must be paraboloidal.

3. Strut scattering effects are not included.

4. The grid size used for aperture integration must be chosen sufficiently small to give a good representation of the aperture field distribution.

5. Array variables associated with the rim data, the principal grid and the feed pattern must be given sufficient dimensions for the required input data.

Several statements are included in the code to print out a warning message if the declared dimension is exceeded for certain array variables. This has been done for the variables mentioned in item 5 above.

A block diagram of the main program is shown in Table IV. A command word system is used to input data into the code. By this method additional computer runs can be made by making small changes in the input data. As seen in Table IV the code can be run by using default data stored in the code (NX: Command). This is useful for initial testing of the code. Also, the default data can be changed as desired by the user to represent a commonly used reflector antenna. Various test options (TO: Command) are available for testing and debugging the code. The input patterns of the feed antenna are specified by the desired number of ϕ-pattern cuts. The input pattern data is controlled by the FD: Command. The feed pattern may be specified either by sample feed data points or as analytic functions. The reflector geometry and dimensions are specified by the DG: Command. The rectangular grid size to be used for aperture integration is also specified by the DG: Command. A do loop for operating frequency was included so that the code could be run for different frequencies without changing any other input data by using the FO: Command. This is useful if the feed pattern can be assumed not to change with frequency. If the feed pattern changes with frequency the feed command (FD:) must be used before the code is executed at each new frequency. The ϕ-planes desired for the output pattern cuts are controlled by the PH: Command. Either evenly spaced pattern cuts or unevenly spaced cuts (up to 10) can be specified. The LP: and PP: Commands provide for line printer and pen plotter outputs, respectively. Comments can be printed on the output data by using the CM: Command. The UN: Command is used to specify the appropriate units for the input data. The code is run or executed by using the XQ: Command. The command word system is described in detail in the user's manual for the code [11].

TABLE IV
BLOCK DIAGRAM OF THE MAIN PROGRAM OF THE FAR FIELD CODE

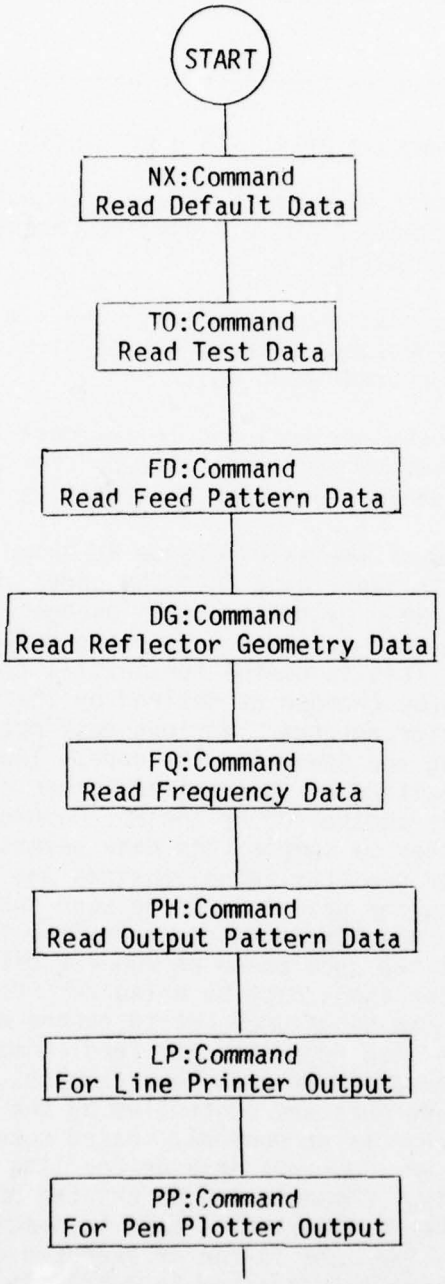

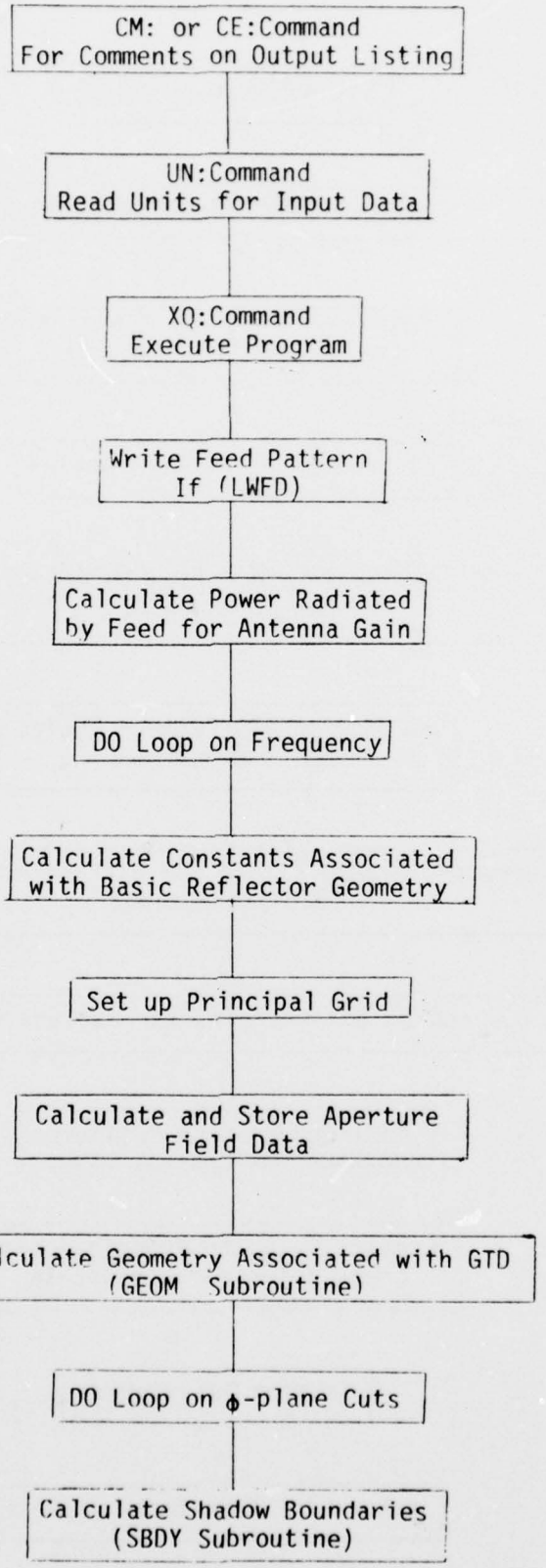
CM: or CE:Command
For Comments on Output Listing
UN:Command
Read Units for Input Data
XQ:Command
Execute Program
Write Feed Pattern
If (LWFD)
Calculate Power Radiated
by Feed for Antenna Gain
DO Loop on Frequency
Calculate Constants Associated
with Basic Reflector Geometry
Set up Principal Grid
Calculate and Store Aperture
Field Data
Calculate Geometry Associated with GTD
(GEOM Subroutine)
DO Loop on ϕ-plane Cuts
Calculate Shadow Boundaries
(SBDY Subroutine)

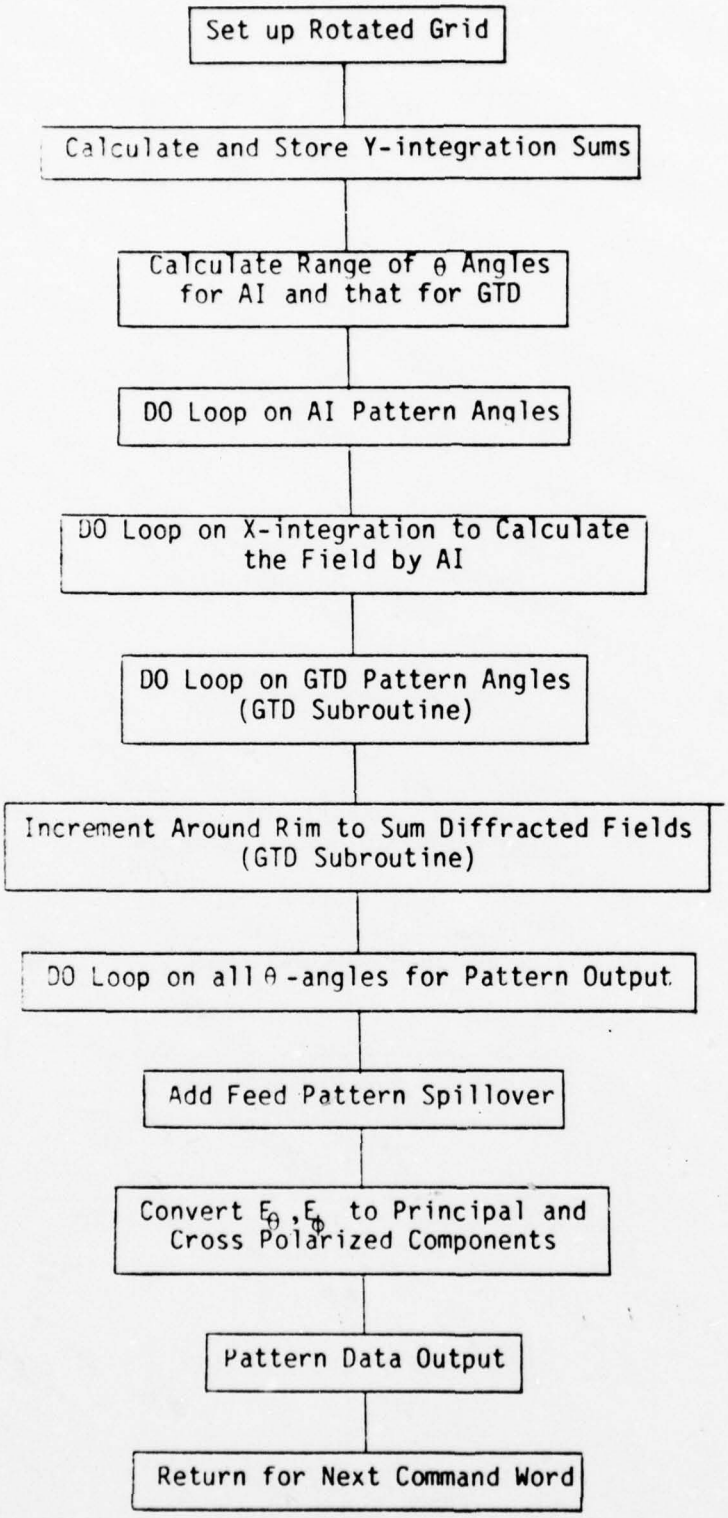
Set up Rotated Grid
Calculate and Store Y-integration Sums
Calculate Range of θ Angles for AI and that for GTD
DO Loop on AI Pattern Angles
DO Loop on X-integration to Calculate the Field by AI
DO Loop on GTD Pattern Angles (GTD Subroutine)
Increment Around Rim to Sum Diffracted Fields (GTD Subroutine)
DO Loop on all θ-angles for Pattern Output
Add Feed Pattern Spillover
Convert E_θ, E_ϕ to Principal and Cross Polarized Components
Pattern Data Output
Return for Next Command Word

E. Computed Far Field Pattern Results

The results of the general reflector code for several example antenna geometries are presented in this section. These examples illustrate the versatility of the code for computing far field patterns of reflector antennas with various rim shapes and feed patterns.

The first example is the common case of a circular reflector with an on-axis feed as shown in Figure 14. A GTD analysis was previously developed for this case as reported in Reference [15]. Calculated results are given in Reference [15] for a 24" diameter reflector with an F/D ratio of 1/3 and a frequency of 11 GHz. The feed is linearly polarized in the y-direction. The measured feed patterns for this antenna as given in Reference [15] are shown in Figure 15. The piece-wise linear feed pattern option of the reflector code was used to approximate the measured H- and E-plane feed patterns as shown in Figures 16a and b, respectively. The far field patterns as computed by the general reflector code are shown in Figures 17a and b for the H- and E-planes, respectively. The results from the general reflector code were found to be in good agreement with the calculated results of Reference [15] without aperture blockage as shown in Figures 18 and 19. Aperture blockage and feed strut scattering effects have not yet been included in the general reflector code. The comparison of the computed results with the measured patterns in Figures 18 and 19 is one indication of the validity of the general reflector code. Other comparisons are given below to further demonstrate the accuracy of the general reflector code.

The next two examples illustrate the flexibility of the general reflector code for treating various rim geometries. One example is a reflector with a $19\lambda \times 11\lambda$ rectangular aperture and a focal distance of 10λ. The other example uses the $19\lambda \times 11\lambda$ rectangular aperture but with chopped corners as shown in Figure 20. The feed patterns were chosen to be the same for both reflectors and are shown in Figures 21a and b. The feed is vertically polarized. The patterns computed by the general reflector code are shown in Figures 22a to c for the rectangular aperture. The corresponding patterns are shown in Figures 23a to c for the same aperture but with chopped corners as shown in Figure 20. Discontinuities occur in the pattern because double diffraction effects are not included. These discontinuities usually occur at low levels in the pattern.

It was originally anticipated that offset-fed reflectors could be handled using this first generation code. However after carefully examining this code, it was determined that several improvements should be made before an offset-fed reflector can be effectively run. Thus, offset-fed reflectors will be treated in the second generation code which is presently being developed. The following examples for offset reflectors were run with a preliminary version of the second generation code.

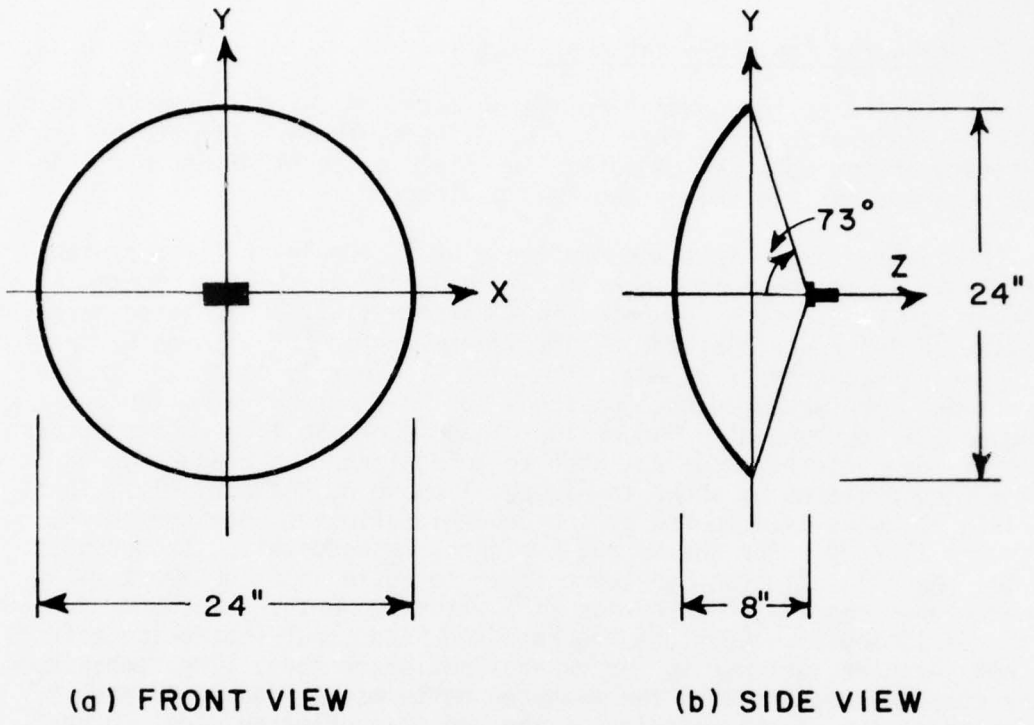

Figure 14. Circular reflector antenna with F/D = $\frac{1}{3}$.

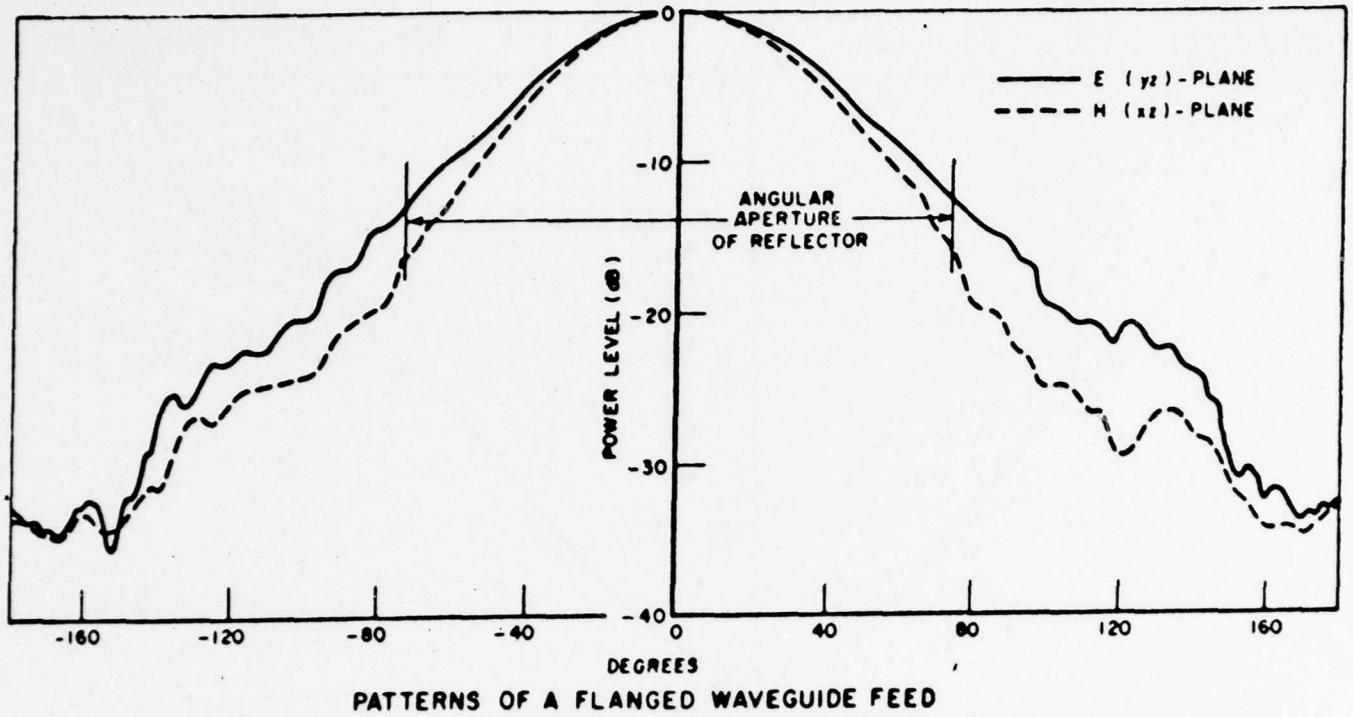

Figure 15. Measured primary field patterns of a flanged waveguide feed.

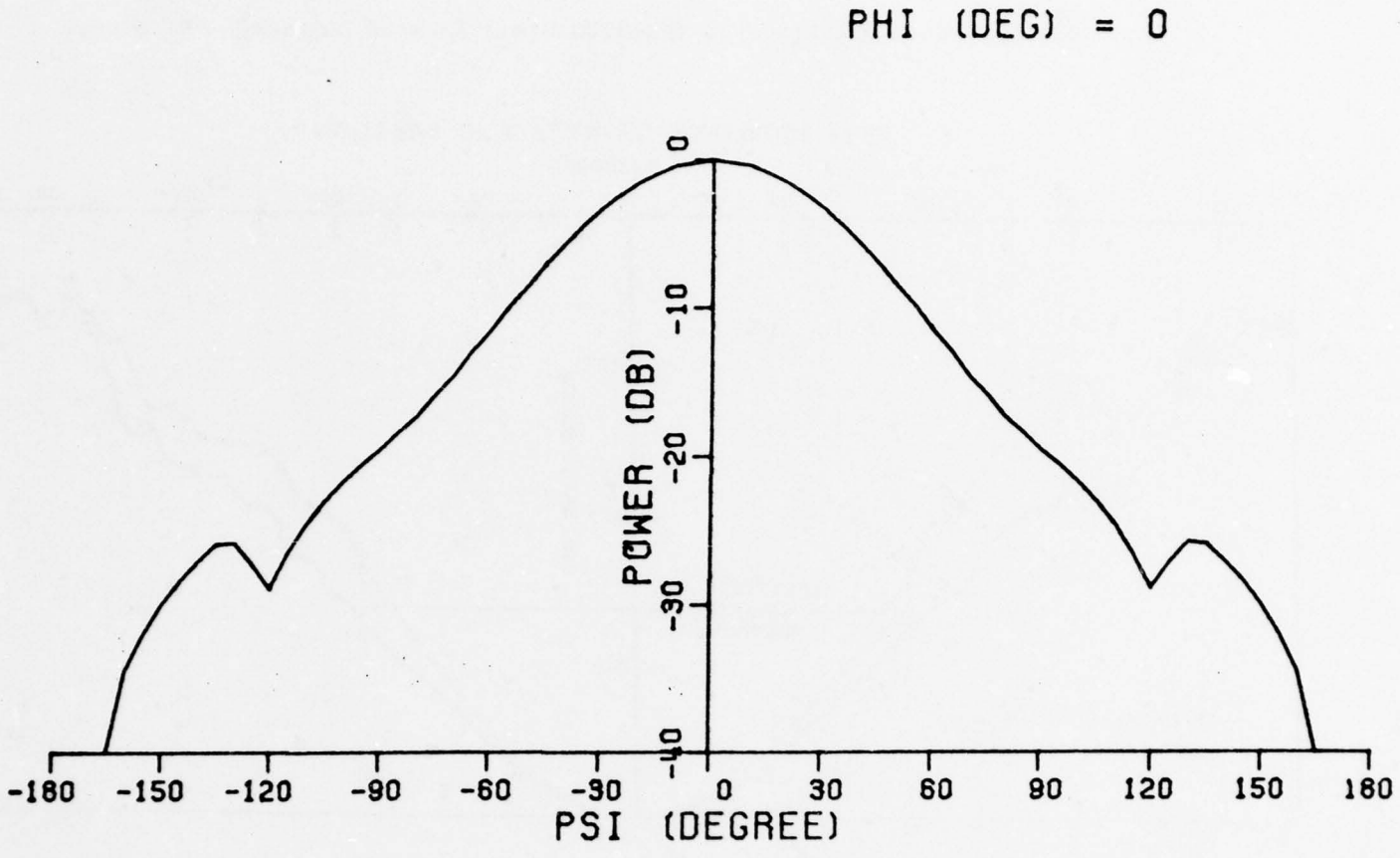

(a)

Figure 16. Input feed patterns for circular reflector example.

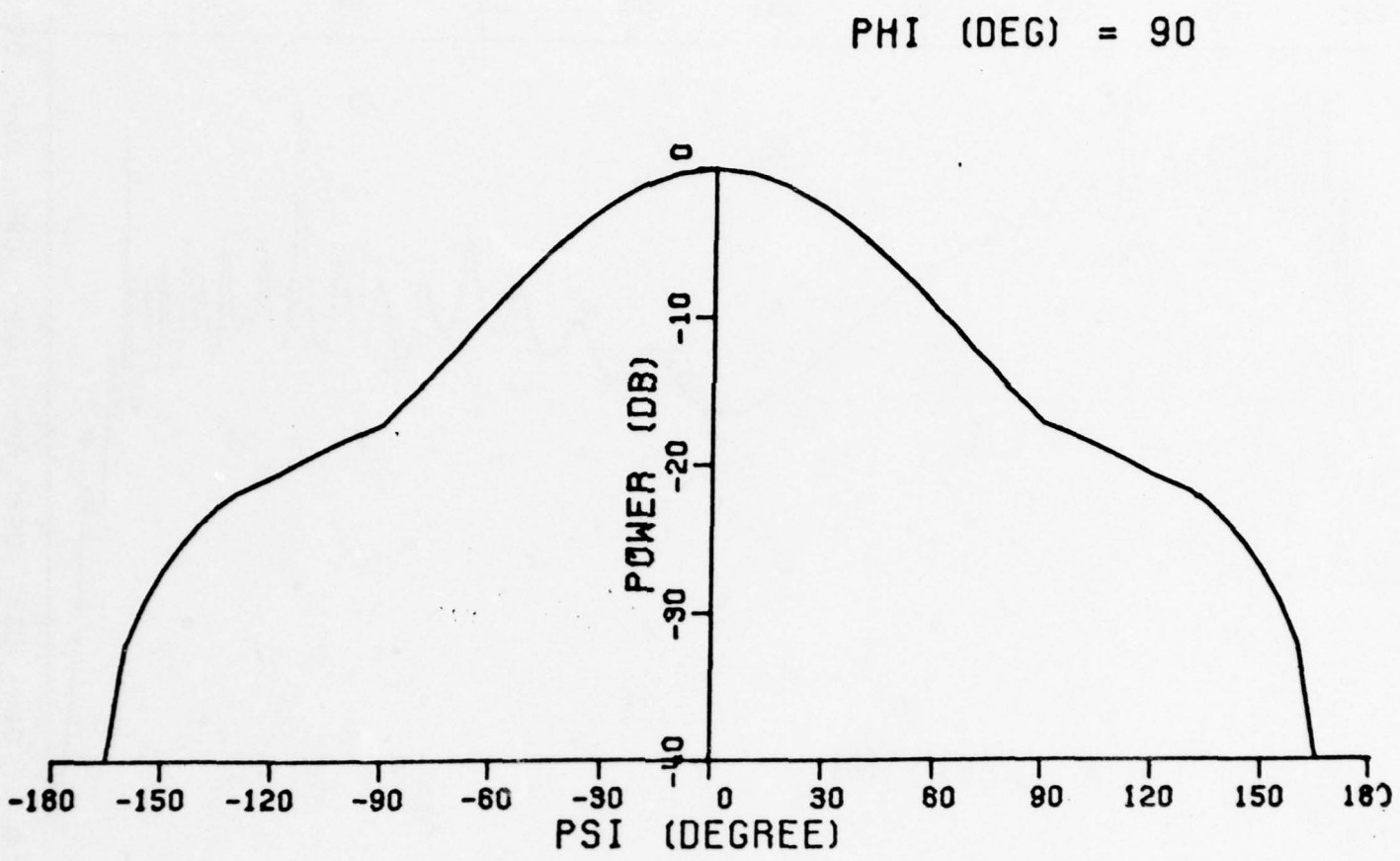

(b)

Figure 16. (Continued)

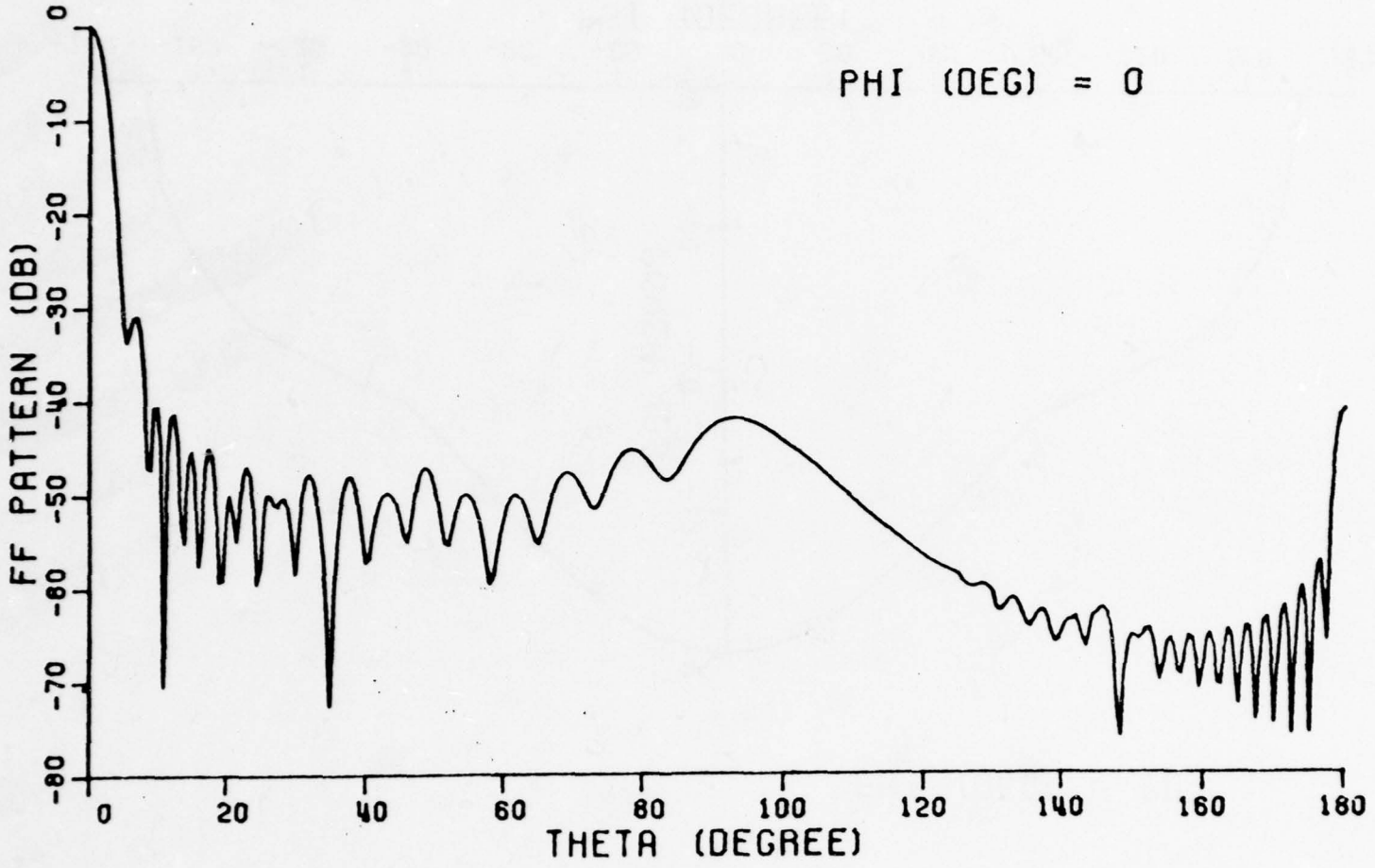

(a)

Figure 17. Far field patterns of circular reflector example computed by general reflector code.

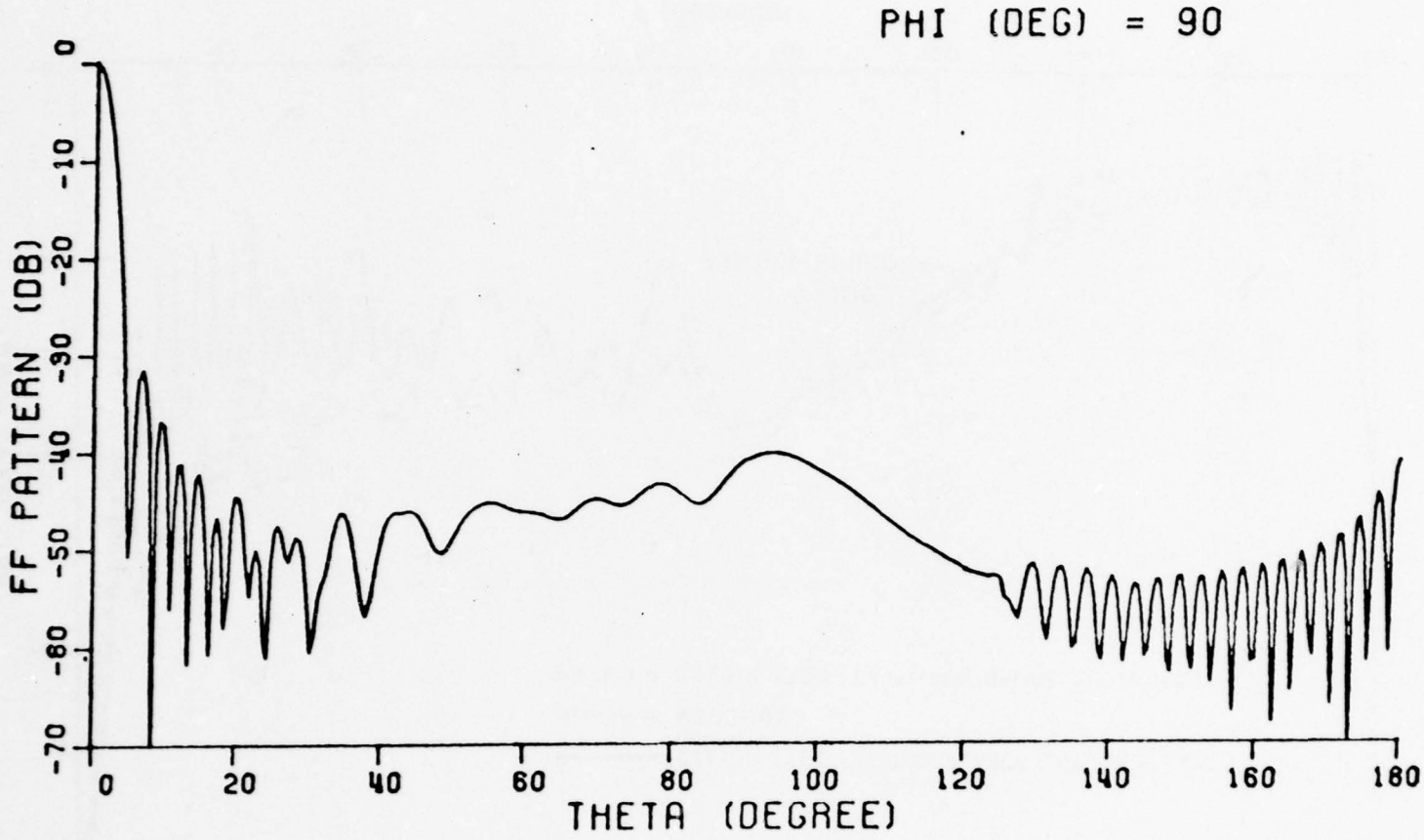

(b)

Figure 17. (Continued)

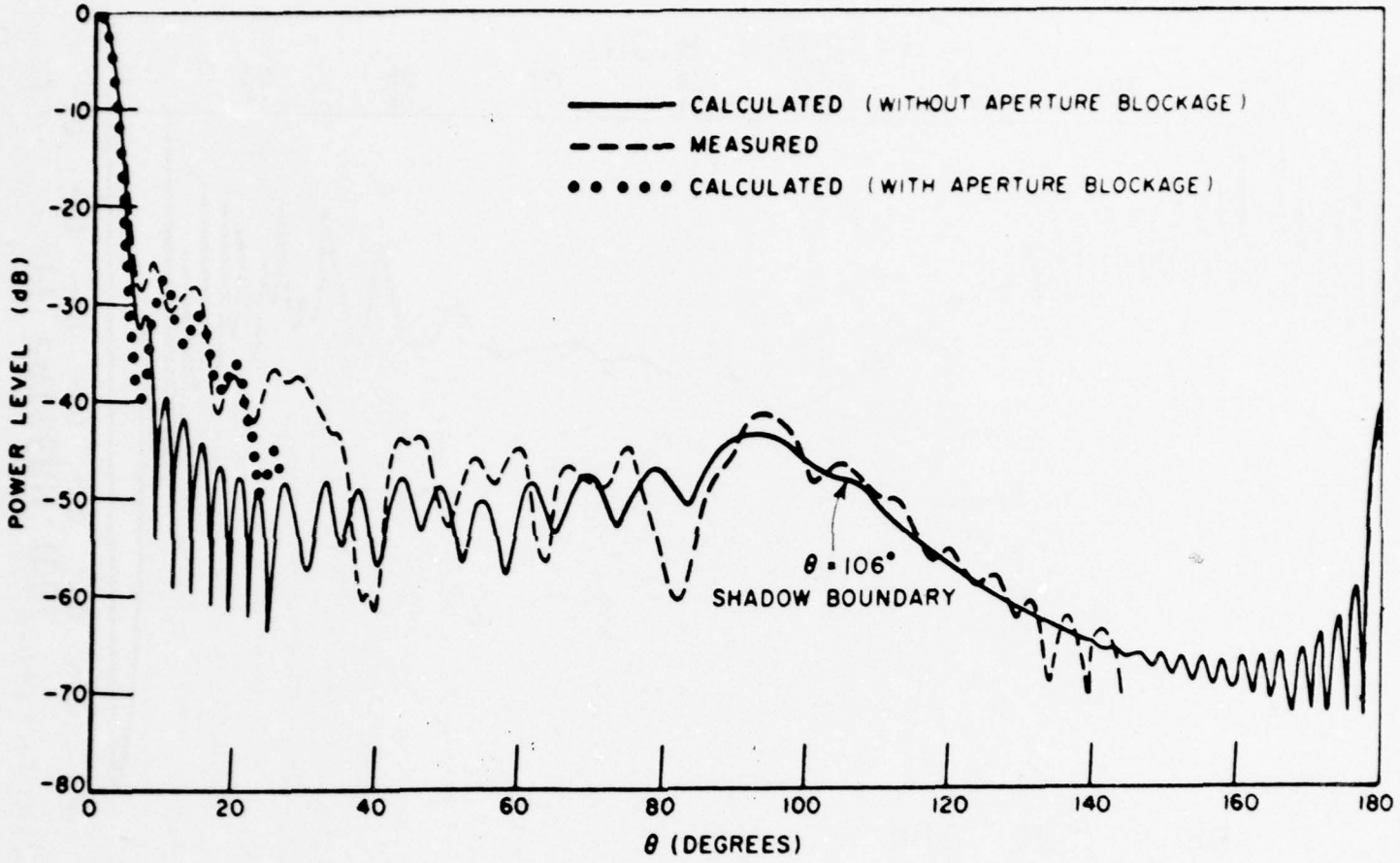

Figure 18. H-plane pattern of a parabolic reflector with a flanged waveguide feed. Computed in Reference [15].

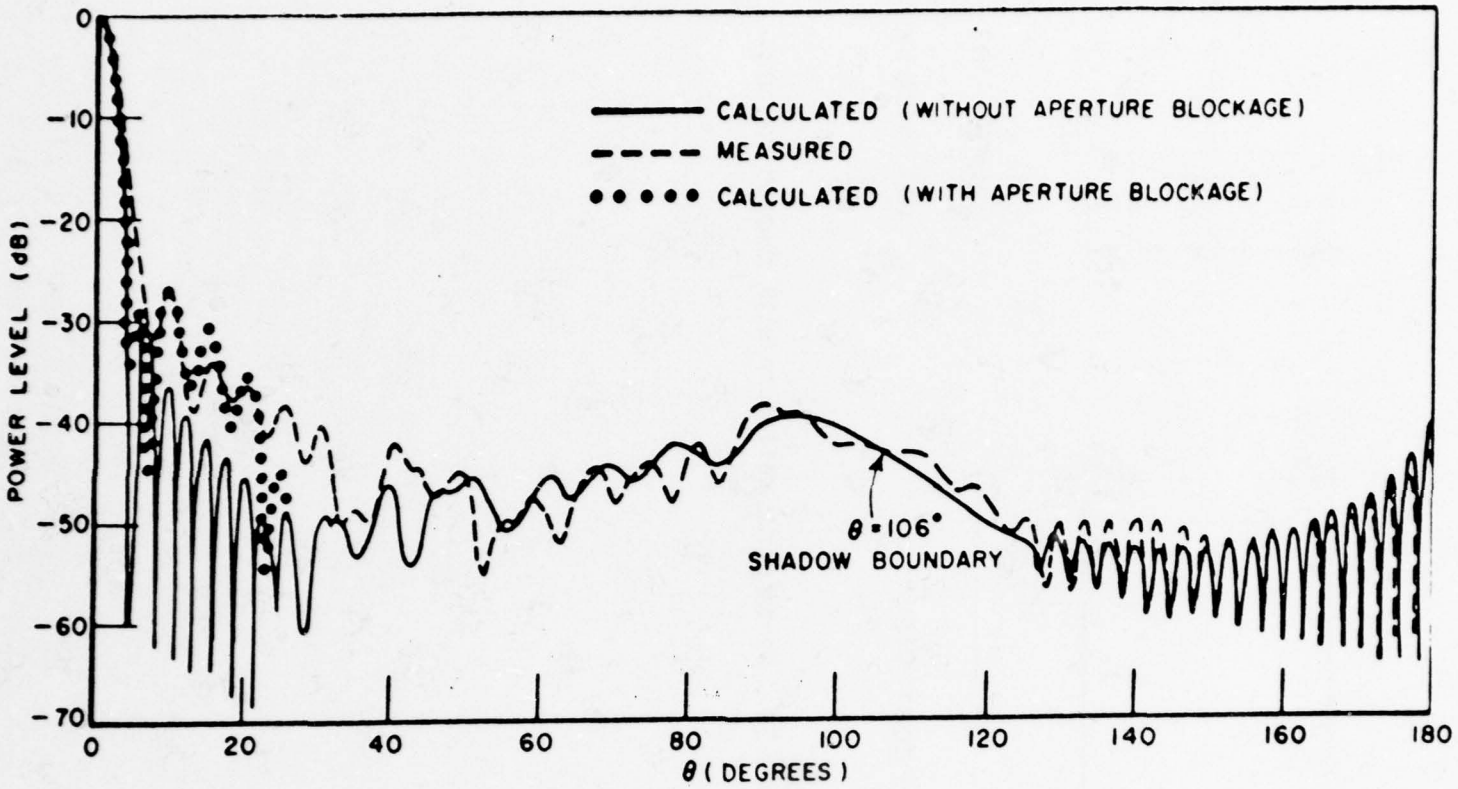

Figure 19. E-plane pattern of a parabolic reflector with a flanged waveguide feed. Computed in Reference [15].

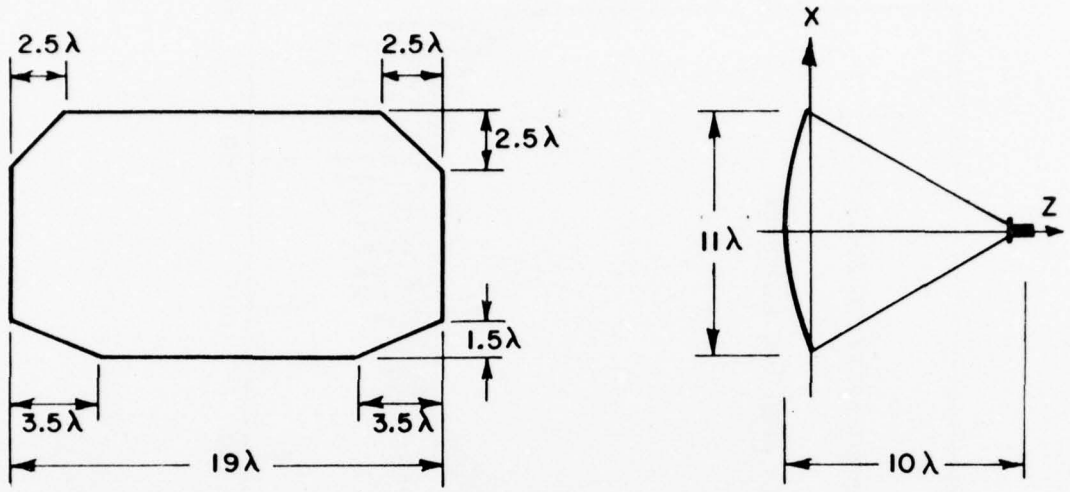

Figure 20. Rectangular reflector with chopped corners.

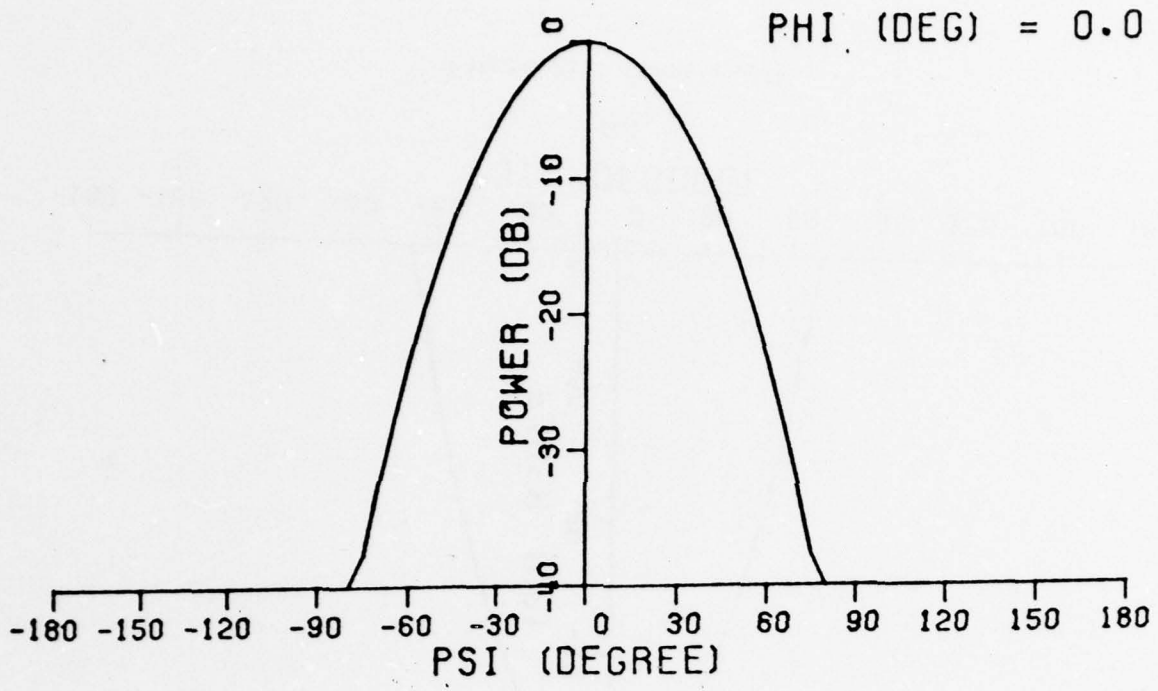

(a)

Figure 21. Input feed patterns for rectangular reflector geometries.

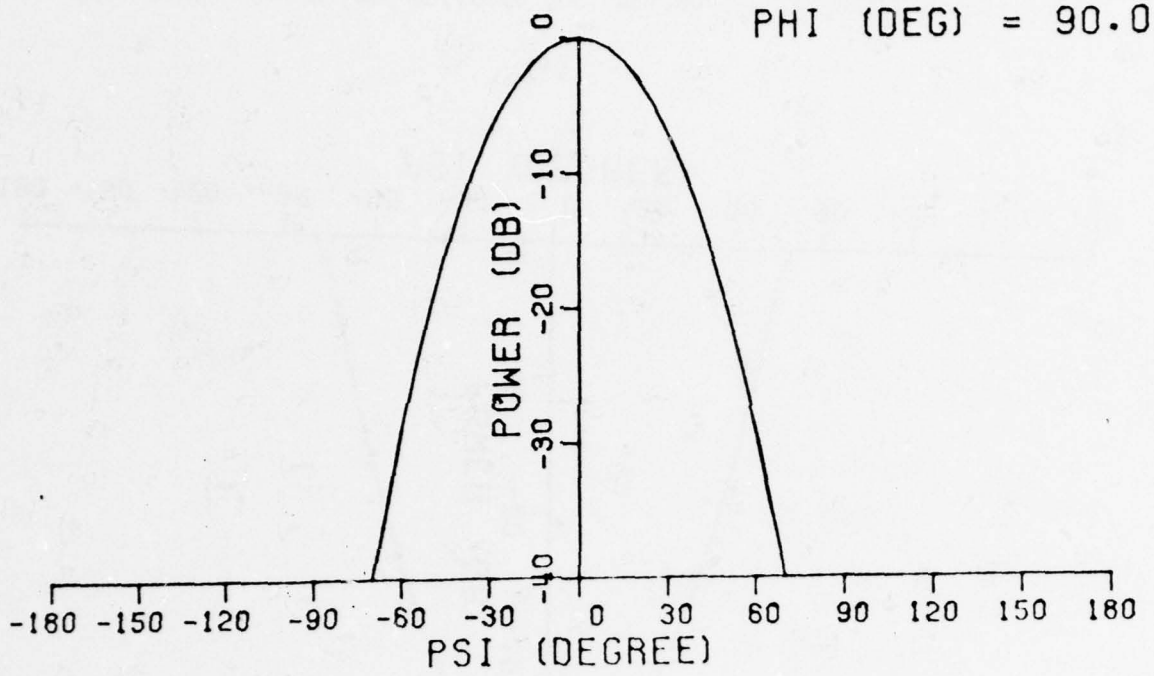

(b)

Figure 21. (Continued)

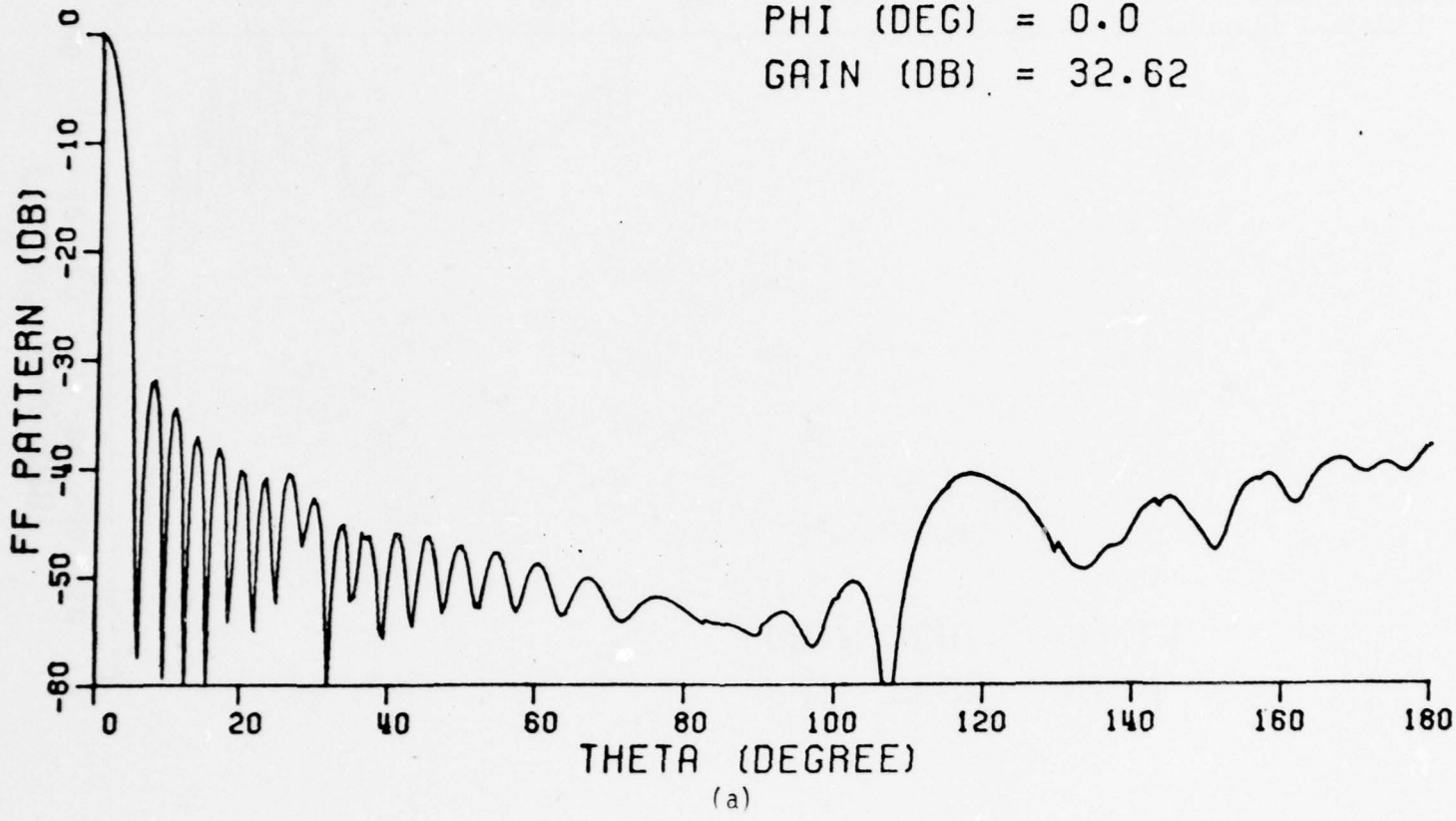

(a)

Figure 22. Far field patterns of rectangular reflector antenna.

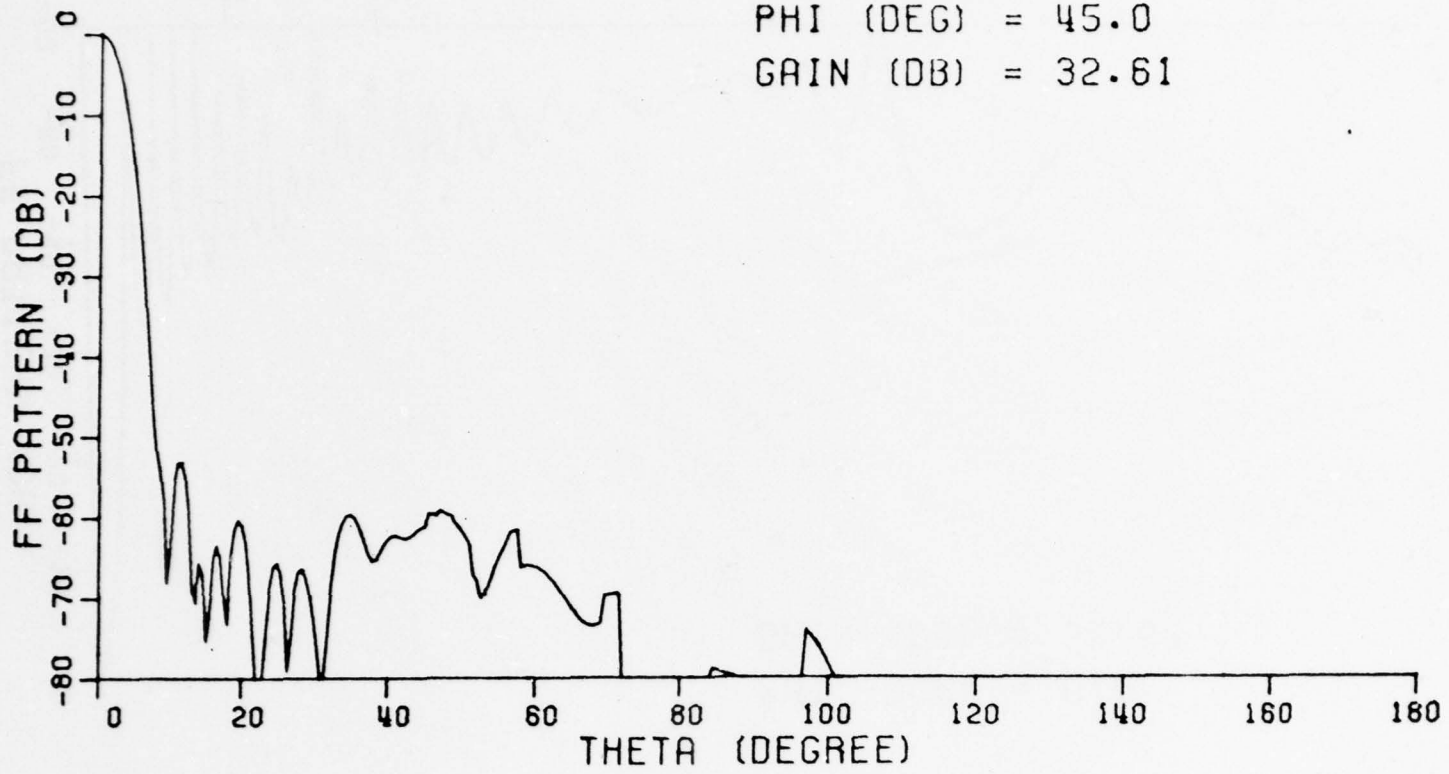

(b)

Figure 22. (Continued)

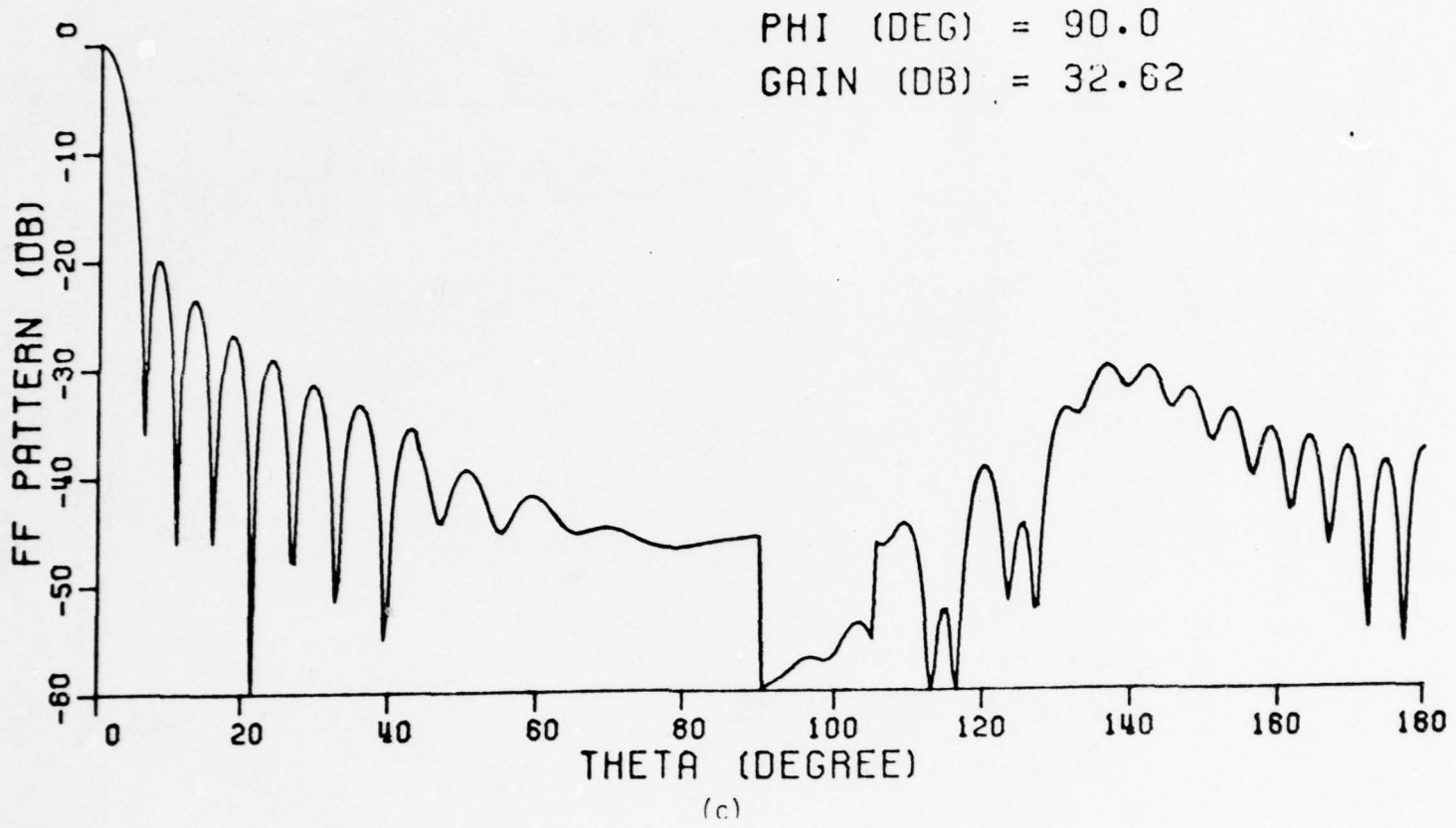

(c)

Figure 22. (Continued)

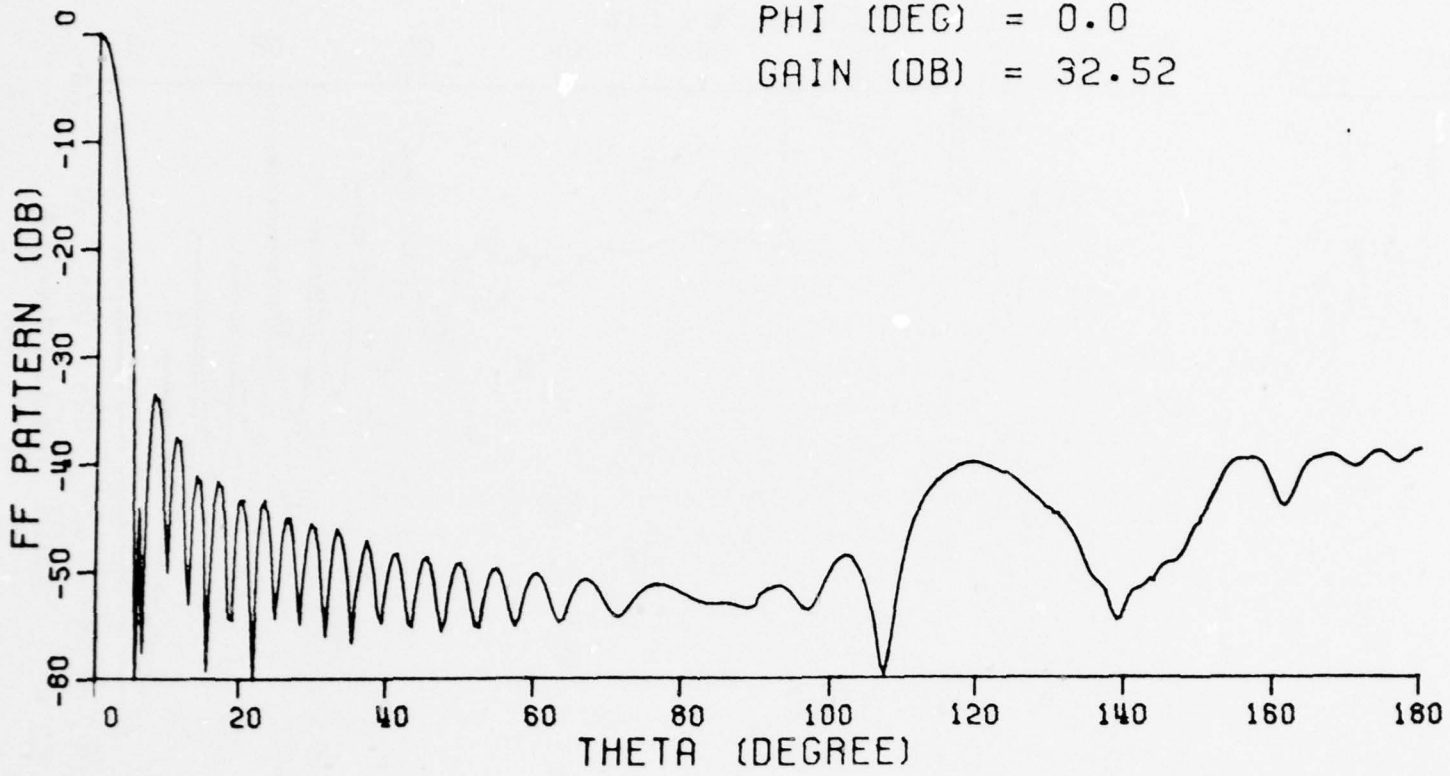

(a)

Figure 23. Far field patterns of rectangular reflector antenna with chopped corners.

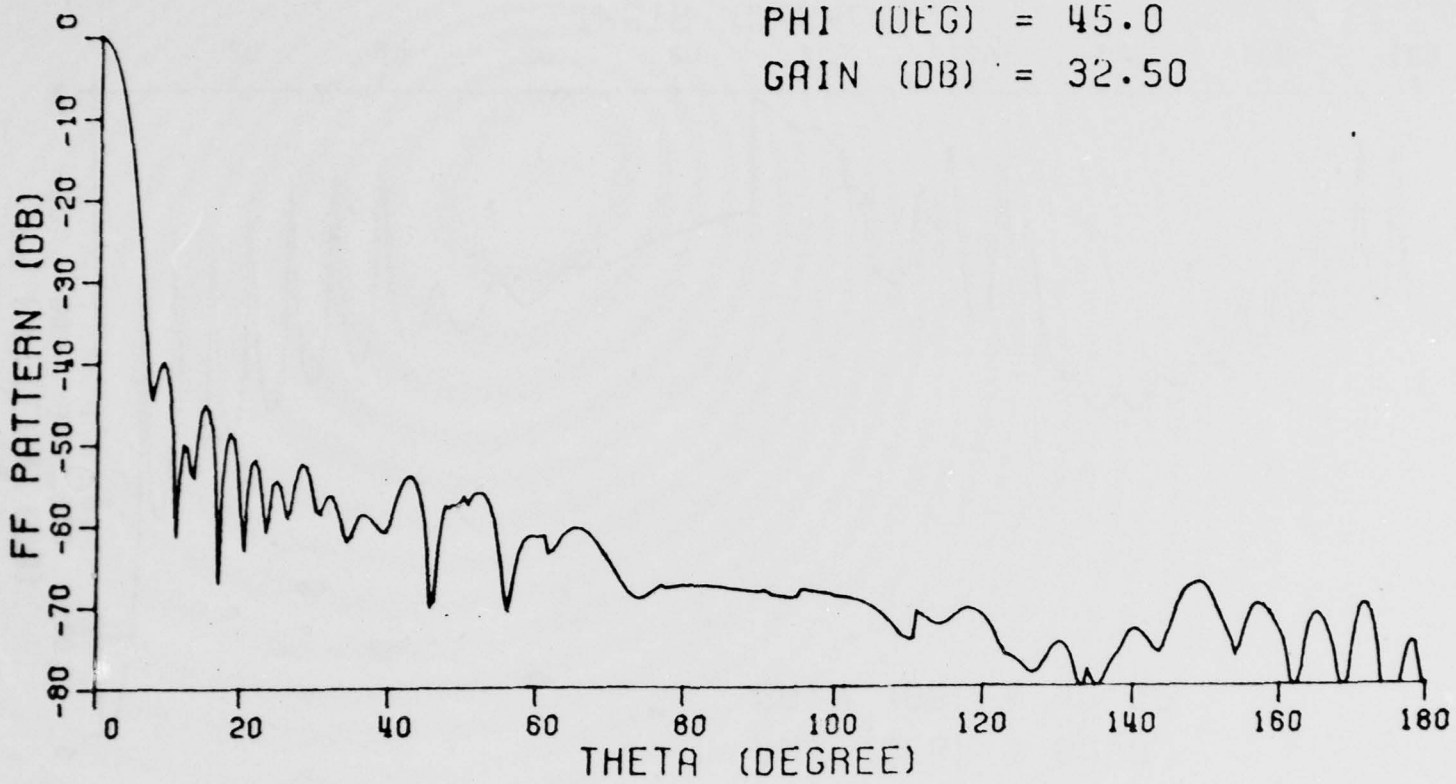

(b)

Figure 23. (Continued)

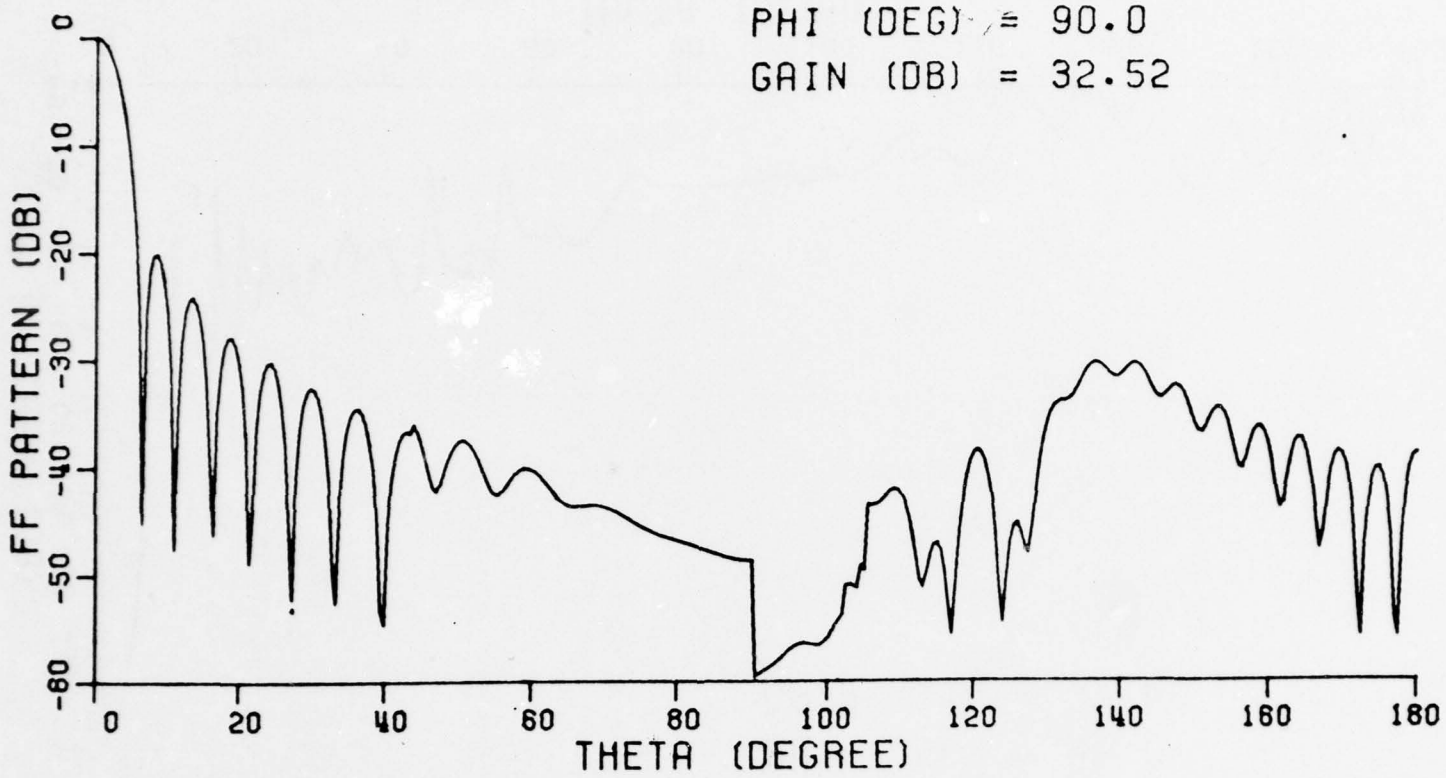

(c)

Figure 23. (Continued)

The first example for an offset reflector is shown in Figure 24. Fortunately, sufficient data were published in Silver [16] to completely specify the antenna and most of its feed pattern. The feed pattern data for this reflector had to be extracted from the published dB contours [16] of the aperture field as shown in Figure 25. The feed is horizontally polarized. The feed patterns were specified by using the option for an offset feed tilt angle (PSIT=20^{o}) and the feed pattern symmetry option (ISYM=3). This feed symmetry option specifies the feed pattern to be symmetrical about the y-z plane. Thus, for example, the feed pattern in the ϕ=-60^{o} cut and $\theta>0$ is the same as shown for $\theta<0$ in the ϕ=$+60^{o}$ cut of Figure 26d. Thus the input feed pattern was specified in the ϕ=-90^{o}, -60^{o}, -30^{o}, -15^{o}, $+15^{o}$, $+30^{o}$, $+60^{o}$ and $+90^{o}$ ϕ plane cuts as shown in Figures 26a through e. The E- and H-plane patterns as computed for 9.2 GHz from the general reflector code are shown in Figures 27a and b. The corresponding measured patterns as published in Silver [16] are shown in Figure 28. The measured and computed patterns are in good agreement considering that feed strut scattering effects are not included in the reflector code. The full 180^{o} patterns as computed by the general reflector code are shown in Figures 29a and b. The feed spillover is evident from the lobes near 90^{o} and 110^{o} in the E- and H-planes, respectively. Since the feed pattern information was obtained from the aperture field contours of Figure 25, the feed spillover was estimated by extrapolating the feed patterns with smooth curves as shown in Figure 26.

The next example is the offset reflector shown in Figure 30. The projected rim shape is circular as shown, although the rim is actually elliptical. The feed is horizontally polarized with an offset angle of 51.5^{o}. A specialized computer code was previously developed by Mentzer et al [17] which is applicable only for this particular antenna. The feed pattern was obtained by calculating values using the special algorithms developed in Reference [17]; and then these values were input using the piecewise linear feed option. The resulting input feed pattern cuts are shown in Figures 31a through c. Although the mid-C band frequency was not precisely known, several frequencies were tried until one was obtained which matched the beamwidths of the patterns calculated in Reference [17]. The patterns computed by the general reflector code are shown in Figures 32a to c. They are in excellent agreement with those calculated in Reference [17] and shown in Figures 33a to c. An antenna gain of 63 dB was computed by the general reflector code; and the gain of the feed horn was computed to be about 37 dB. Thus the general reflector code predicts the antenna gain as 26 dB above the feed horn gain. This is within about 1 dB of that shown in Figure 33.

The depolarization properties of offset reflector antennas were studied by Chu and Turrin [18]. They calculated the maximum cross polarization produced by a linearly polarized feed and checked their result with a measured cross polarized pattern of the offset reflector with an offset angle of θ_c=45^{o} shown in Figure 34. Kauffman et al [19] also checked this case with calculated patterns from their computer program for circular

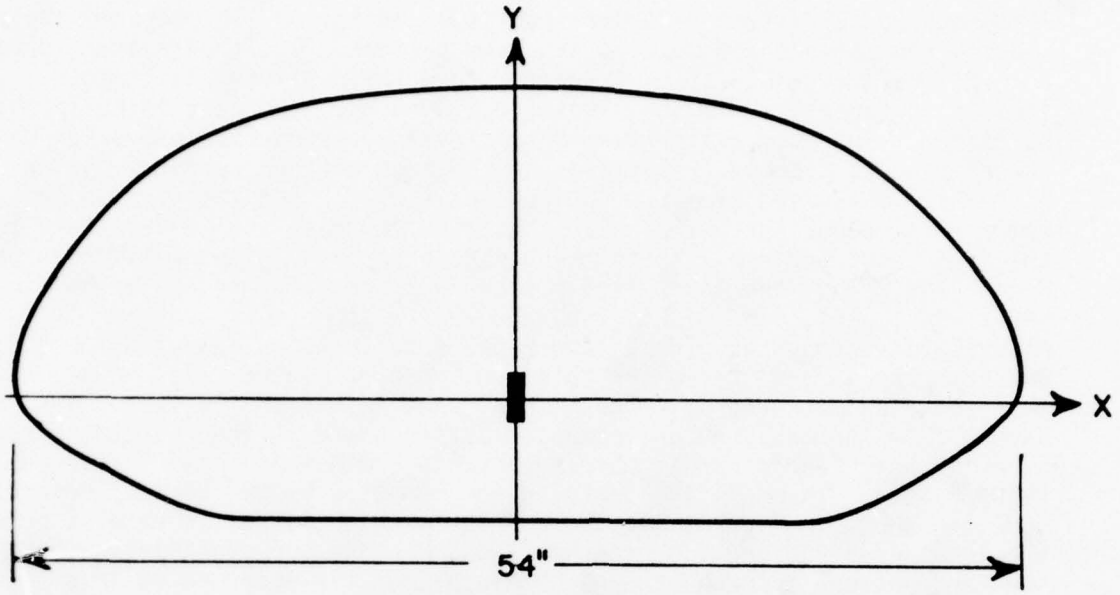

(a) FRONT VIEW

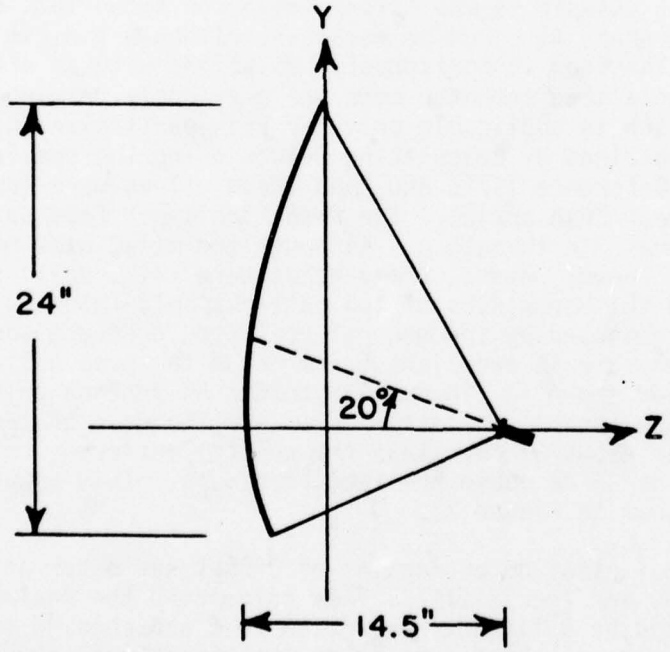

(b) SIDE VIEW

Figure 24. Offset reflector rim shape and crossection.

reflector antennas. Their computer program is based on an aperture integration analysis involving the quantizing and sorting of numerous aperture field data. In the calculations of [18] and [19] for this offset reflector example, a circularly symmetric feed pattern was assumed. The feed pattern was taken to be the same as the H-plane pattern of an open ended circular waveguide as shown in Figure 35. The patterns computed by the general reflector code, as shown in Figures 36 through 38, are in excellent agreement with those computed in [19] and with the measured patterns of [18]. Note that excellent agreement is achieved for the cross polarized beam as shown in Figure 37 for the $\phi=0^{o}$ plane. There is no cross polarized beam in the $\phi=90^{o}$ plane for a symmetrical feed pattern.

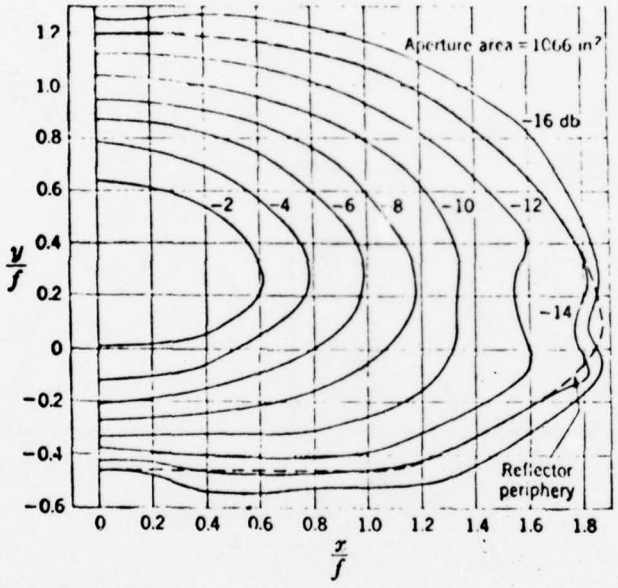

Figure 25. Constant intensity contours in paraboloid aperture (horn feed axis titled 20^{o} relative to paraboloid axis).

No cross polarization occurs when the offset reflector is fed by a circularly polarized feed; but the depolarization property manifests itself by a beam shift for circular polarization. The left and right circularly polarized beams shift in opposite directions [18]. The corresponding circularly polarized cases as computed by the general reflector code are shown in Figures 39 and 40. The calculated beam shift in each case was 0.35^{o}, or a total shift of 0.70^{o} between left and right circular polarizations. This compares well with the value of 0.75^{o} as determined from measured patterns [18]. The latter are reproduced in Figure 41.

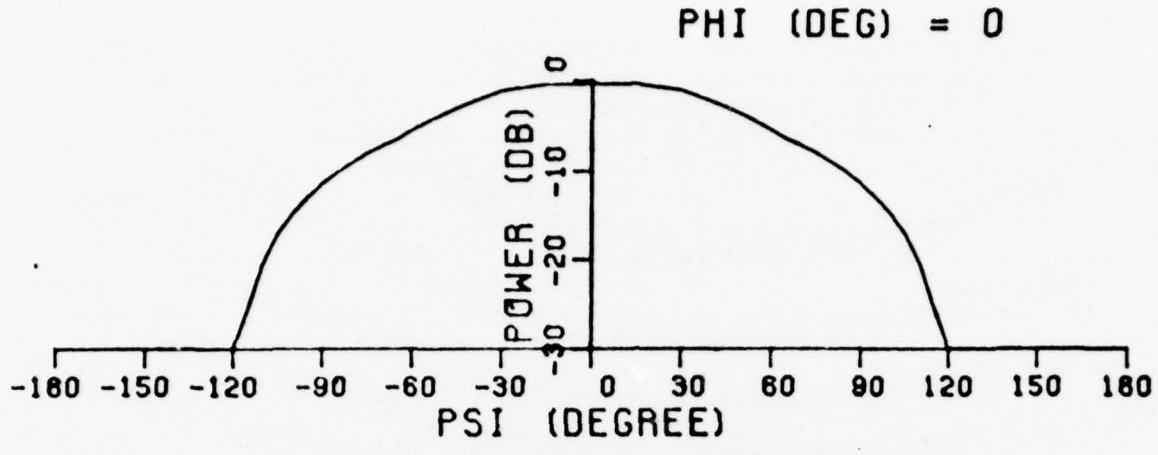

(a)

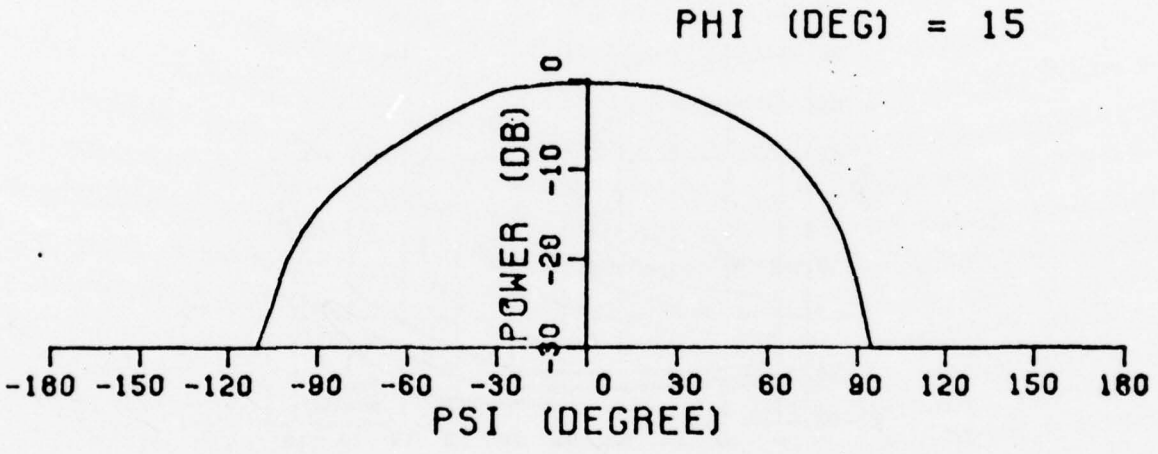

(b)

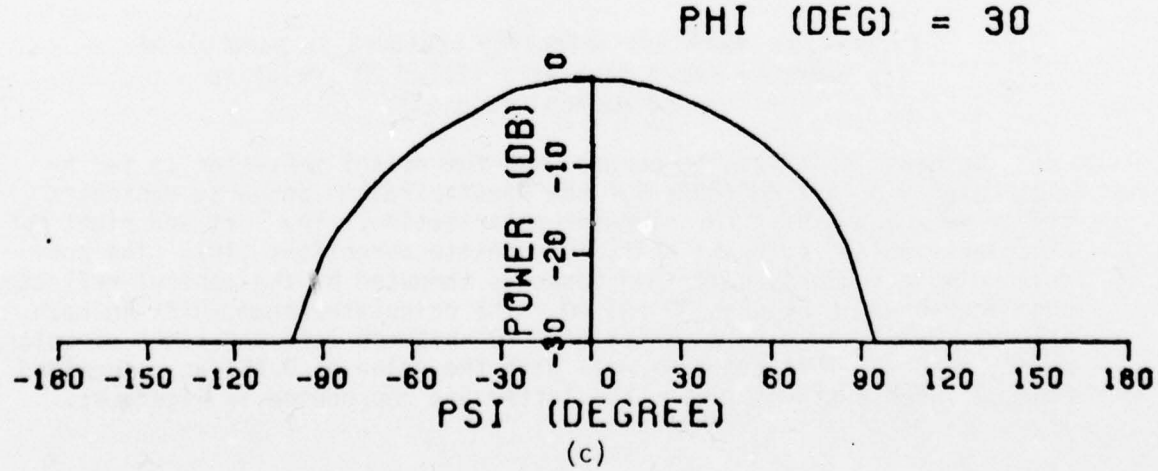

(c)

Figure 26. Input feed patterns for offset reflector example.

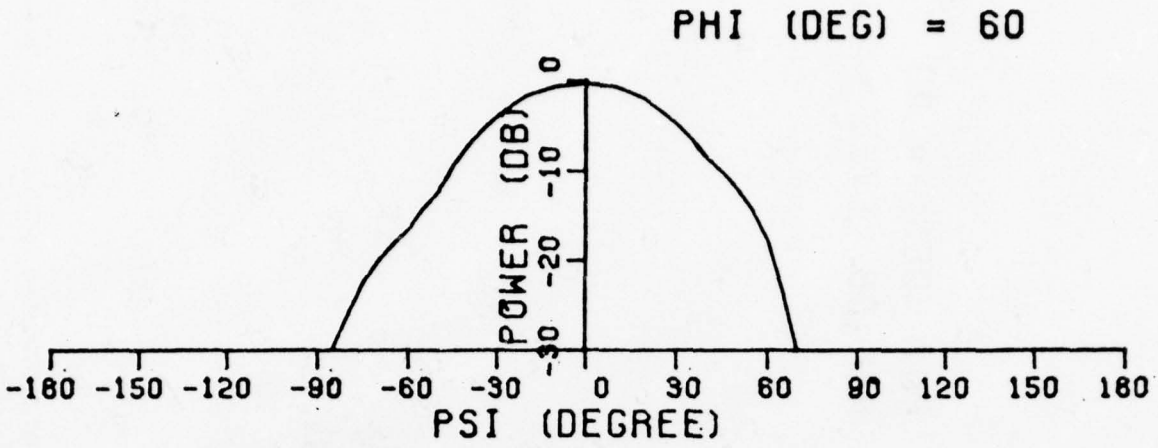

(d)

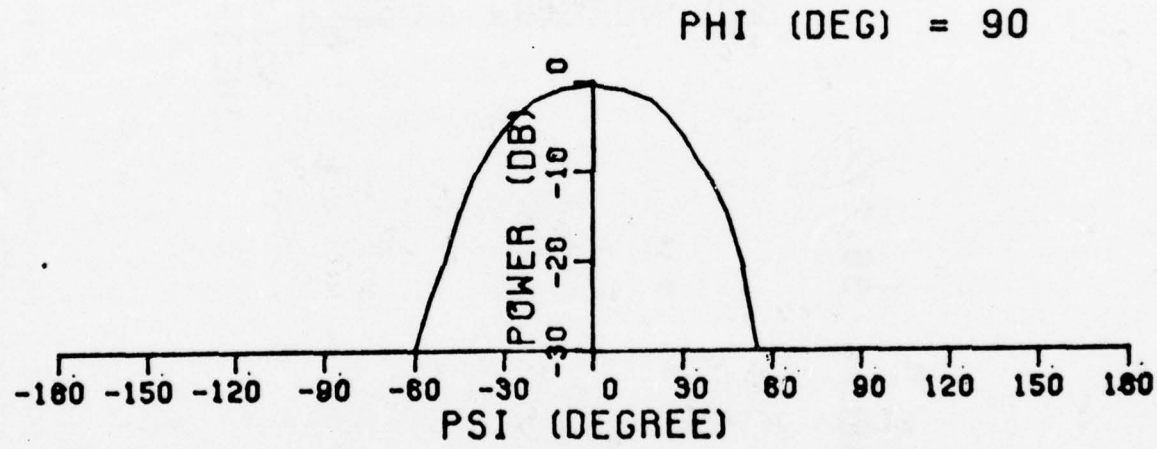

(e)

Figure 26. (Continued)

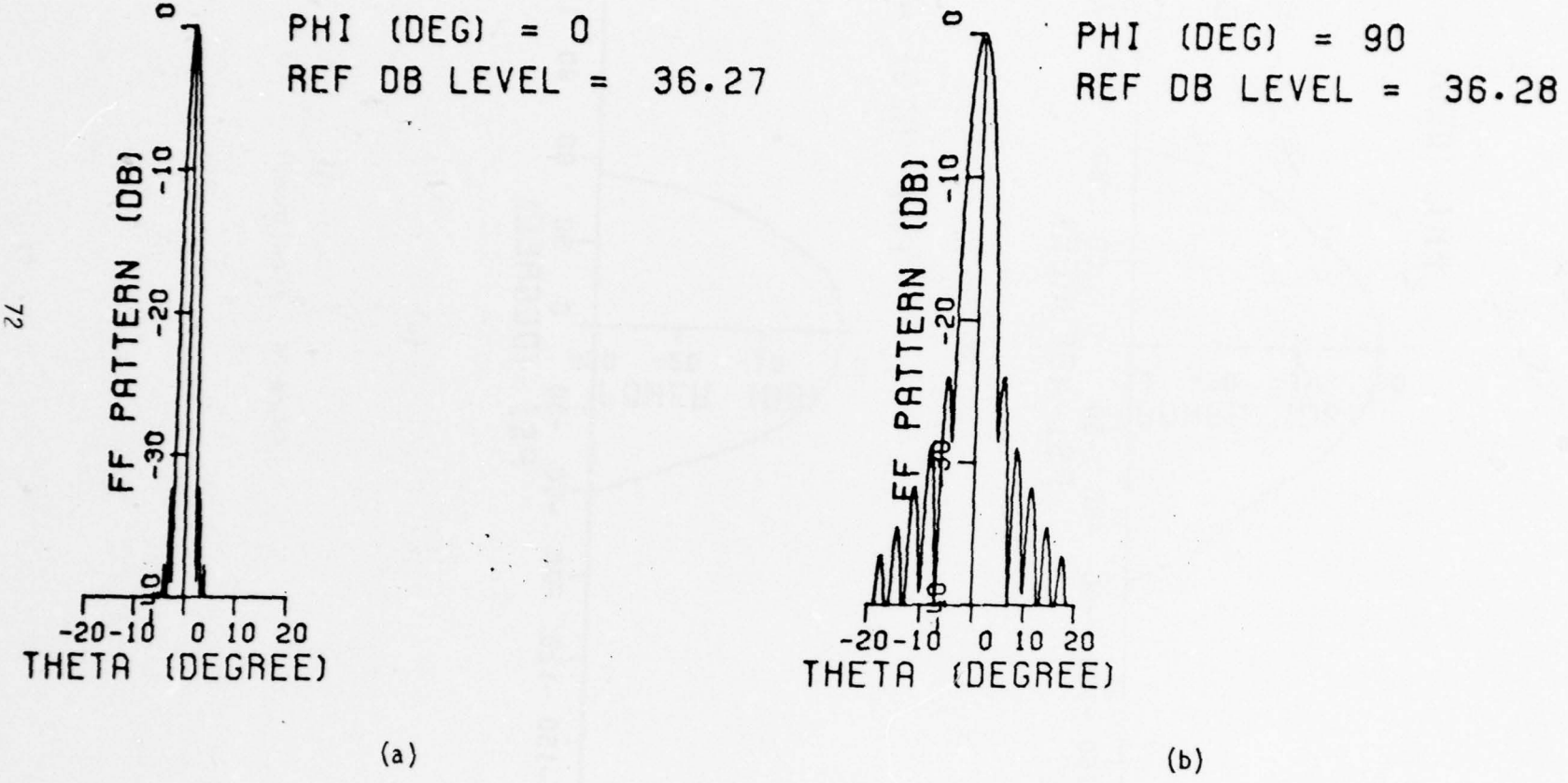

Figure 27. Far field patterns of offset reflector example computed by general reflector code. Main beam and near sidelobes.

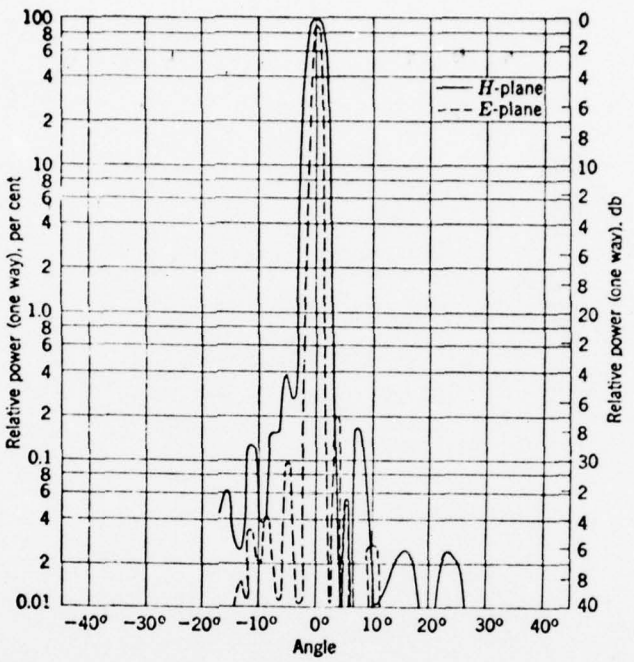

Figure 28. Principal E- and H-plane polar diagrams of the antenna shown in Figure 24.

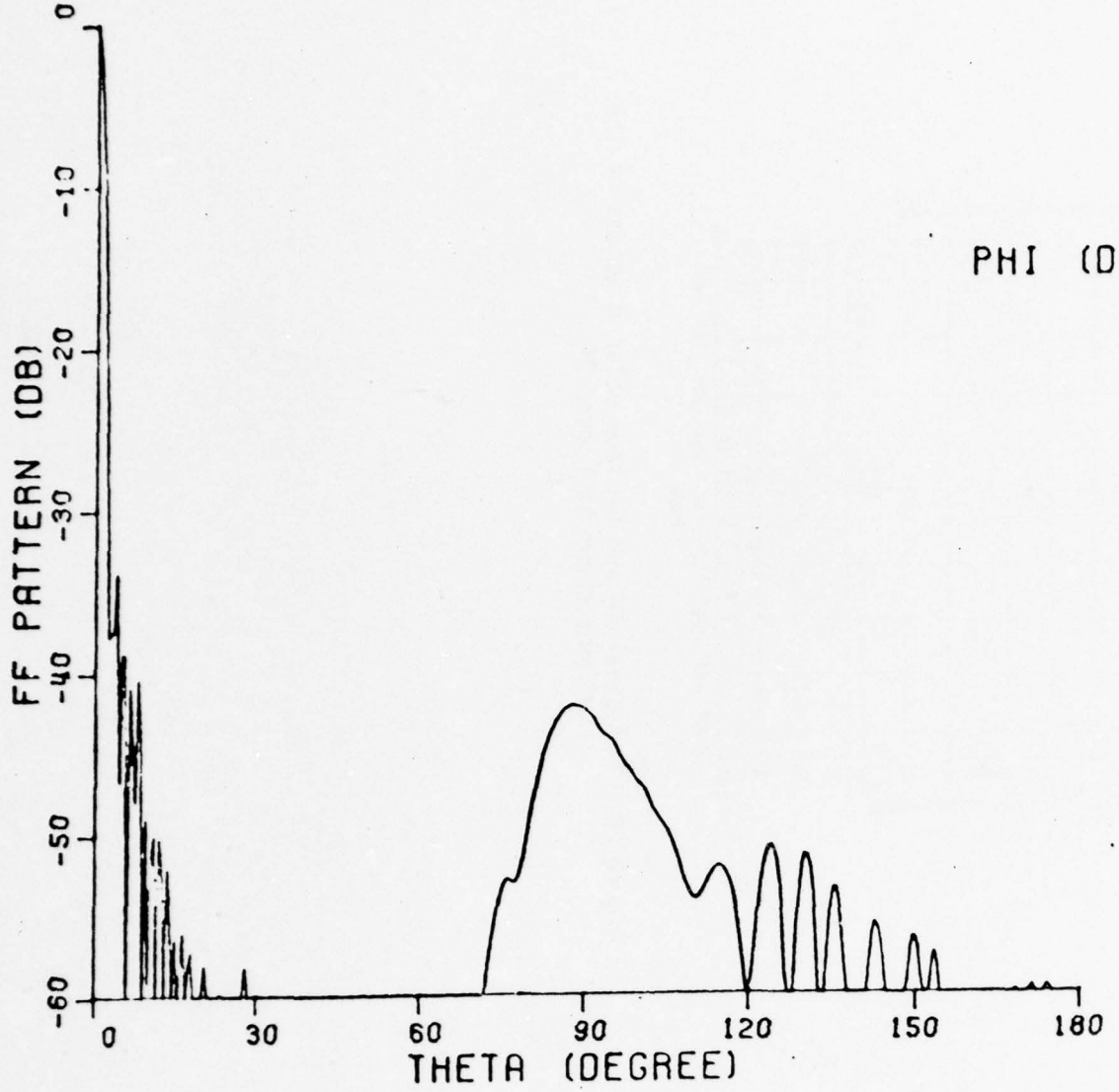

(a)

Figure 29. Far field patterns of offset reflector example computed by general reflector code.

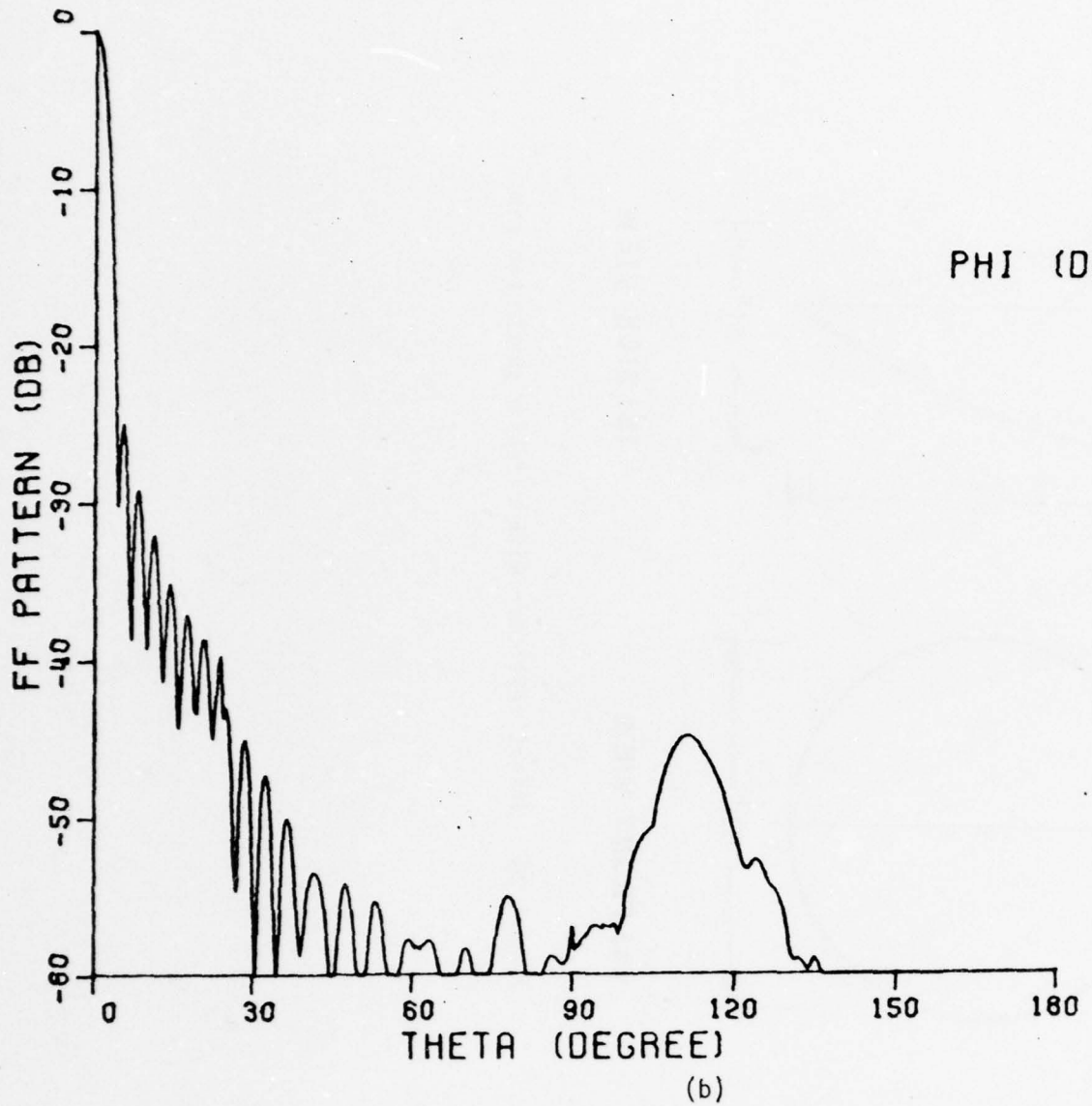

(b)

Figure 29. (Continued)

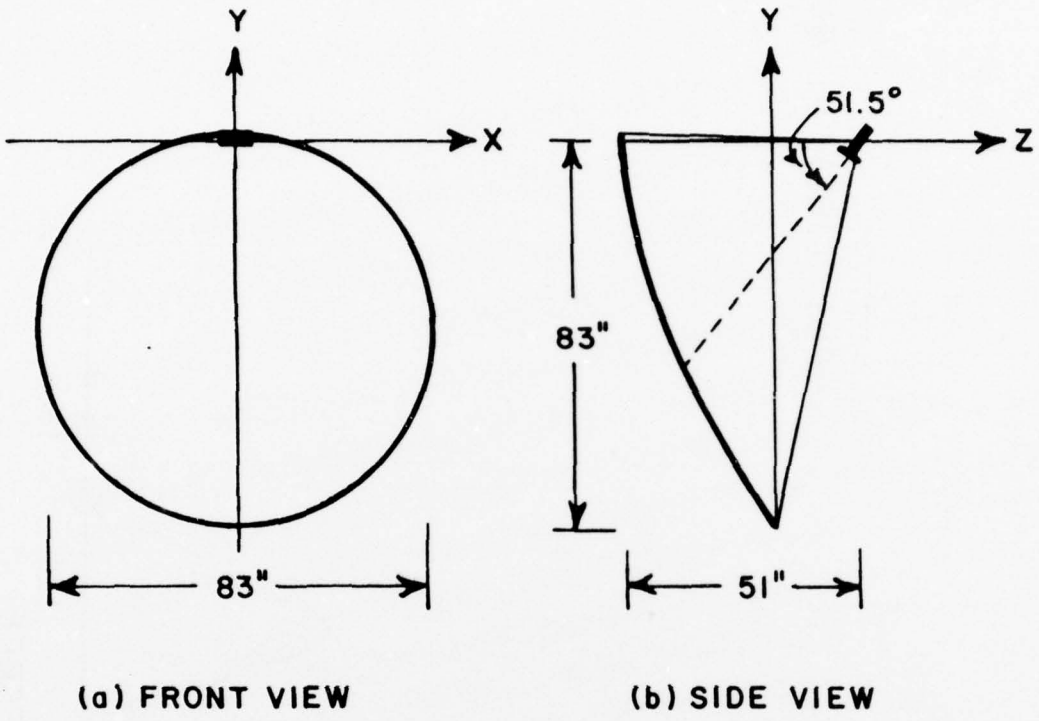

Figure 30. Offset reflector with circular projected rim.

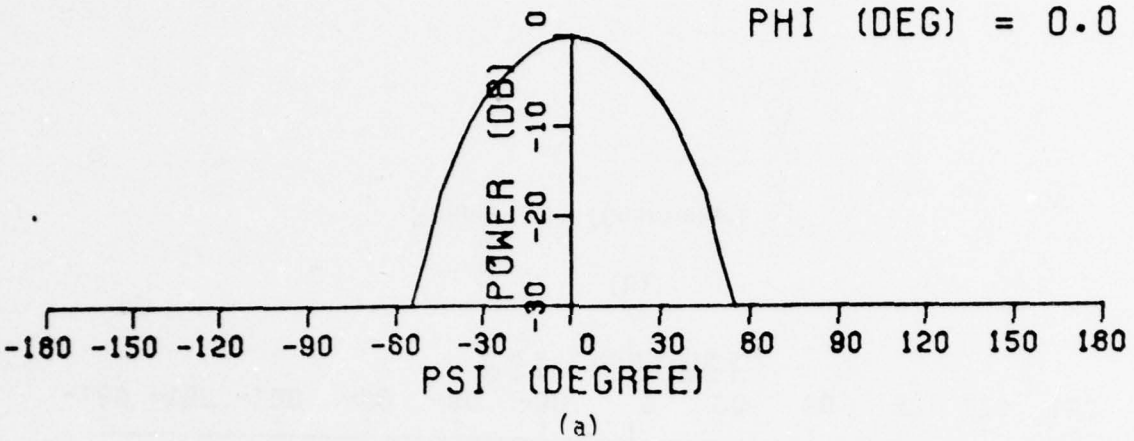

(a)

Figure 31. Input feed patterns for offset reflector with circular projected rim.

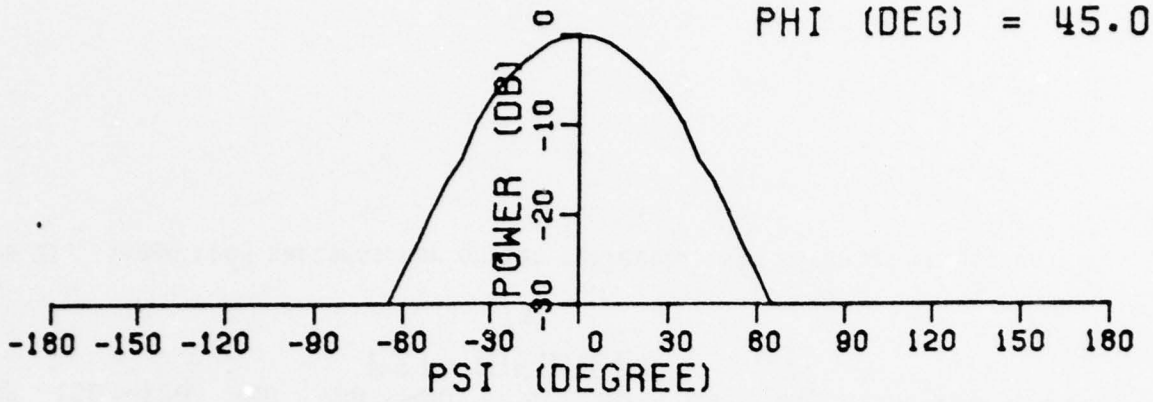

(b)

Figure 31. (Continued)

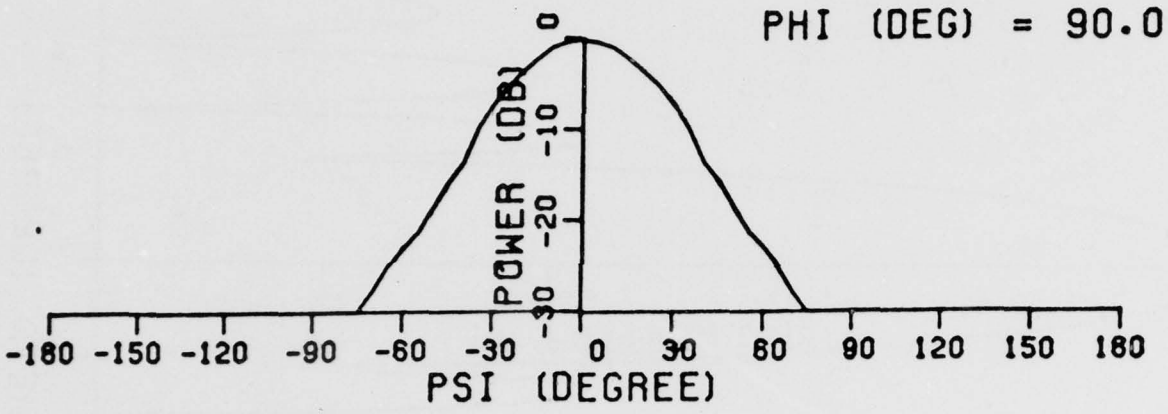

(c)

Figure 31. (Continued)

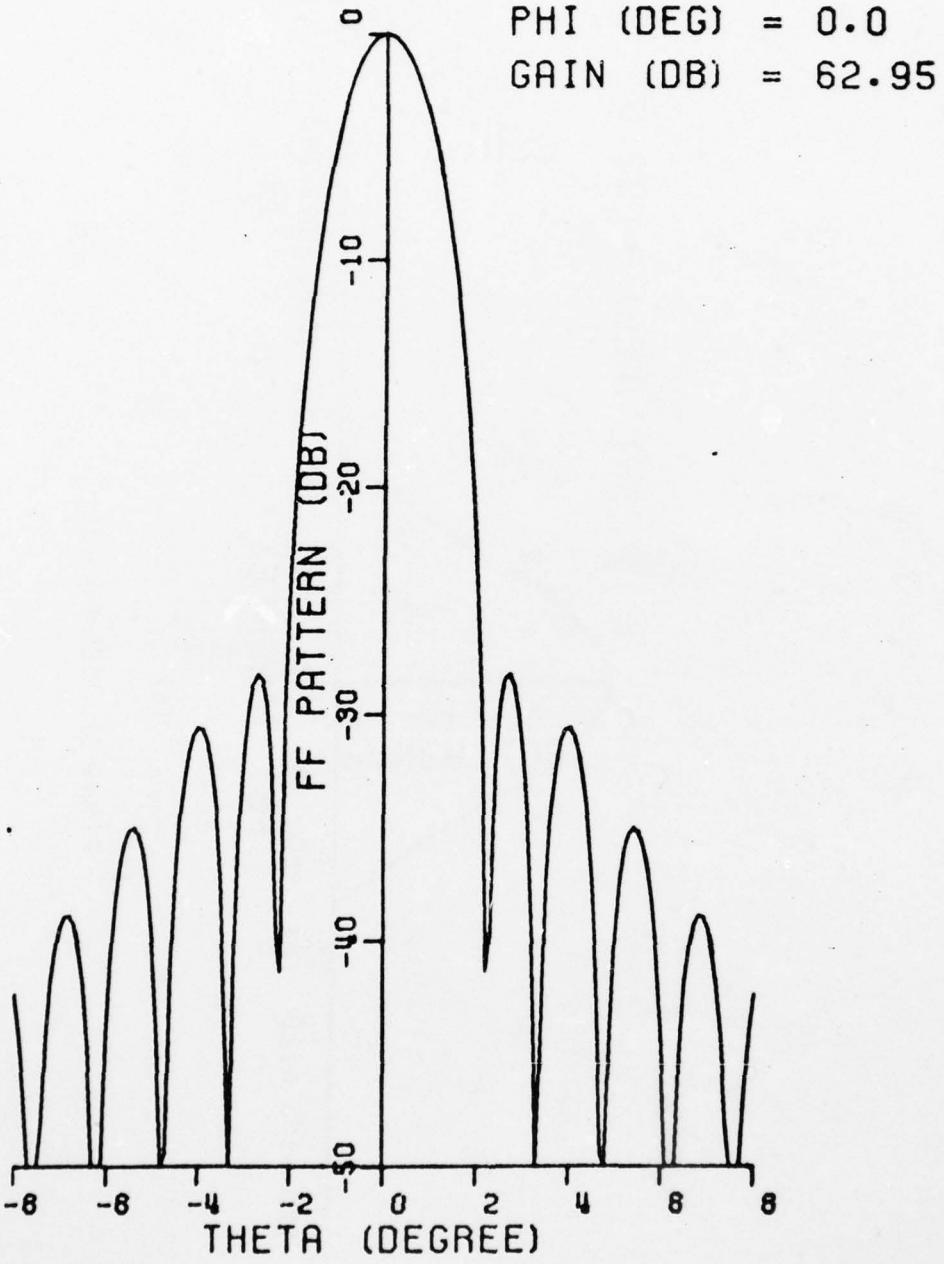

(a)

Figure 32. Far field patterns of offset reflector with circular projected rim computed by general reflector code.

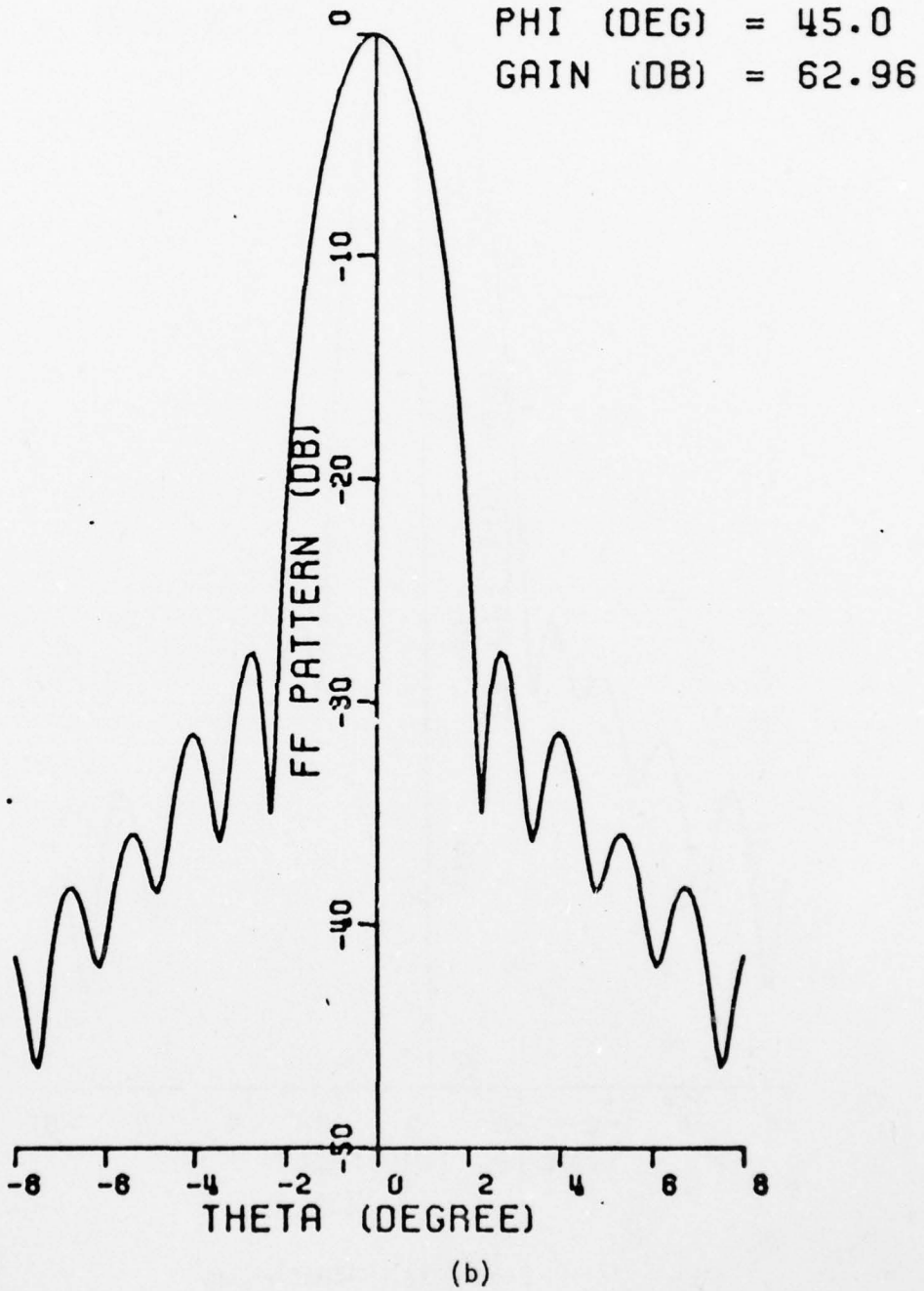

(b)

Figure 32. (Continued)

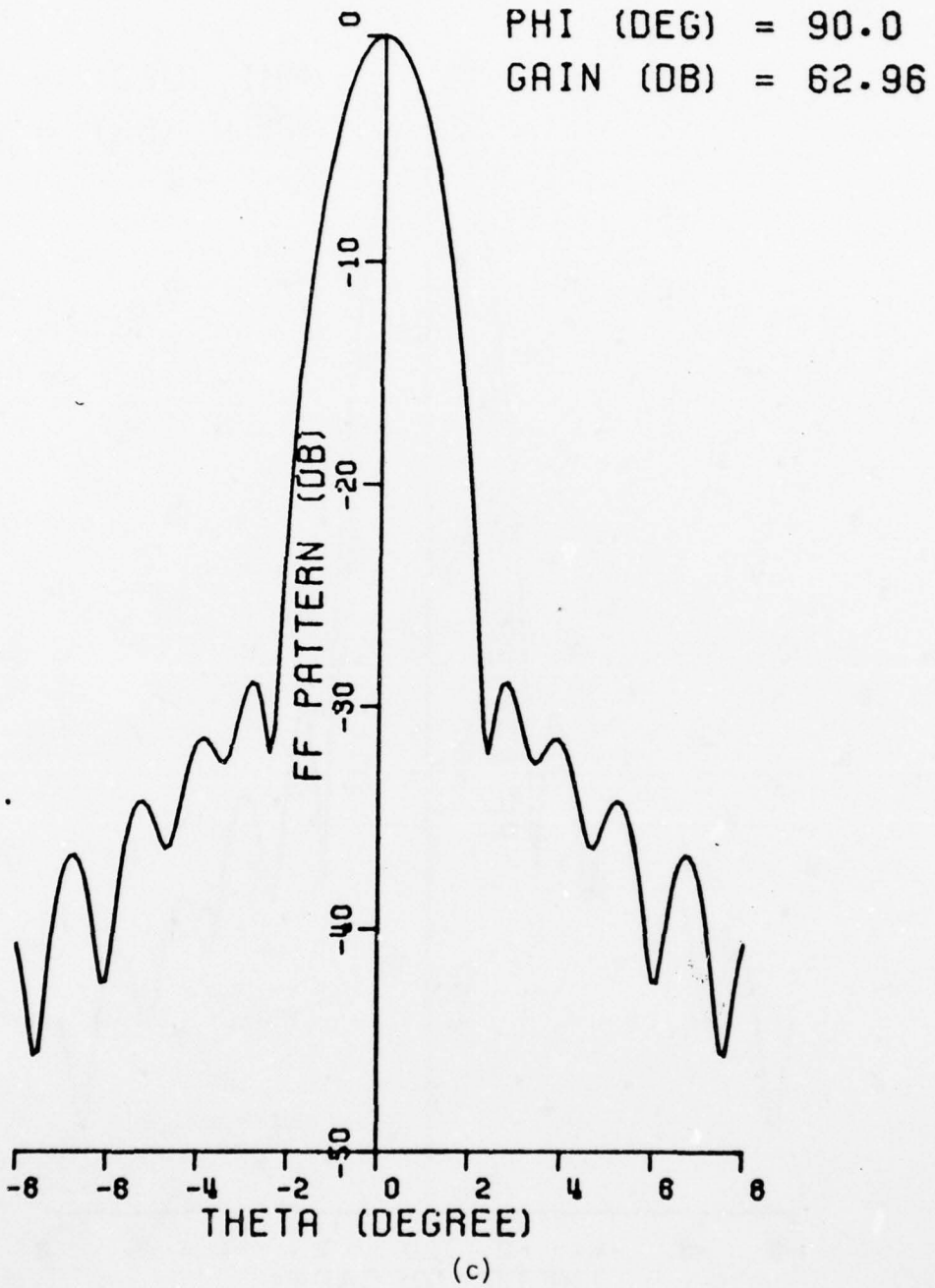

(c)

Figure 32. (Continued)

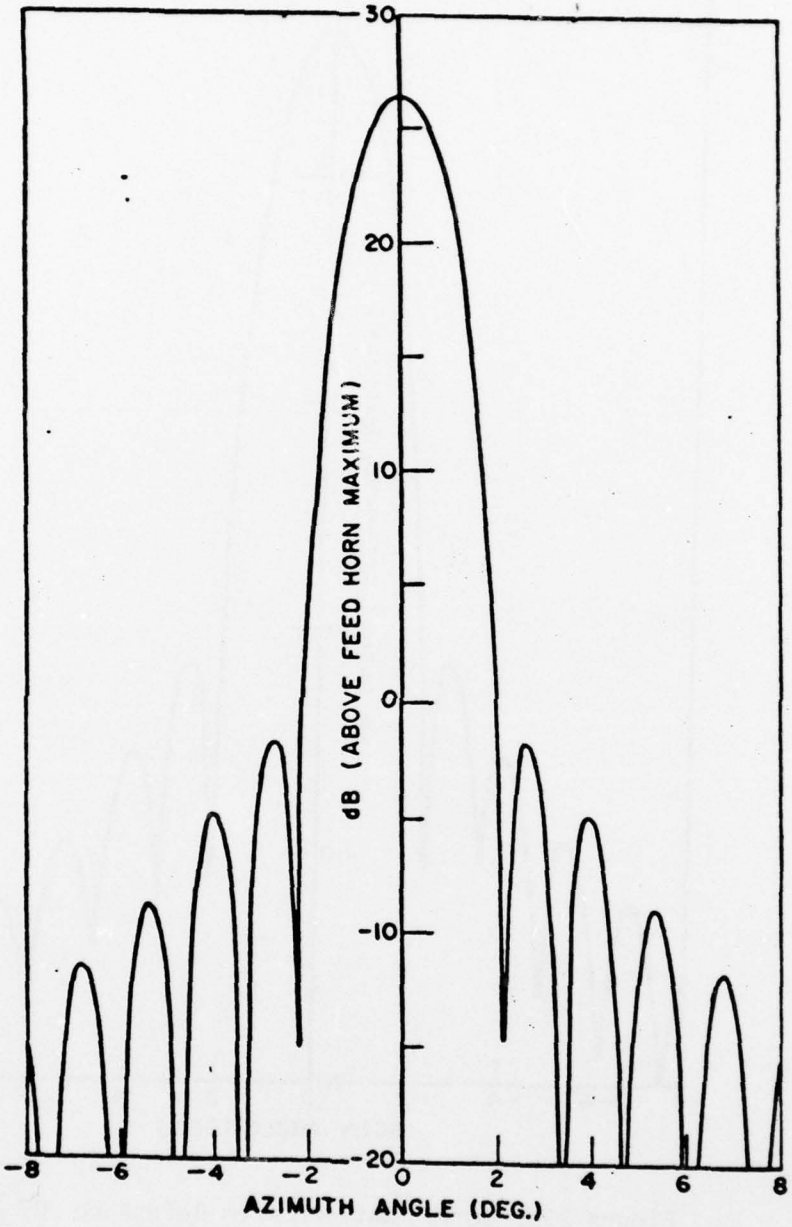

Figure 33a. $\phi = 0^{o}$ pattern from Reference [17].

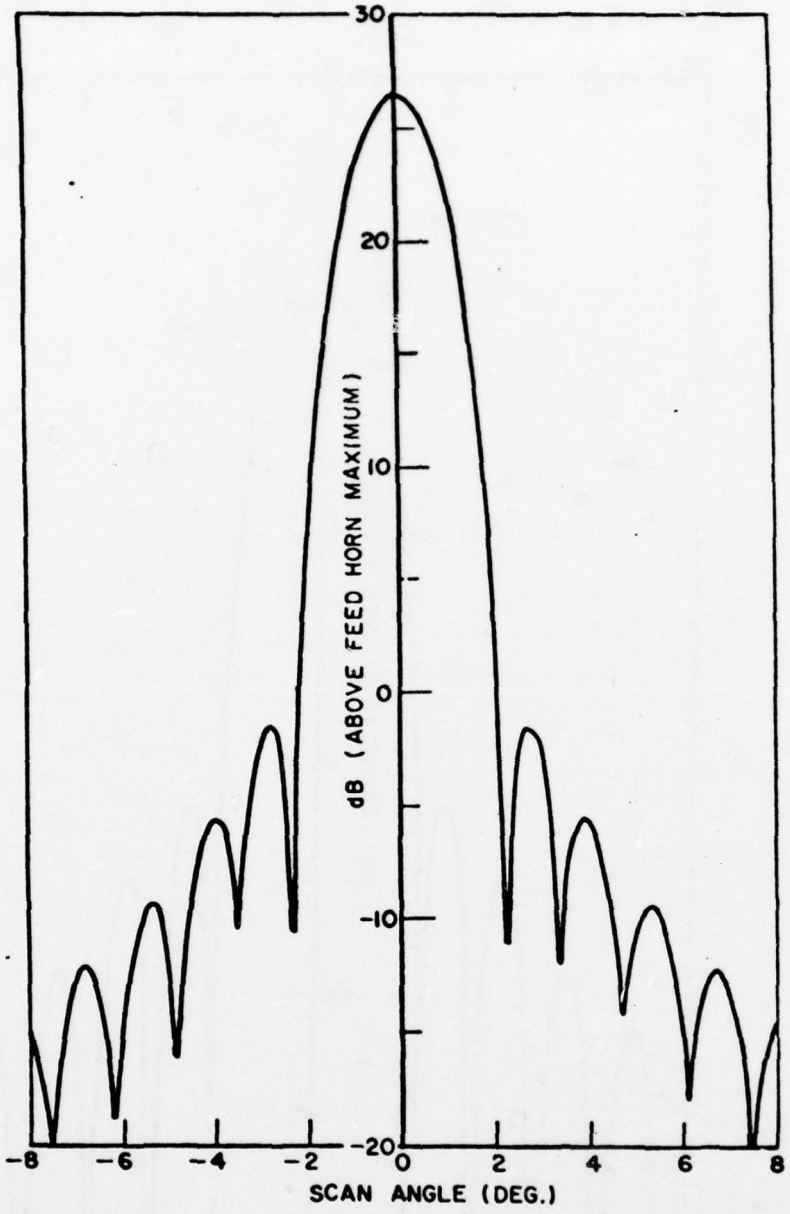

Figure 33b. $\phi = 45^{\circ}$ pattern from Reference [17].

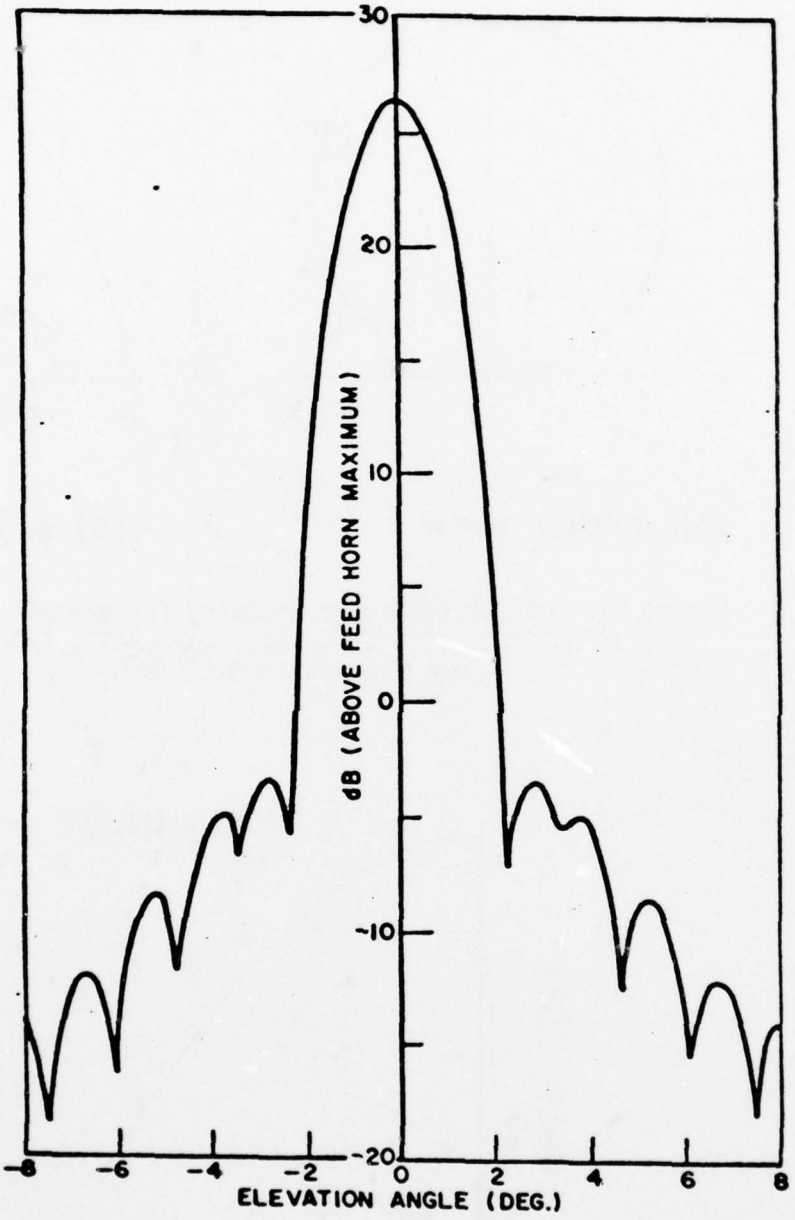

Figure 33c. $\phi = 90^{\circ}$ pattern from Reference [17].

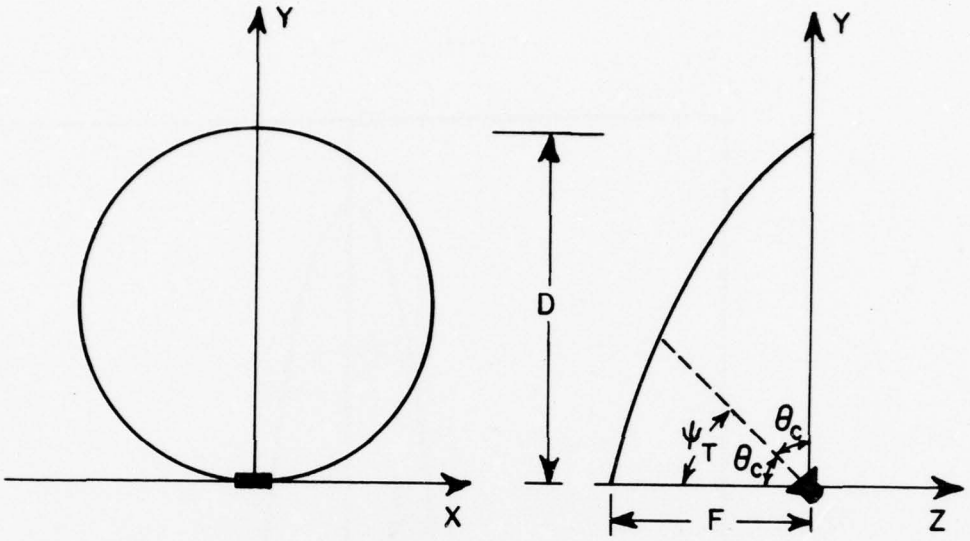

(a) FRONT VIEW (b) SIDE VIEW

Figure 34. Offset reflector geometry for example of Chu and Turrin [18]. D = 12 inches, $\psi_T = \theta_c = 45^0$, f/D=0.25 and frequency = 18.5 GHz.

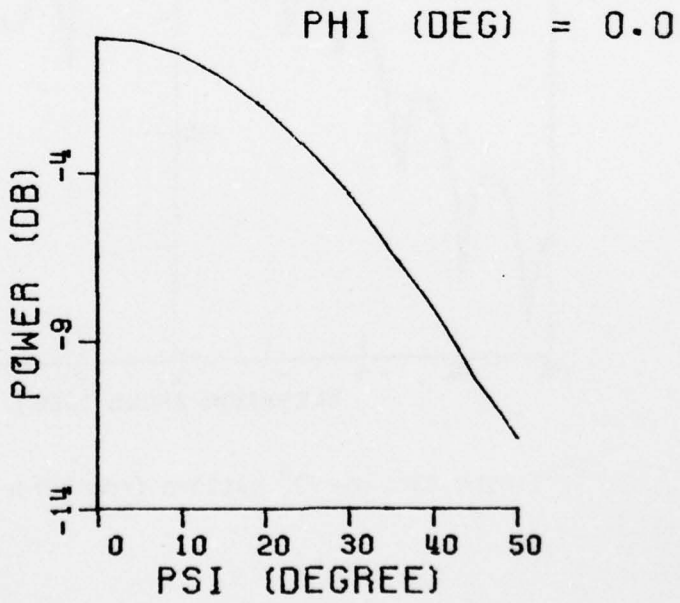

Figure 35. Feed pattern for offset reflector example of Reference [18].

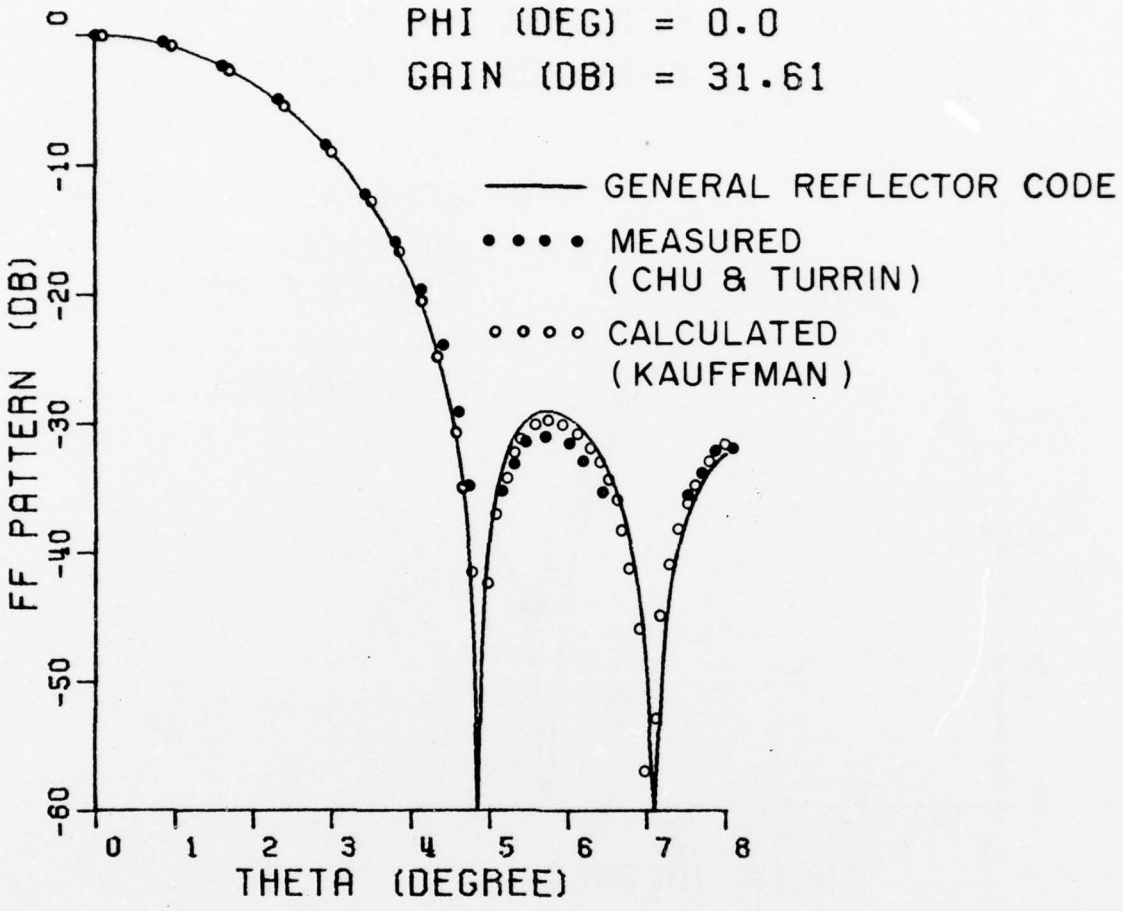

Figure 36. Far field pattern for example of Reference [18], computed by general reflector code. Principal polarization is $\phi=0^{o}$ plane.

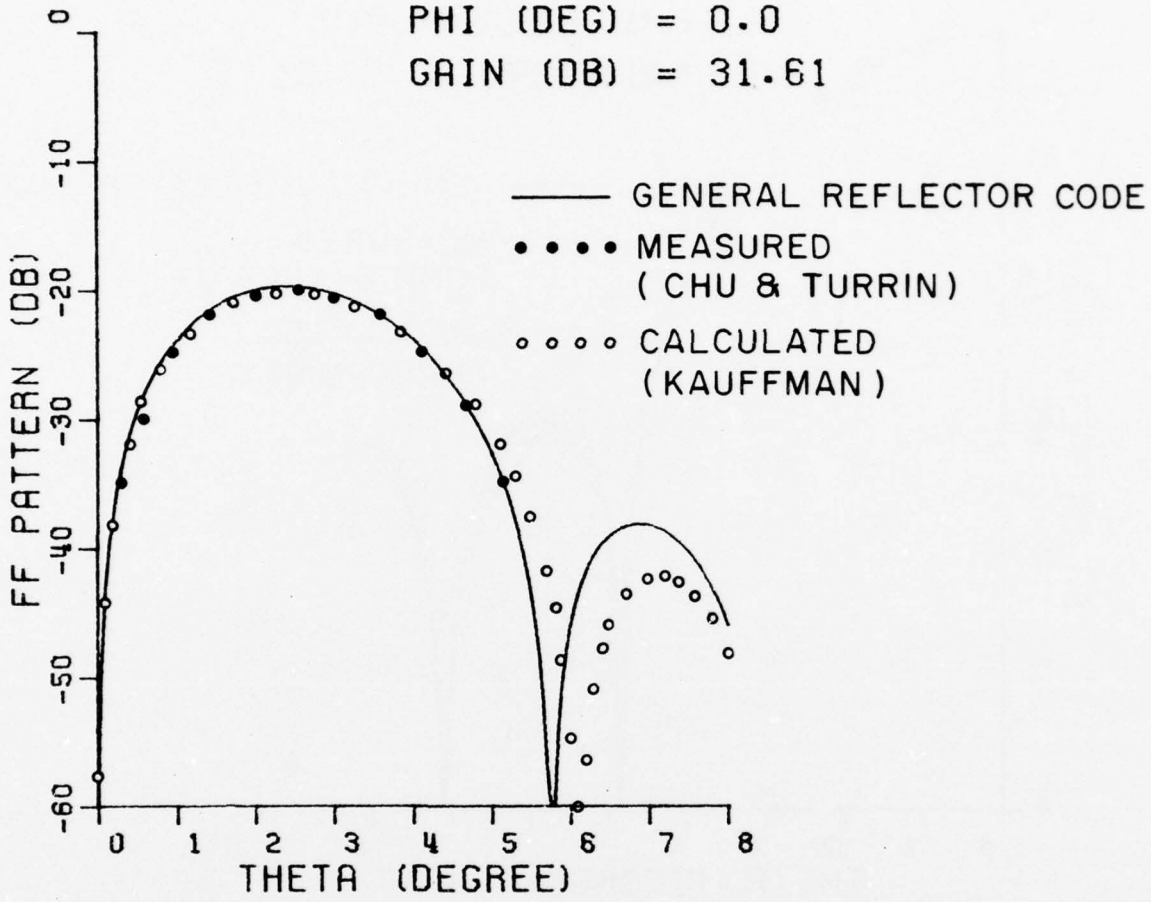

Figure 37. Far field pattern for example of Reference [18], computed by general reflector code. Cross polarization in $\phi=0^{0}$ plane.

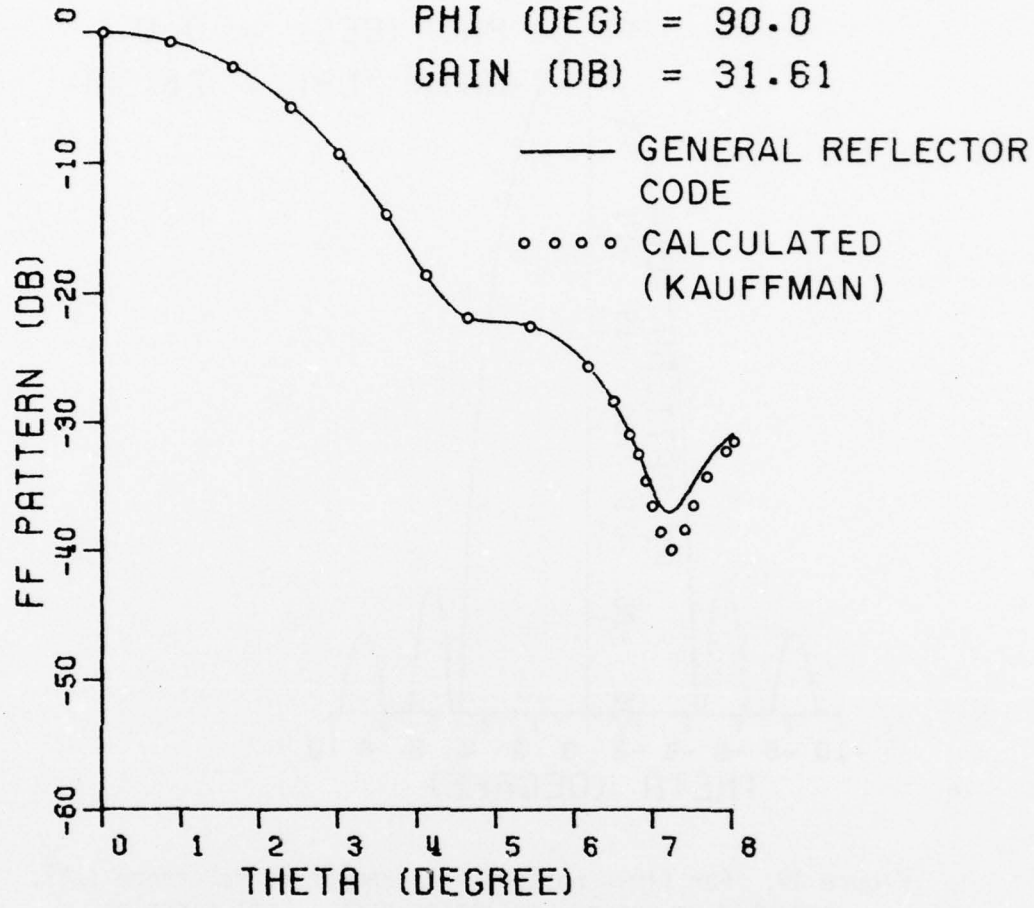

Figure 38. Far field pattern for example of Reference [18], computed by general reflector code. Principal polarization in $\phi=90^{o}$ plane.

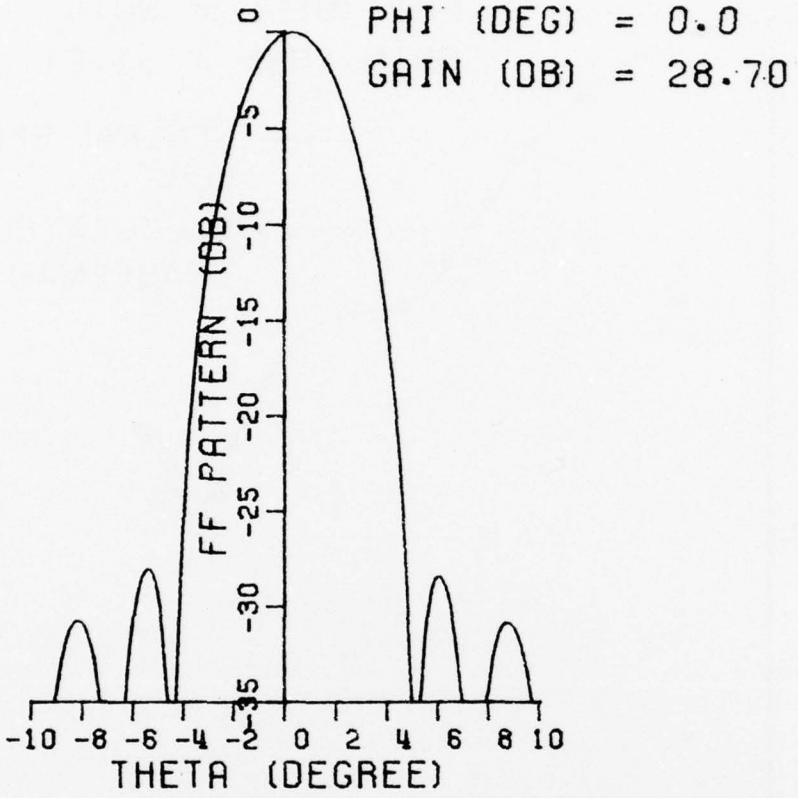

Figure 39. Far field pattern for example of Reference [18], computed by general reflector code. Left circular polarization in $\phi=0^{0}$ plane.

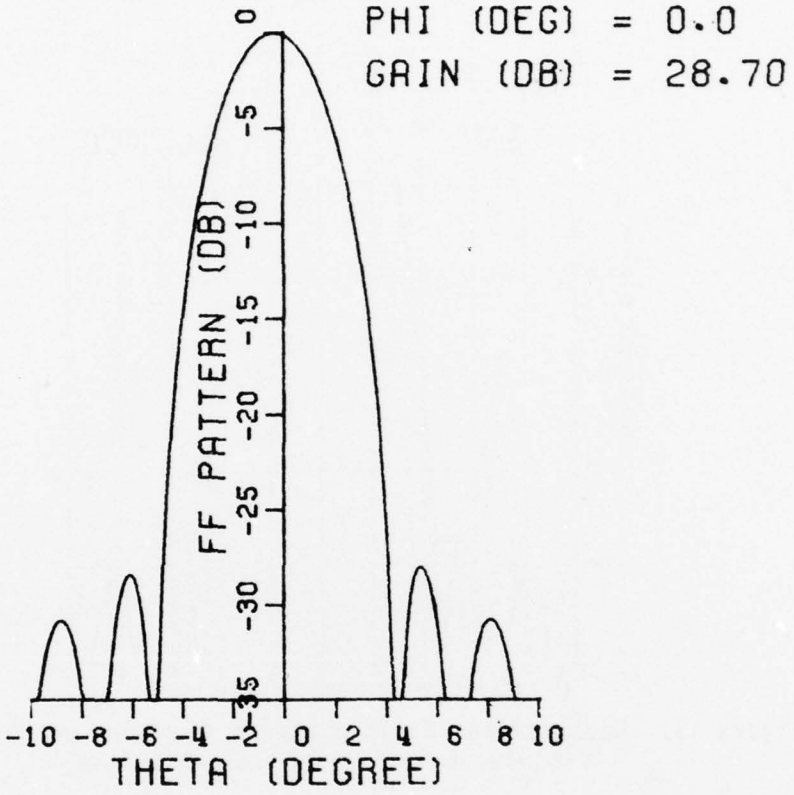

Figure 40. Far field pattern for example of Reference [18], computed by general reflector code. Right circular polarization in $\phi = 0^{0}$ plane.

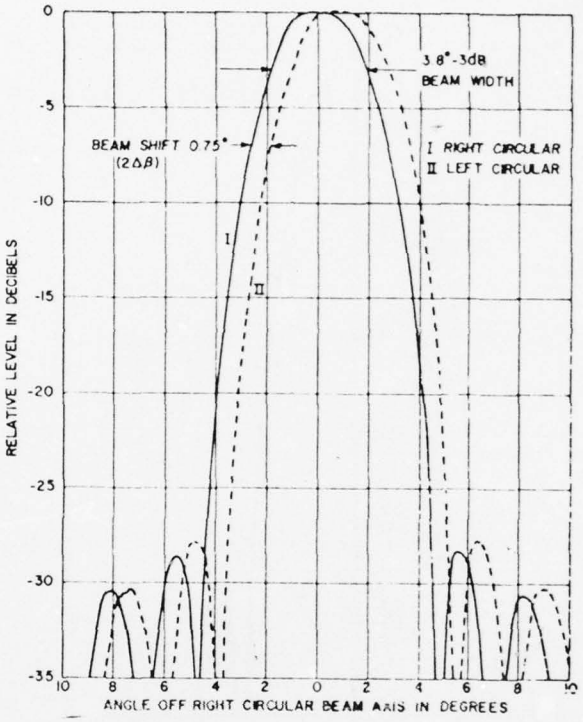

Figure 41. Measured far field patterns from Chu and Turrin [18]. Circular polarization in $\phi=0^{0}$ plane.

AD-A063 870 OHIO STATE UNIV COLUMBUS ELECTROSCIENCE LAB F/G 9/5
ASYMPTOTIC HIGH FREQUENCY TECHNIQUES FOR UHF AND ABOVE ANTENNAS--ETC(U)
OCT 78 R C RUDDUCK, R J MARHEFKA N00123-76-C-1371
UNCLASSIFIED ESL-4508-12 NL

2 OF 2
AD
A063870

END
DATE
FILMED
4 -79
DDC

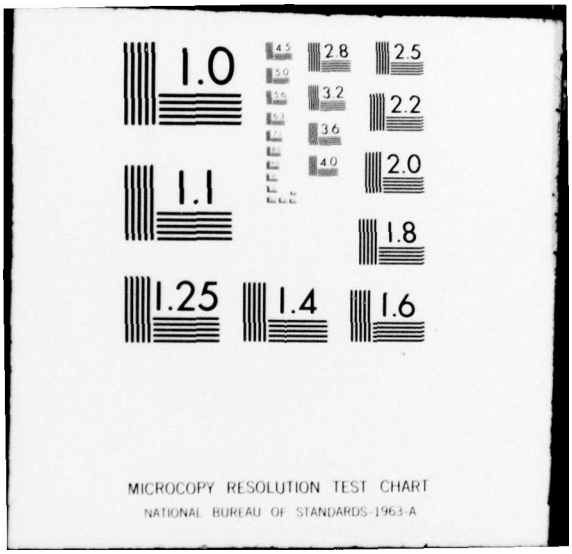
1.0
1.1
1.25
1.4
1.6
2.8
2.5
3.2
2.2
3.6
2.0
4.0
1.8
MICROCOPY RESOLUTION TEST CHART
NATIONAL BUREAU OF STANDARDS-1963-A

V. THEORETICAL STUDIES

Substantial progress has been made in the work relating to the extension of the GTD to treat the diffraction from an edge illuminated by a non ray-optical field. In the configurations under study, the non-ray optical field is the transition region field of a second edge. This topic has been described earlier on pp. 67 and 68 of [4508-6]; it has also been mentioned on p. 26 of [4508-7].

It should be pointed out that Equation (41) in [4508-6] applies to a pair of staggered wedges with different wedge angles, as well as to the half planes shown in Figure 45 of that report. In the present period, the analysis has been extended to the case of the thick edge, as shown in Figure 42.

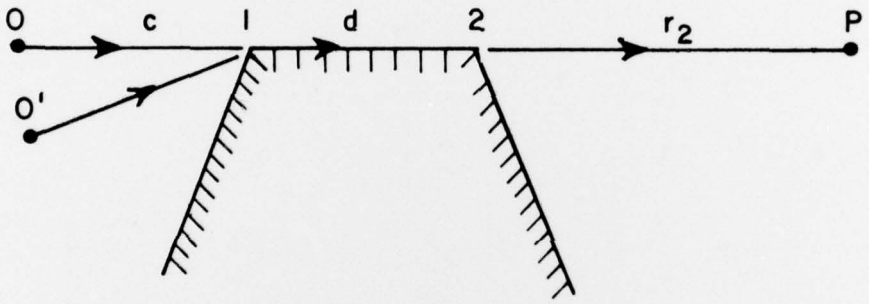

Figure 42. Thick edge illuminated by a source at O or O'.

The solutions for the field at P when the source O, edge 1, edge 2 and P are all in line can be summarized as follows.

A. The electric field incident from O is perpendicular to the top surface (hard boundary condition).

$$U(P) = \frac{1}{2} f(c+d+r_2)+O(k^{-1/2}) .$$

B. The electric field incident from O is parallel to the top surface (soft boundary condition)

$$U(P) = \left[\frac{1}{\pi} \tan^{-1}\sqrt{\frac{cr_2}{d(c+d+r_2)}}\right] f(c+d+r_2) + O(k^{-1}) .$$

where f(x) is defined by Equation (42) in [4508-6].

The preceding formulas have been applied to an example where the thick edge is part of a rectangular cylinder; however one is still dealing with grazing incidence on the top surface, as indicated in Figure 42. Calculations of the field at P when P is in the far-zone of the rectangular cylinder are compared with those obtained from the moment method. The agreement is found to be very close, generally within a few percent, even when the surface exposed to grazing incidence is only 0.2λ wide.

Also the solution has been generalized to the case where the source (or field point) is not in line with edges 1 and 2, as in the case of the source at O'.

This research is essentially complete and a technical report is being prepared. A paper describing this work was presented at the USNC/URSI Spring Meeting in Washington, D.C.

REFERENCES

1. R. G. Kouyoumjian and P. H. Pathak, "A Uniform Geometrical Theory of Diffraction for an Edge in a Perfectly-Conducting Surface," Proc. IEEE, Vol. 62, November 1974, pp. 1448-1461.

2. R. G. Kouyoumjian, "The Geometrical Theory of Diffraction and Its Applications," Numerical and Asymptotic Techniques in Electromagnetics, edited by R. Mittra, Spring-Verlag, New York, 1975.

3. P. H. Pathak and W. D. Burnside, "A Uniform Asymptotic Result for the Scattering of Plane Waves by a Circular Cylinder," Report 3973-1, March 1976, The Ohio State University ElectroScience Laboratory, Department of Electrical Engineering; prepared under Contract N62269-74-C-0788 for Naval Air Development Center, Warminster, Pa.

4. G. J. Burke and A. J. Poggio, "Numerical Electromagnetic Code (NEC) - Method of Moments," NOSC/TD 116, July 1977, Naval Ocean Systems Center, San Diego, California 92152.

5. R. J. Marhefka, "Analysis of Aircraft Wing-Mounted Antenna Patterns," Report 2902-25, June 1976, The Ohio State University ElectroScience Laboratory, Department of Electrical Engineering; prepared under Grant No. NGL 36-008-138 for National Aeronautics and Space Administration.

6. W. D. Burnside, "User's Manual Flat Plate Program," Report 4508-4, May 1977, The Ohio State University ElectroScience Laboratory, Department of Electrical Engineering; prepared under Contract N00123-76-C-1371 for Naval Regional Procurement Office, Long Beach, California.

7. R. J. Marhefka, "User's Manual for Plates and Cylinder Computer Code," Report 4508-8, March 1978, The Ohio State University ElectroScience Laboratory, Department of Electrical Engineering; prepared under Contract N00123-76-C-1371 for Naval Regional Procurement Office, Long Beach, California.

8. H. Bach, "Pattern Measurements of High Frequency Satellite-Mounted Antennas," Electromagnetic Institute, Technical University of Denmark, R154, January 1976.

9. C. H. Walter, Traveling Wave Antennas, Dover Publications, Inc., New York, 1969, pp. 15-16.

10. R. F. Harrington, Time Harmonic Electromagnetic Fields, McGraw-Hill Book Company, New York, 1961, p. 79.

11. R. C. Rudduck,S. H. Lee and W. D. Burnside, "Far Field Reflector Antenna Computer Code User's Manual," Report 4508-11, July 1978, The Ohio State University ElectroScience Laboratory, Department of Electrical Engineering; prepared under Contract N00123-76-C-1371 for Naval Regional Procurement Office, Long Beach, California

12. R. C. Rudduck, R. J. Marhefka, W. D. Burnside, R. G. Kouyoumjian, C. H. Walter, "Asymptotic High Frequency Techniques for UHF and Above Antennas," Report 4508-10, June 1978, The Ohio State University ElectroScience Laboratory, Department of Electrical Engineering; prepared under Contract N00123-76-C-1371 for Naval Regional Procurement Office, Long Beach, California.

13. W. D. Burnside, R. G. Kouyoumjian, R. J. Marhefka, R. C. Rudduck and C. H. Walter, "Asymptotic High Frequency Techniques for UHF and Above Antennas," Report 4508-6, August 1977, The Ohio State University ElectroScience Laboratory, Department of Electrical Engineering; prepared under Contract N00123-76-C-1371 for Naval Regional Procurement Office.

14. A. C. Ludwig, "The Definition of Cross Polarization," IEEE Trans. on Antennas and Propagation, AP-21, pp. 116-119, January 1973.

15. P. A. J. Ratnasiri, R. G. Kouyoumjian and P. H. Pathak, "The Wide Angle Side Lobes of Reflector Antennas," Report 2183-1, March 1970, The Ohio State University ElectroScience Laboratory, Department of Electrical Engineering; prepared under Contract AF 19(628)-5929 for Air Force Cambridge Research Laboratory.

16. S. Silver, Microwave Antenna Theory and Design, MIT Rad. Lab Series, Vol. 12, McGraw Hill (1949), pp. 455-457.

17. C. A. Mentzer, P. H. Pathak and L. Peters, Jr., "Pattern Analysis of An Offset Fed Parabolic Reflector Antenna," Final Report 3220-2, Department of Electrical Engineering; prepared under Contract N00178-71-C-0264 for U. S. Naval Weapons Laboratory.

18. T. S. Chu and R. H. Turrin, "Depolarization Properties of Offset Reflector Antennas," IEEE Trans. on Ant. and Prop., AP-21, pp. 339-345, May 1973.

19. J. H. Kauffman, W. F. Croswell and L. J. Powers," Analysis of Radiation Patterns of Reflector Antennas," AP-24, pp. 53-65, January 1976.